SEOS Frame Camera Applications Study

Final Report

Prepared for:
National Aeronautics and Space Administration
Goddard Space Flight Center
Greenbelt, Maryland

Contract NAS5-21989
AED R-4045
Issued: September 13, 1974 (Preliminary)
November 14, 1974 (Final)

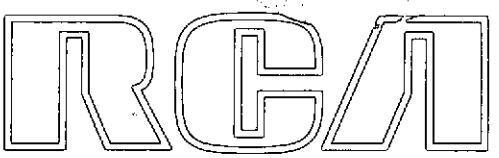

RCA Government and Commercial Systems
Astro-Electronics Division, Princeton, New Jersey

SEOS Frame Camera Applications Study

Final Report

Prepared for:
National Aeronautics and Space Administration
Goddard Space Flight Center
Greenbelt, Maryland

Contract NAS5-21989
AED R-4045
Issued: September 13, 1974 (Preliminary)
November 14, 1974 (Final)

RCA Government and Commercial Systems
Astro-Electronics Division, Princeton, New Jersey

PREFACE

This report contains the results of a Frame Camera Applications Study performed by the Astro-Electronics Division (AED) of RCA for the National Aeronautics and Space Administration to support GSFC engineering and planning effort for the Synchronous Earth Observatory Satellite (SEOS).

The work was performed by RCA-AED under Contract NAS 5-21989 during the period from January to September 1974.

TABLE OF CONTENTS

TABLE OF CONTENTS (CONTINUED)

TABLE OF CONTENTS (CONTINUED)

LIST OF ILLUSTRATIONS

LIST OF ILLUSTRATIONS (CONTINUED)

LIST OF ILLUSTRATIONS (CONTINUED)

LIST OF TABLES

LIST OF TABLES (CONTINUED)

I. INTRODUCTION

This Frame Camera Application Study was undertaken by RCA Astro-Electronics Division in January 1974 to support the NASA Goddard Space Flight Center study and planning effort for the Synchronous Earth Observatory Satellite (SEOS). SEOS is a research and development satellite which will provide opportunities for observation of transient phenomena at any time, provided they fall within the fixed viewing circle of the spacecraft. On-going disasters can be monitored continuously, large areas of potential danger can be surveyed at any desired interval, and changing conditions of the earth's resources can be observed at regular intervals. Current planning efforts for SEOS are aimed toward identifying and evaluating potential applications and determining requirements for SEOS subsystems and payload instruments.

The initial thrust of the study was directed toward the evaluation of possible applications for frame cameras for SEOS. Consistent with this primary objective, a survey of potential sensors with their important operational characteristics was performed (Section III of this report). This effort was paralled with an assessment of potential applications for SEOS in the meterological and earth resources areas. Matching of these applications with potential cameras was intended, with an eventual comparison of the performance of alternate, e.g. pushbroom and point scanning, sensors.

The course originally intended for this effort was thwarted by the lack of available performance data for the scanning instruments and conflicting applications definitions. It was therefore decided, with NASA agreement, to undertake the evaluation of three potentially attractive applications and to characterize the performance capabilities of suitable frame cameras.

The frame cameras that are characterized in this report are intended to provide:

1) Highest possible resolution in daylight - A resolution of about 50 meters in a minimum frame of 150 km square, for a single, broad spectral band.

2) Nighttime operation in a single visible spectral band with a goal of 300 meters resolution for cloud motion observation in noonlight.

3) Multispectral observations extending to low daylight condition - taking advantage of the integration time potential of frame cameras to provide spectral observations with 150 meters resolution.

Selected from the possible frame camera sensors were the 2-inch Return Beam Vidicon (RBV), a 40 mm Silicon Intensifier Target (SIT) vidicon, and a 1-inch silicon vidicon for the three applications. In addition, a 25 mm Secondary Electron Conduction (SEC) tube was considered as a potential alternative to the SIT.

The study then consisted of an examination of these sensors, together with the scene characteristics corresponding to their particular applications. Performance levels achievable, and design and operations concepts are also presented in the following sections. The results are promising and indicate the feasibility and usefulness of frame cameras for SEOS.

II. SUMMARY

Each of the frame cameras considered in this study appears to offer a useful approach to the application intended. While the level of definition attempted in this study is necessarily first order, substantial confidence in the results has been acquired. Judgements as to soundness of the derived performance numbers, e.g., for coverage, sensitivity, resolving power, is based on the described analysis and substantial practical experience with similar systems.

Contrast ratios and scene highlights available for each camera vary substantially with the particular application, the time of day and year, i.e., the sun (or moon) angle, and for the multispectral camera with the spectral bands of interest. For example, for the high resolution applications from nadir to 80° zenith angles, contrasts range from over 12:1 to about 1.2:1. For moonlit scenes (which we limit only to cloud motion observations), contrasts for the same lunar zenith angles go down to about 1.6:1. On the other hand, for the multispectral case, where detection of very small surface reflectance changes is desired, several of the bands offer contrasts of 1.02:1 to 1.05:1 for the minimum contrast conditions. The computed resolving powers for each of the frame cameras, for contrast ratios typical of the intended applications, are listed in Table II-1. The computations clearly indicate the capability of the frame cameras to achieve the desired resolutions for each application.

Note that the specific ground resolution numbers are the result of not only the available sensor packing density, but are also directly relatable to the specific scaling factor employed for the optics. The values shown, for example 41 meters per TV line at a contrast ratio of 2 for the high resolution case,

TABLE II-1. SUMMARY OF CAMERA RESOLVING POWER PERFORMANCE

CAMERA	NADIR GRD COVERAGE KM. SQ	SCENE CONTRAST RATIO	RESOLVING POWER AT NADIR METERS/TV LINE
HI RESOLUTION	150	2.0	41
		1.6	44
NIGHTTIME			
SIT	283	∞	266
		4	284
SEC	216	∞	233
		4	248
MULTISPECTRAL	100	2.0	121
		1.2	141
		1.05	194

increase as the contrast ratio decreases. If improved resolution at low contrast is desired, it may be obtained at the expense of decreased coverage.

The difference in resolving power values shown for the two nighttime cameras (SIT and SEC sensors) are the result of initial estimates required to start the computation and were not intentionally different. Note that the increased format of the SIT provides larger area coverage per frame. The difference in coverage would be somewhat smaller for a recomputation for more nearly equal resolving power.

The performance of these cameras is maintained by adjusting the exposure time to provide the proper highlight exposure at the faceplate of the sensor. This may be obtained within the operating radiance levels of the camera.

Highlight exposures can be achieved by a combination of exposure time control, using the programmable shutter available with each camera, and neutral density filters. The shutter, which is accurately controllable down to 4.5 milliseconds, can reduce exposure time or extend it to the operational limit of each tube. The filters are useful to cut down the light further when even 4.5 milliseconds is too long an exposure time. Small decreases in peak exposure, say 20 percent, result in relatively small changes in resolving power. The same effect is true in terms of operation beyond the normal radiance levels of the sensor, the fall off in resolution being relatively slow with decreasing radiance at a specific contrast ratio.

Exposure time analyses during this study indicate that for both the high resolution camera and the multispectral camera, normal operation and satisfactory performance can be achieved at greater than 80° solar zenith angles, thus approaching sunset

(90°) conditions. For the nighttime camera, operation extends to below half-moon, depending on seasonal and yearly variation.

All of the cameras described are assumed to operate in conjunction with the Large Earth Survey Telescope (LEST) with specific optical elements tailored for the field of view and format of each frame camera. As a starting point, NASA suggested that the basic LEST be considered a 1.5 meter telescope with 9 meter focal length (f/6), and that the field of view provides coverage of 400-by-400 km of the surface at nadir. Required, in addition, is MTF data to permit resolving power computations.

The assumed LEST MTF curve is shown in Figure II-1. This curve is based on an early and preliminary curve generated by the Itek Corporation for an f/20 version of LEST, at a wavelength of .63 micrometers, with extrapolation to low packing density. It is anticipated that the final version of the LEST will provide a somewhat different MTF. This will change the resolving power values computed in later sections, but since the LEST component is less significant than the sensor MTF, substantial changes are not anticipated. Probably of more significance, changes in the effective aperture of the telescope will directly impact the computed exposure times for all of the cameras (Section V).

The computed lens characteristics for each of the cameras are listed in Table II-2. Note that the cameras require elements to shorten the focal length, which in turn results in a numerically lower f number (increased effective aperture). The mechanism employed to establish the desired scaling factor (described later) is a function of both the desired coverage and the available sensor packing density.

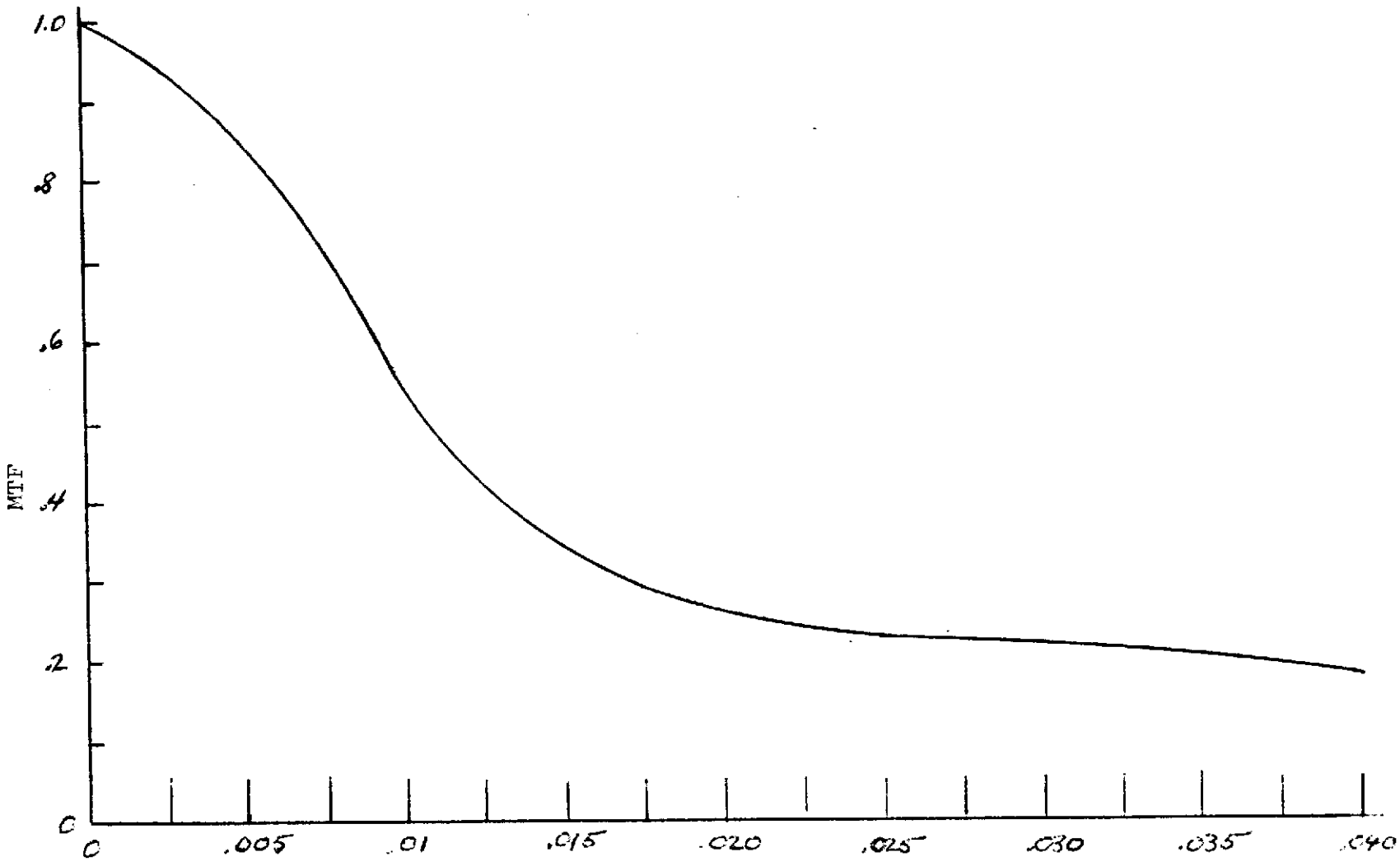

Figure II-1. Assumed LEST Modulation Transfer Function

TABLE II-2. SUMMARY OF OPTICAL CHARACTERISTICS

CAMERA	OPTICS FOCAL LENGTH IN METERS	f/NO.	NADIR GRND COVERAGE KM SQ.
HI RES.	6.06	4	150
NIGHTTIME			
SIT	3.58	2.4	283
SEC	2.98	2.0	216
MULTISPECTRAL	4.05	2.7	100

III. SENSOR PERFORMANCE COMPARISON

1. Introduction

Performance features and operational characteristics of a number of frame camera sensors were reviewed and normalized for comparison purposes. The outstanding characteristics, particularly sensitivity, spectral responsivity and resolution, were used as the basis for overall characterization of camera operating features. This material was reviewed with NASA and formed the basis for selection of three specific sensors which were analyzed in greater detail and are treated in later sections of this report. This section deals with the earlier comparative material and contains a discussion of the processes followed in arriving at the sensor evaluation.

2. Sensor Performance Characteristics

A total of eleven (11) frame camera sensors[1] were considered. These are listed in Table III-1 together with physical and performance characteristics. Physically the tubes fall in 1, 2 or 3-inch generic sizes. While other possibilities are sometimes available, the format chosen was intended to permit more direct comparison among the various units.

The format employed for the measurements provided in the data sheets or, in some cases, laboratory measurements at AED are also listed. Typically a one-inch sensor has an available image diagonal of 16 millimeters (mm). The format of the other sensors are not directly relateable to the physical size. For example, the 2-inch RBV has an available diagonal of 35 mm which is the same as the three-inch isocon.

---

1. For definition of sensor types and other terminology used in this report see Glossary, Appendix A.

TABLE III-1. SUMMARY OF SENSOR PERFORMANCE CHARACTERISTICS

TYPE	SIZE	RES LP/MM	SENSIT FC-SEC	DYNAMIC RANGE	SPECTRAL	GEOM-ETRY	SHAD-ING	STOR-AGE	FORMAT MM x MM	γ	CONDITIONS
Vidicon - ASOS	1"	33	.08	55	ASOS	B	B	B	12.2 x 12.2	.7	6.5 Sec Frame
Vidicon - PbO	1"	36	$.75 \times 10^{-3}$	32	PbO	A	A	C	9.6 x 12.8	1.0	BDCST
Vidicon - Silicon	1"	28	$.18 \times 10^{-3}$	32	Sil	B	A	C	9.6 x 12.8	1.0	BDCST
SIT/EBS	1"	25	1×10^{-3}	32	S-20	C	B	C	9.6 x 12.8	1.0	BDCST
SEC	2"	16	$.13 \times 10^{-3}$	32	S-20	B	B	A	15.2 x 20.3	1.0	BDCST
ISIT	1"	21	$.1 \times 10^{-3}$	32	S-20	C	B	C	9.6 x 12.8	1.0	BDCST
Image Orthicon	3"	11	$.8 \times 10^{-3}$	32	S-20	B	A	C	27.4 x 36.5	1.0	BDCST
Image Isocon	3"	16	$.27 \times 10^{-3}$	100	S-20	B	A	C	21.3 x 28.5	1.0	BDCST
RBV - ASOS	2"	70	.15	40	ASOS	A	C	B	25.4 x 25.4	.8	3.5 Sec Frame
RBV - SILICON	2"	45	.01	32	Sil	A	C	C	25.4 x 25.4	1.0	.25 Sec Frame
Intensif. RBV(ASOS)	2"	35	1.8×10^{-3}	40	S-20	C	C	B	25.4 x 25.4	.8	3.5 Sec Frame

QUALITY RANK	STORAGE TIME
A - Best B - Moderate C - Poorest	A - Long B - Moderate C - Short
See Appendix B for definitions	

The resolution entry in the second column of Table III-1 is the packing density at 20 percent response to a square wave test pattern. This data was obtained from manufacturer data sheets, for the first eight entries, where the information is usually provided in TV lines per picture height. For example, for the RCA 4532, the one-inch silicon vidicon, the response curve indicates 530 TV lines at 20 percent response for a 3/8-inch high picture. This corresponds to about 28 line pairs per mm.

The resolution entries for the first two return-beam-vidicon (RBV) sensors are typical results obtained from samples measured at AED. In both cases the test lens response was taken into account by converting the overall square wave response to sine wave response, dividing by the sine wave MTF of the lens, and then converting the sensor MTF to square wave response.

For the intensifier RBV, the MTF of the intensifier was cascaded with the sensor response. Note that the packing density available from the RBV is halved by the addition of the intensifier (from 70 lp/mm to 35 lp/mm).

The sensitivity column entries are in foot-candle-seconds (fc-sec) exposure for 30 dB signal-to-noise ratios (SNR). Operating conditions for these data entries are not completely normalized. Typical data sheet light transfer characteristics are provided for open shutter, at broadcast rates, and with a tungsten illumination source. These scan rates were not changed for the data entries, but shuttered exposure was assumed, and computation of the light transfer characteristic for 6000° Kelvin (sunlight) illumination was performed. Data for those sensors listed under conditions other than broadcast standards were obtained (or extrapolated) from measurements made at AED.

The transformation of the light transfer characteristic was accomplished by first assuming that normalizing 2850° color - temperature tungsten and 6000° sunlight spectral curves (Figure III-1) for equal engergy at 550 nanometers will provide equal luminous input to the sensor. (More exactly, the standard luminous efficiency curve, Figure III-2, should be cascaded with the spectral energy of the two sources and the resultant response integrated over the visible wavelengths. The amplitudes of the two sources should then be adjusted for equality of luminous inputs). Step-wise integration was then performed for the spectral response of each sensor type at both color temperatures. The process is illustrated in Figure III-3 where the S-20 spectral response is shown together with the illumination energy assumed for each 50 nanometer interval.

The eleven sensors which were considered include four distinct spectral characteristics. These four are plotted in Figure III-4 and the resulting computed ratio of spectral sensitivities at the two temperatures are listed in Table III-2. It is apparent that for applications involving spectral stimulus in specific narrow bands, a sensor providing an indicated high sensitivity for full spectrum stimulus may be unsuitable. The particular application together with the data provided in Table III-1 must be weighed to establish the potential suitability of each sensor.

TABLE III-2. RATIO OF SENSOR SENSITIVITY AT 6000°K TO SENSITIVITY AT 2850°K

SENSOR TYPE	RATIO
S-20	1.24
Silicon	.52
Lead Oxide	1.55
ASOS	1.03

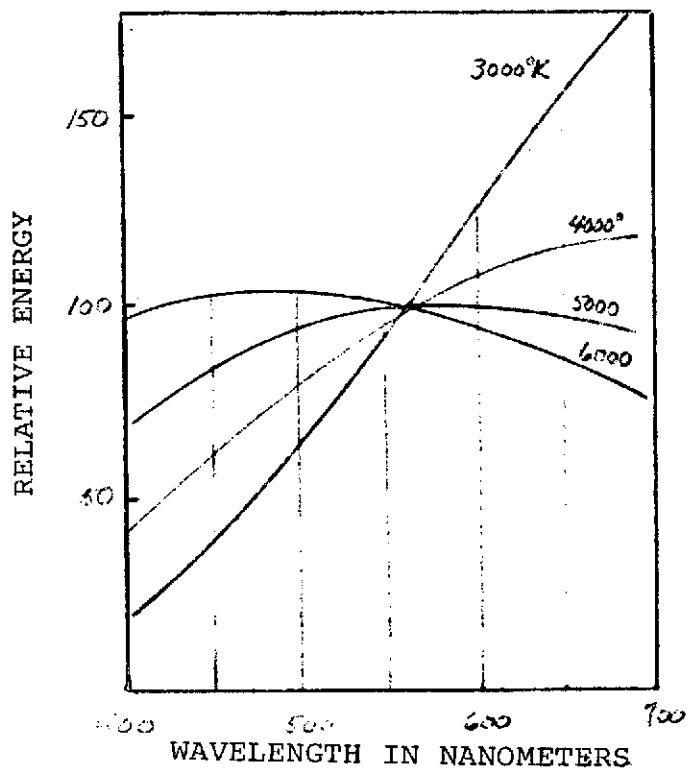

Figure III-1. Spectral Emittance as a Function of Color Temperature

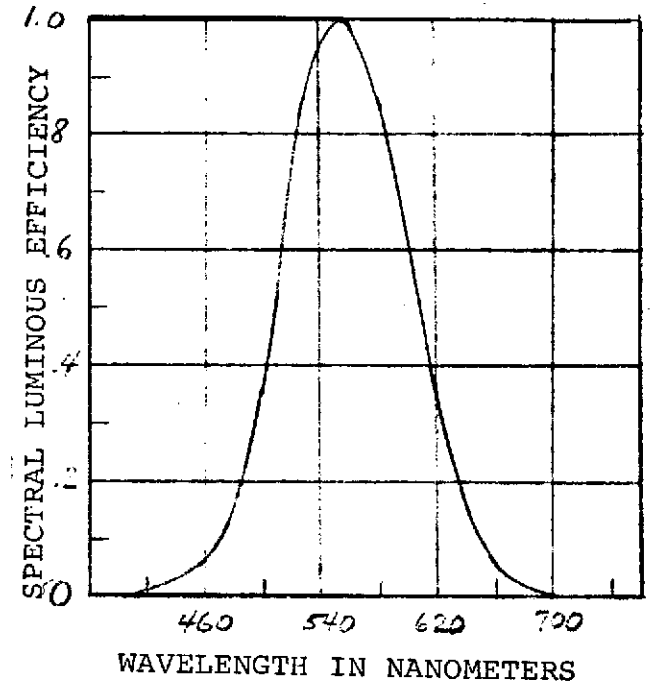

Figure III-2. Standard Luminosity Curve

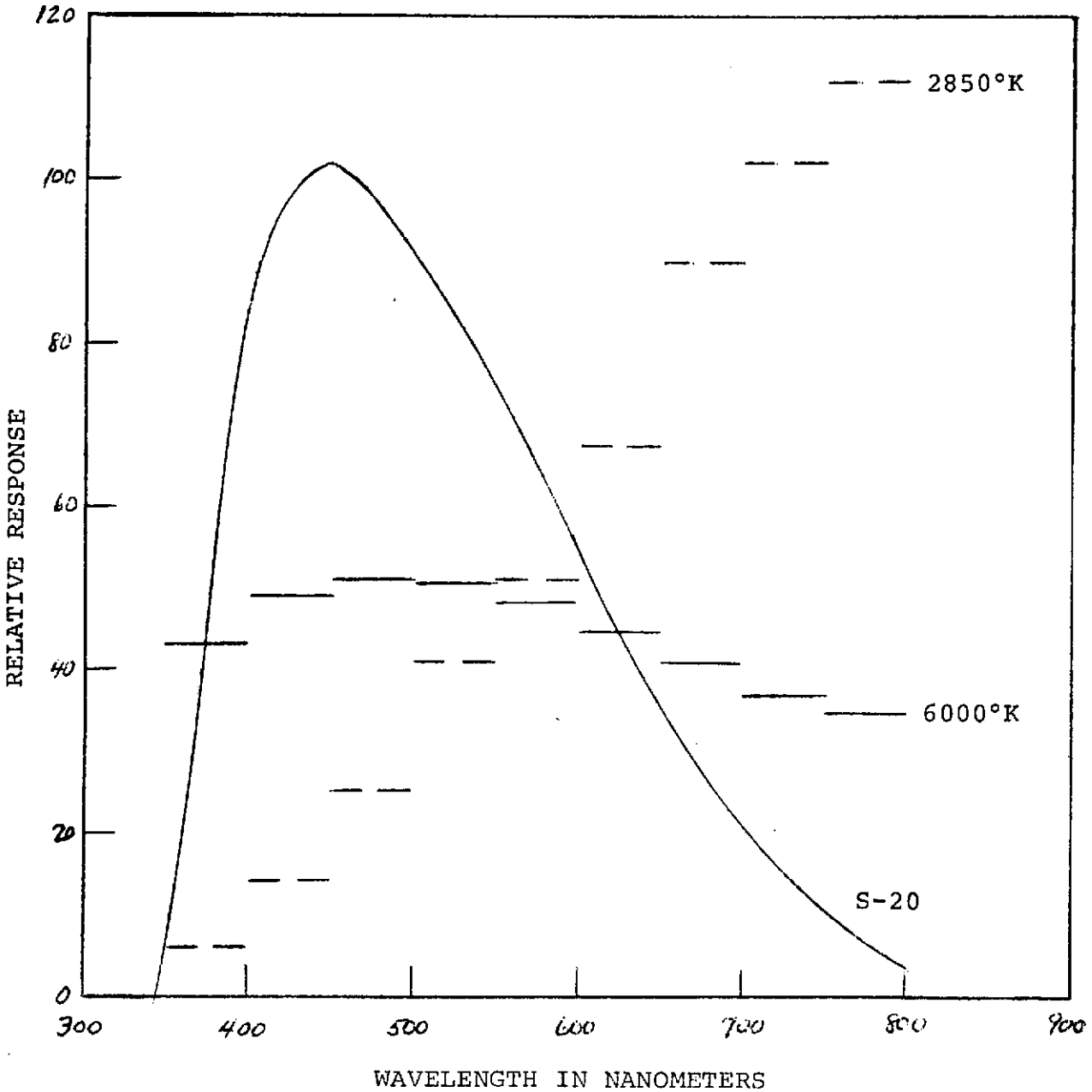

Figure III-3. Integration Increments for S-20 at 2850° and 6000°K

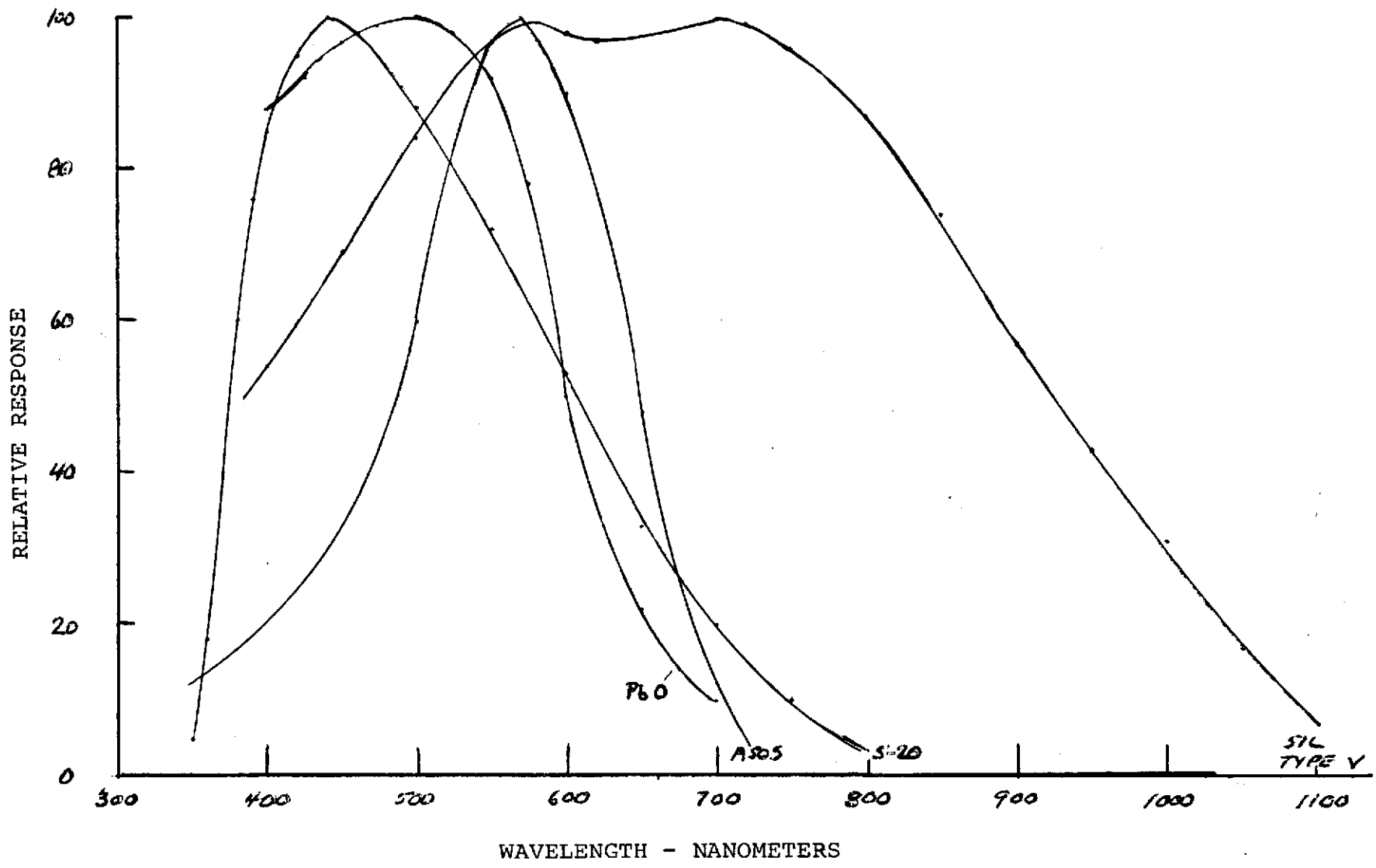

Figure III-4. Spectral Responsivity of Sensors

Other characteristics contained in Table III-1 may be important for a particular application. (Definitions of column headings and entries are contained in Appendix "B"). For example, if nighttime picture-taking is desired, long exposure times will be required and the storage characteristic of the sensor will be important. The SEC sensor, in particular, has very low target leakage and may be employed for long exposure times without significant loss in information (characterized as "A", the longest storage time under "storage" heading in the table). Another example: where excellent geometry is required (better than 1%), entries "A" in the geometry column should be selected.

3. Sensor Coverage Time

The portion of daily coverage that each type of sensor is capable of providing was computed. It was assumed for this computation that the LEST was an f/6 optical system and that the scene reflectivity was 0.25 with a solar illumination of 12,000 foot-candles (fc) at high noon. Then the faceplate illumination is given by:

$$fc = \frac{0.25 \times 12000 \times T}{4(6)^2} = 20.8T$$

where T is the lens transmission. A transmission of .72 was assumed[1], providing a faceplate illumination of 15 fc.

The illumination level and the sensor sensitivity (highlight exposure for a given SNR) were then used to compute the exposure times for each sensor. These computed values are given in the second column of Table III-3. For lower sun angle values, the

1. A more pessimistic transmission value of 50% was assumed for the computations appearing in later sections of this report.

TABLE III-3. SENSOR EXPOSURE RANGE

SENSOR TYPE	SENSITIVITY FC-SEC	LIGHT COND =	REQUIRED EXPOSURE TIMES FOR 30 DB SNR IN SEC						MAXIMUM EXPOSURE TIMES SEC
			SUN NORMAL	SUN 84.26°	SUNSET	TWI-LIGHT	DEEP TWI-LIGHT	FULL MOON	
		REL ILLUM =	1.0	.1	5×10^{-3}	10^{-4}	10^{-5}	10^{-6}	
Vidicon-ASOS	.08		5.3×10^{-3}	5.3×10^{-2}	1.0				2
Vidicon-PbO	$.75 \times 10^{-3}$		5×10^{-4}	5×10^{-3}	.01				.1 - .2
Vidicon-Silicon	$.18 \times 10^{-3}$		1.2×10^{-5}	1.2×10^{-2}	2.4×10^{-3}	.12			.1 - .2
SIT/EBS	$.1 \times 10^{-3}$		$.67 \times 10^{-5}$	$.67 \times 10^{-4}$	1.33×10^{-3}	.067			.1 - .2
SEC	$.13 \times 10^{-7}$		$.87 \times 10^{-5}$	$.87 \times 10^{-4}$	1.73×10^{-3}	.087	.87	8.7	100
ISIT	$.1 \times 10^{-3}$		$.67 \times 10^{-5}$	$.67 \times 10^{-4}$	1.33×10^{-3}	.067			.1 - .2
Image Orth	$.8 \times 10^{-3}$		5.3×10^{-5}	5.3×10^{-4}	1.07×10^{-2}				.1 - .2
Image Isocon	$.27 \times 10^{-7}$		1.8×10^{-5}	1.8×10^{-4}	3.6×10^{-3}	.18			.1 - .2
RBV-ASOS	.15		10×10^{-3}	.1	2				2
RBV-Silicon	.01		$.7 \times 10^{-3}$	7×10^{-3}	.14				.1 - .2
Intensif-RBV	1.8×10^{-3}		1.2×10^{-4}	1.2×10^{-3}	2.4×10^{-2}	1.2			2

relative illumination levels are shown at the top of the columns of this table, with required exposure times for each sensor as the column entries. The final column in this table lists the assumed maximum exposure times for each sensor. For longer exposure times, with typical units, some loss of signal and/or loss of resolution might be anticipated.

The entries for maximum exposure time are quite conservative at this point, since requirements were not yet factored into the performance numbers. Longer exposure times can be used for several of the sensors. Silicon, for example, can be improved in this regard by cooling. A 2-to-1 increase in maximum permissible exposure times can be assumed for each 7.5°C decrease in temperature below the 30°C faceplate temperature used for data sheet entries. Similarly, many low leakage ASOS units are available permitting exposure times up to an order of magnitude higher than the 2 seconds maximum time listed.

It should be emphasized that the computations for exposure time are made to bracket the performance levels anticipated and provide comparative data among sensors, and were redone more accurately as described in a later section where particular applications are described. Factors that need to be considered in detail include: additional optical elements required to provide specific earth coverage per frames; the portion of the spectrum required for a particular observation and the target reflectivity; atmospheric effects as influenced by times of operation (sun angle); and camera operating rates and bandwidth.

4. Camera Operating Conditions

Operating cycles were estimated for each of the sensors considered. This data is shown in Table III-4 where minimum and maximum scan rates and frame times are presented. Data is based on sensor capabilities relating to information packing density, storage time, and erase/prepare requirements.

TABLE III-4. CAMERA OPERATING CONDITIONS

SENSOR TYPE	LINES/ FRAME MAX	READOUT RATES				PRE-PARE TIME SEC	EXPOS TIME MAX	TOTAL FRAME TIME	
		LINE RATES		FRAME RATE					
		MIN /SEC	MAX /SEC	MIN /SEC	MAX /SEC			MIN SEC	MAX SEC
Vidicon - ASOS	1200	120	2400	.1	2	5	2	7.5	17
Vidicon - PbO	1200	4800	120 K	40	100	.2	.1	.3	.55
Vidicon - Sil	1000	2000	60 K	2.0	60	.2	.1	.3	.8
SIT	800	1600	48 K	2.0	60	.2	.1	.3	.8
SEC	800	8	80 K	.01	100	.1	100	Expos T	200
ISIT	700	1400	42 K	2.0	60	.2	.1	.3	.8
Image Orth	1000	2000	100 K	2.0	100	.1	.1	.2	.4
Image Isocon	1200	2400	120 K	2.0	100	.1	.1	.1	.4
RBV-ASOS	5000	500	10,000	.1	2	5	2	7.5	17
RBV-Silicon	3200	6400	16,000	2.0	10	.2	.1	.4	.8
Intensifier RBV (Sil)	2500	250	5,000	.1	2	5	2	7.5	17

The first column in the table lists the lines per frame assuming a factor of about 20 percent excess scan lines over the available picture elements. Picture elements were determined by assuming a square format with a diagonal given by the available format listed in Table III-1.

Maximum time per frame (last column) is determined by the sum of the maximum expose and read times, and prepare time. Maximum expose and read is limited by the sensor leakage characteristic and operating temperature. Erase time is devoted to removing old information and preparing the surface for the subsequent exposure. Factors such as target capacity, beam current, and surface acceptance coefficient were combined to provide a reasonable time interval for this function.

As an example of the process followed to specify the maximum frame time, consider the RBV with the ASOS surface. Experience had indicated that the total time for expose and read should be limited to about 10 to 15 seconds to prevent excessive loss of stored information and loss of resolution due to transverse leakage. This time is limited here to 12 seconds, 10 for read (0.1 second minimum frame rate) 2 for expose. Erasure and preparation may be accomplished in 5 seconds leading to a total frame time of 17 seconds.

At the other extreme, for minimum frame time, the read rate can be speeded up until no substantial reduction in total frame time results. For the RBV example, if 5 seconds is used for prepare and 2 seconds for exposure, decreasing the read time to 0.5 seconds results in a total time of 7.5 seconds with only a small portion devoted to read. This kind of trade-off has assumed adequate bandwidth available from the satellite communication link and no adverse SNR effects from the quite high rates involved.

Again for the RBV case, with a 0.5 second read interval and 5000 lines per frame, the scan rate is 10,000 scans per second. Ignoring blanking and retrace time, 4500 picture elements scanned at a 10,000 scan line per second rate will require a bandwidth of:

$$BW = \frac{4500}{2} \times 10{,}000 = 22.5 \text{ MHz}$$

Numbers listed for the other sensors in the table have been computed following a similar line of reasoning.

IV. OBSERVATION REQUIREMENTS

1. Introduction

There are many potential applications for frame cameras on SEOS which can take advantage of such features as programmable extended exposure times, light intensification, high packing density and resolution, snapshot coverage of large areas, stable image geometry, and rapid readout and repeat coverage. Some of the applications can also be handled by other instruments such as scanning radiometers or "push broom" linear arrays, while for others, frame cameras offer considerable extensions over the capabilities of the other instruments. For the purposes of this study, we have only concentrated on applications for which features of the frame camera are unique. Specifically, two features are exercised - the abilities to achieve higher resolution and to operate in much lower illumination conditions than discrete detector instruments. Accurate measurements of boundaries and motions are desirable for several meteorological (e.g., snow, clouds) and earth resources (land-water boundaries) applications. Scenes for these applications are described below with 50 meter resolution in a single band set as a goal. In addition, night time cloud motion observations are desired to determine wind velocities. A goal of 300 meters resolution in the visible was set for observation of moonlit scenes described below. This is about four times better than the resolution expected for an IR radiometer. Finally, several earth resources applications require multispectral observations at all daylight hours, including near sunrise and sunset. Scenes for these applications are described below at gradually increasing solar zenith angles.

2. Scene Descriptions

A. High Resolution, Daylight Observation Required

High accuracy measurements are desired for many earth

resources and meteorological applications. Cloud edges versus various backgrounds are needed accurately to provide motion information as well as edge formations at all meteorological scales. Snow field boundaries are of interest in both meteorology and earth resources. Variations in land-water lines in estuaries and flood-prone areas must also be determined accurately.

Snow boundaries can be observed during the best sunlight conditions, but only during winter and early spring. The others, especially cloud motions, may be required at any time. A typical set of scenes of this type are listed in Table IV-1. All scenes are assumed located at 40°N, 100°W. We have not included clouds versus snow scenes. The reflectances are too similar for these items and normal variations in either cloud or snow reflectances could make either appear brighter at different times (especially for low clouds). Since other backgrounds occur much more frequently than snow, we do not use clouds versus snow for determining camera design parameters.

The sun angles chosen represent a typical range from the best, 16.5° (noon at summer solstice) to relatively poor illumination conditions. Even poorer illumination conditions can be estimated from the results for these angles by extrapolating plotted results. Note, that each of the other angles (except 16.5°) corresponds to different times of day at different times of year. For example, 48° is noon in mid-February and about 1400 at the vernal equinox, 68.5° is 1350 at the winter solstice and 1610 at the equinox, and 25.5° is 1455 at the winter solstice and 1645 at the equinox.

Table IV-2 gives the other parameters of interest - reflectivity (ρ), altitude, and optical thickness (m) - for each observable. A standard atmosphere is assumed in all cases. Reflectance values are taken from Reference 1.

TABLE IV-1. HIGH RESOLUTION SCENES

Scenes		Sun Angles (Zenith)
High Cumulus Over	Water	16.5^{o}, 48^{o}, 68.5^{o}, 75.5^{o}, 80^{o}
	Vegetation	16.5^{o}, 48^{o}, 68.5^{o}, 75.5^{o}, 80^{o}
	Soil	48^{o}, 68.5^{o}, 75.5^{o}, 80^{o}
Low Stratus Over	Water	16.5^{o}, 48^{o}, 68.5^{o}, 75.5^{o}, 80^{o}
	Vegetation	16.5^{o}, 48^{o}, 68.5^{o}, 75.5^{o}, 80^{o}
	Soil	48^{o}, 68.5^{o}, 75.5^{o}, 80^{o}
Vegetation vs Water (boundaries)		16.5^{o}, 48^{o}, 68.5^{o}, 75.5^{o}, 80^{o}
Snow vs Soil		48^{o}, 68.5^{o}

TABLE IV-2. PARAMETERS FOR EACH OBSERVABLE

Observable	Reflectivity (ρ)	Altitude (ft)	Optical Thickness (for normal illumination)
Cumulus Clouds	.8	30,000	.3
Stratus Clouds	.55	5,000	.85
Water	.05	0	1
Vegetation	.04 - .17 (linear from .35 - .7μ) .30 (.7-.75μ) .45 (.75-.8μ)	0 0 0	1 1 1
Snow	.64	0	1
Soil	.12 - .4 (linear from .35 - .8μ)	0	1

B. Moonlight Observations

The most significant night-time observation is of cloud motion in order to determine wind velocity. Thus, the scenes involving high and low clouds listed in Table IV-1 with corresponding parameters in Table IV-2 are also of interest for night-time observations. We will use the same zenith angles as typical of the moon's position in the sky since the moon's orbital plane makes only a 5^{o} angle with the ecliptic. The maximum elevation varies from an 11.5° zenith angle to 68.5° (for a 40°N. latitude scene) depending both on season and year. Phases of the moon from full moon down to 1/3 moon will be used to determine illumination. It must be recognized, of course, that a moon phase less than full is only visible in the night sky (even at low elevation) for approximately the same fraction of the night as the phase. E.g., a half moon is visible only half the night; it is also visible during half the day. Thus, night-time observations with partial moons are limited both by the available light and the time in view.

C. Low-light Multispectral Applications

ERIM has been conducting a study of potential earth resources applications for SEOS (Reference 2). Thirty-two applications have been identified and ranked according to importance, feasibility of observation, and uniqueness to SEOS capabilities. The top twenty of these are considered significant for SEOS. All of them require multispectral observations. Of this group of twenty, four applications require mostly visible/near infrared observations throughout the daylight hours. These four are (using ERIM's ranking numbers):

[2] Estuarine Dynamics and Pollution Dispersal

Observation times correspond to high, mid, and low tides, which vary to any time during the day.

[6] Detecting and Monitoring Fish Location and Movement

Noon daily plus 0600, 0900, 1500, and 1800 during the local fishing season (April-September for the test sites).

[12] Detecting and Monitoring Oil Pollution

Noon daily plus 1/hr. whenever oil spill occurs.

[18] Diurnal and Seasonal Variations for Thematic Mapping

By definition, throughout the day and year.

ERIM's study identified typical test sites for each of these applications and provided radiances at the spacecraft corresponding to these sites in spectral bands of interest (Reference 3). For each site two sun angles were used in the computations, one corresponding to noon at the summer solstice, the other to a mid-morning or afternoon sun on a day in mid winter or spring. The latter are not the most poorly illuminated scenes we wish to examine for frame camera applications, but they are the only low-light multispectral scenes for which total radiances including target and path radiances are available. Table IV-3 gives the parameters for each of the scenes. Table IV-4 lists the spectral bands of interest for each application. In subsequent sections we will indicate how we can provide rough extrapolations to lower light levels.

3. Computation Procedures for Radiances Seen from Spacecraft

A. High Resolution Scenes - Daylight

Radiance values seen at the LEST are made up of two components, one (L_t) from reflections off the target surface, the other (L_p) from the path radiance. The latter is itself composed of two parts, the backscattered sky radiance (L_s) and the ground radiance (L_g), forward scattered after reflections from the background surrounding the target.

TABLE IV-3. APPLICATIONS REQUIRING MULTISPECTRAL OBSERVATION THROUGHOUT THE DAY

Application	Test Site Location		Times		Solar Zenith (deg.)	S/C Zenith (deg.)
	Lat. (deg.)	Long. (deg.)	Day	Time		
2. Estuaries	39°N	75°W	6/22	1200	15.5°	52°
			12/22	0900	75.3°	52°
6. Fishing Areas	30.25°N	88.5°W	6/22	1200	6.75°	37.5°
			4/22	1500	47.8°	37.5°
12. Oil Pollution	29.75°N	95°W	6/22	1200	6.25°	35.1°
			12/22	0900	68.6°	35.1°
18. Thematic Mapping	38.6°N	76°W	6/22	1200	15.1°	51.2°
			1/22	0900	68.1°	51.2°

TABLE IV-4. SPECTRAL BANDS OF INTEREST FOR DIURNAL VARIATION OBSERVATIONS

Spectral Bands (μm.) / Applications	.42-.46	.47-.52	.53-.57	.56-.60	.60-.65	.65-.69	.70-.73	.78-.82	.89-.95
Estuaries	X	X	X	X	X	X	X		
Fishing Areas	X	X	X	X	X	X	X		
Oil Pollution		X	X	X		X			
Thematic Mapping	X	X	X	X	X	X	X	X	X

Each of these radiances is separately calculated. E.g., target radiance is:

$$L_t = H_s(\lambda)\ e^{-m\tau\lambda} \left(\frac{1}{\cos\ \theta_z} + \frac{1}{\cos\ \theta_s} \right) \cos\ \theta_z\ \rho(\lambda) \qquad (1)$$

where: $H_s(\lambda)$ = radiance outside the atmosphere in a small band around λ in $\mu w/cm^2$-ster-μ

m = vertical optical thickness thru atmosphere

τ_λ = extinction optical air mass at wavelength λ

θ_z = solar zenith angle from target

θ_s = spacecraft zenith angle from target

$\rho(\lambda)$ = target reflectance at wavelength λ

The values for $H_s(\lambda)$ and τ_λ are taken from the Handbook of Geophysics and Space Environments (Reference 4), while other parameters appeared in Tables IV-1 and IV-2. L_t is computed over 0.05μ intervals from 0.55 to 0.8μ and summed over appropriate intervals. Generally, the interval of interest for this application is accepted as 0.55 - 0.7μ. However, 0.7 - 0.8μ would offer better contrast for vegetation vs water.

For path radiance, $$L_p = L_s + L_g. \qquad (2)$$

L_s is dependent only on wavelength, target altitude, and the solar and spacecraft zenith angles. The ERIM atmosphere computer model was used to generate L_s for zero spacecraft zenith angle at sea level. For higher altitudes (i.e., for clouds), we have made a first order approximation of L_s by multiplying the sea level value by the optical thickness from Table IV-2.

L_s for non-zero angles would be slightly smaller, but the computer was not set up for such computations. We will use the zero zenith values of L_s in our analyses. L_g for the same conditions (i.e., vertical viewing) can be shown from outputs of ERIM (Reference 5) to be linearly dependent on L_t if we assume that the target and background have the same reflectances. ERIM outputs showed that G, the ratio of L_g to L_t, was linearly dependent on background reflectance and independent of solar zenith angle. G, under these conditions, is dependent on wavelength and is shown in Figure IV-1. We shall assume G is independent of spacecraft zenith angle also. If we assume we are interested in measuring boundaries of a target of reflectance ρ_1 against a background of reflectance ρ_2, then:

$$L_g(\lambda) = \tfrac{1}{2} \left(L_g\ (\lambda,\ \rho_1) + L_g\ (\lambda,\ \rho_2)\right)$$

$$= \tfrac{1}{2}\ G_\lambda\ \left(L_t\ (\lambda,\ \rho_1) + L_t\ (\lambda,\ \rho_2)\right) \qquad (3)$$

where $L_t\ (\lambda,\ \rho_i)$ is the radiance at wavelength λ from a target of reflectance ρ_i sitting in a background of reflectance ρ_i. As was the case for L_t, L_s and L_g would each have to be summed over the appropriate wavelength intervals.

B. Moonlight Observations

Since we are using the same elevation angles and some of the same scenes for our moonlight observations that we did for the high resolution sunlight observations, we will generate the appropriate radiances by using sun-moon conversion factors on the corresponding sunlight radiances. These factors were not available to us directly in any known source, but they were derivable using the following procedure:

Let $H_s(\lambda)$ = the radiance at the top of the atmosphere from sunlight over a small band centered at λ.

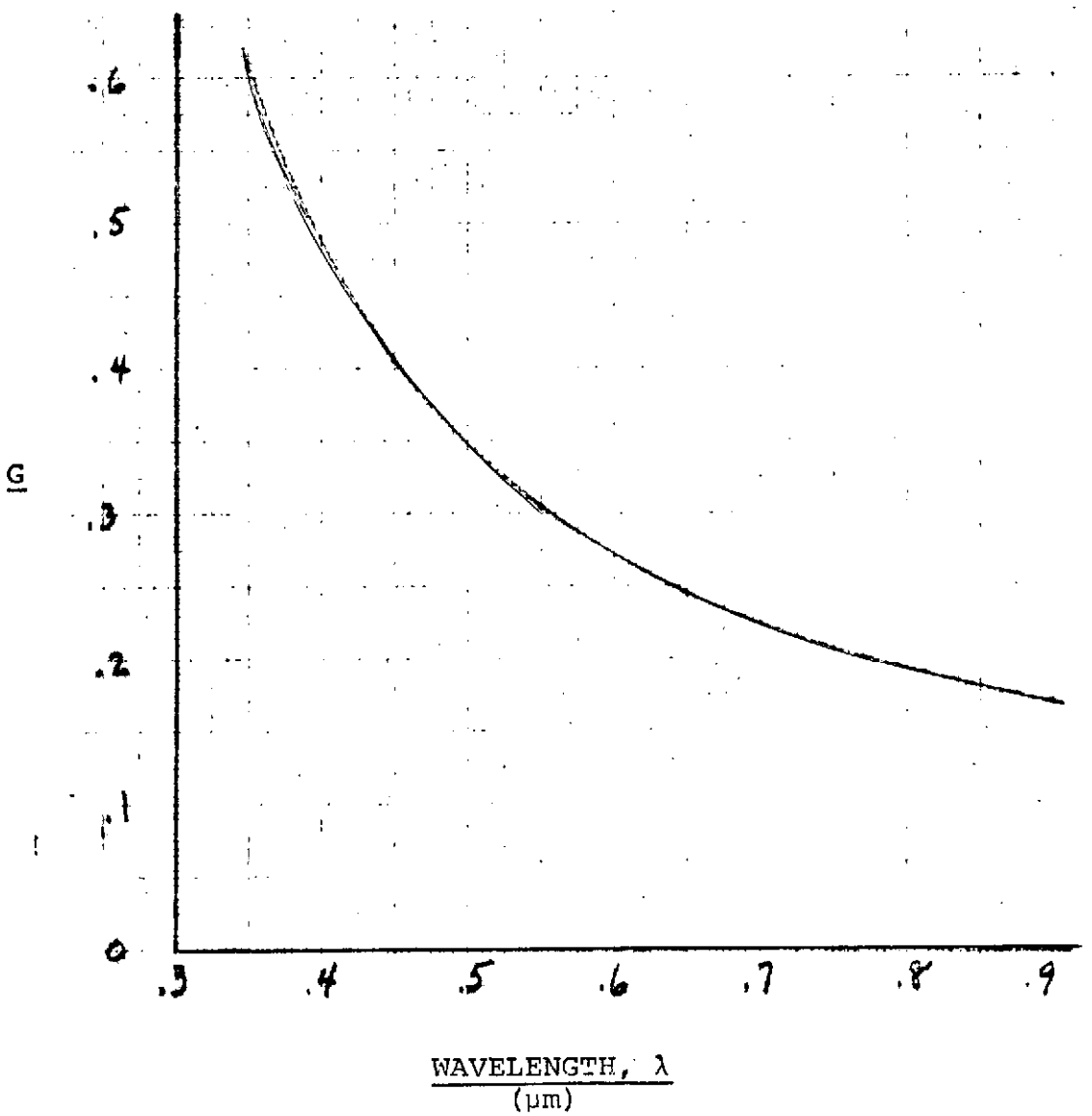

Figure IV-1. Variation of Ratio (G) of Forward Scattered Background Radiance to Target Radiance at Different Wavelengths (λ) for the Same Target and Background Reflectances

$H_m(\lambda)$ = the radiance at the top of the atmosphere from full moonlight over a small band centered at λ.

$$R(\lambda) = \frac{H_m(\lambda)}{H_s(\lambda)} \tag{4}$$

The $R(\lambda)$'s are the conversion factors we want to derive.

To determine $H_m(\lambda)$, we note that the illuminance, I_m, provided at sea level thru a standard clear atmosphere from the moon at zenith is 0.267 lumens/meter^2 (Reference 6). But:

$$I_m = \int_0^\infty K(\lambda)\ H_m(\lambda)\ T(\lambda)\ d\lambda \tag{5}$$

where: $K(\lambda)$ = luminosity in lumens/watt at wavelength λ (Figure IV-2, taken from Reference 6)

$T(\lambda) = e^{-\tau(\lambda)}$, where $\tau(\lambda)$ is the extinction optical thickness (see Reference 4) (6)

For small $\Delta\lambda$, say 0.05μ, equation (5) can be approximated by:

$$I_m \approx \sum_{i=0}^{6} K(.425+.05i)\ H_m(.425+.05i)\ T(.425+.05i)\ X\ .05 \tag{7}$$

since $T(\lambda)$ is essentially zero outside the interval (.4 - .75μ).

Figure IV-3 (from Reference 7) gives us a relative spectral distribution $E(\lambda)$ of emittance from the moon. If $H_{m,\ max}$ is the maximum value of $H_m(\lambda)$ averaged over an interval of length $\Delta\lambda$, then:

$$H_m(\lambda) = H_{m,\ max}\ E(\lambda) \tag{8}$$

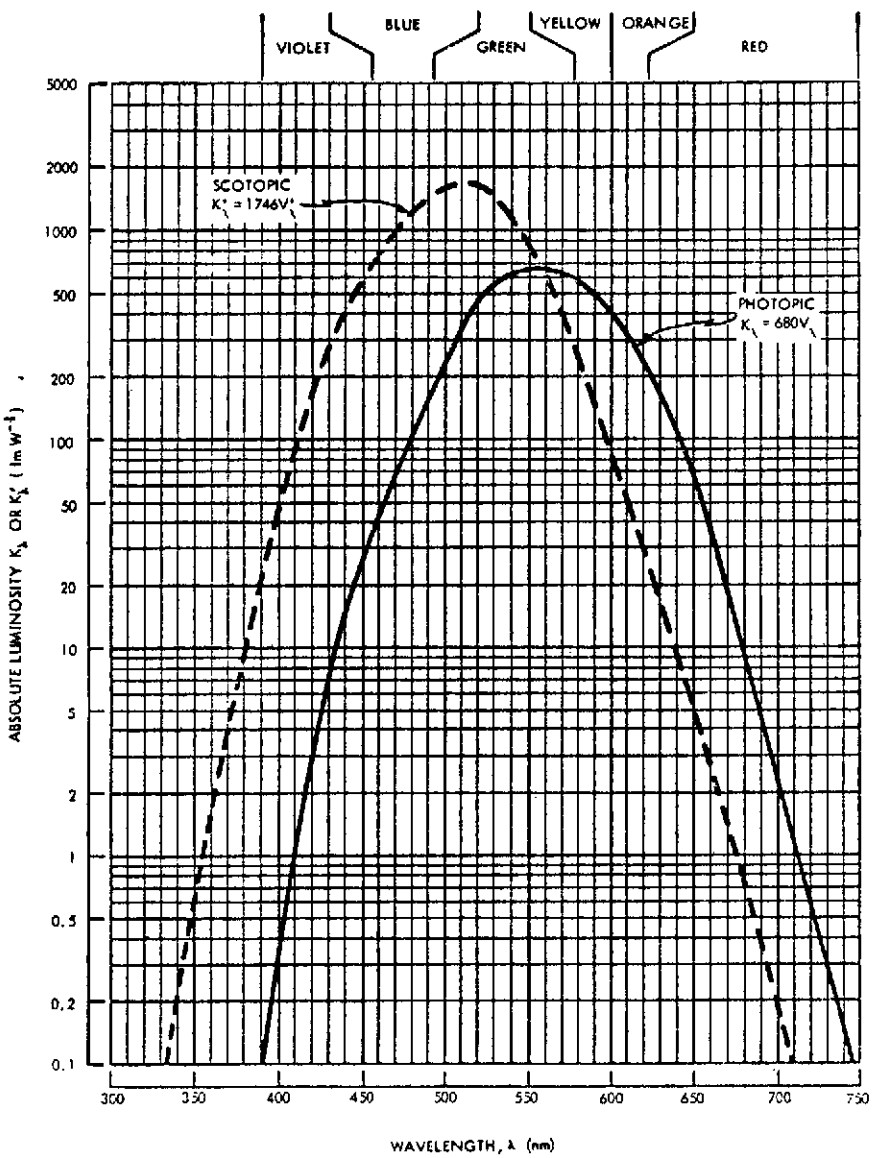

Figure IV-2. Absolute Luminosity Curves K_λ and K'_λ, as Functions of Wavelength (Response of the Human Eye to Radiation of a Given Wavelength).

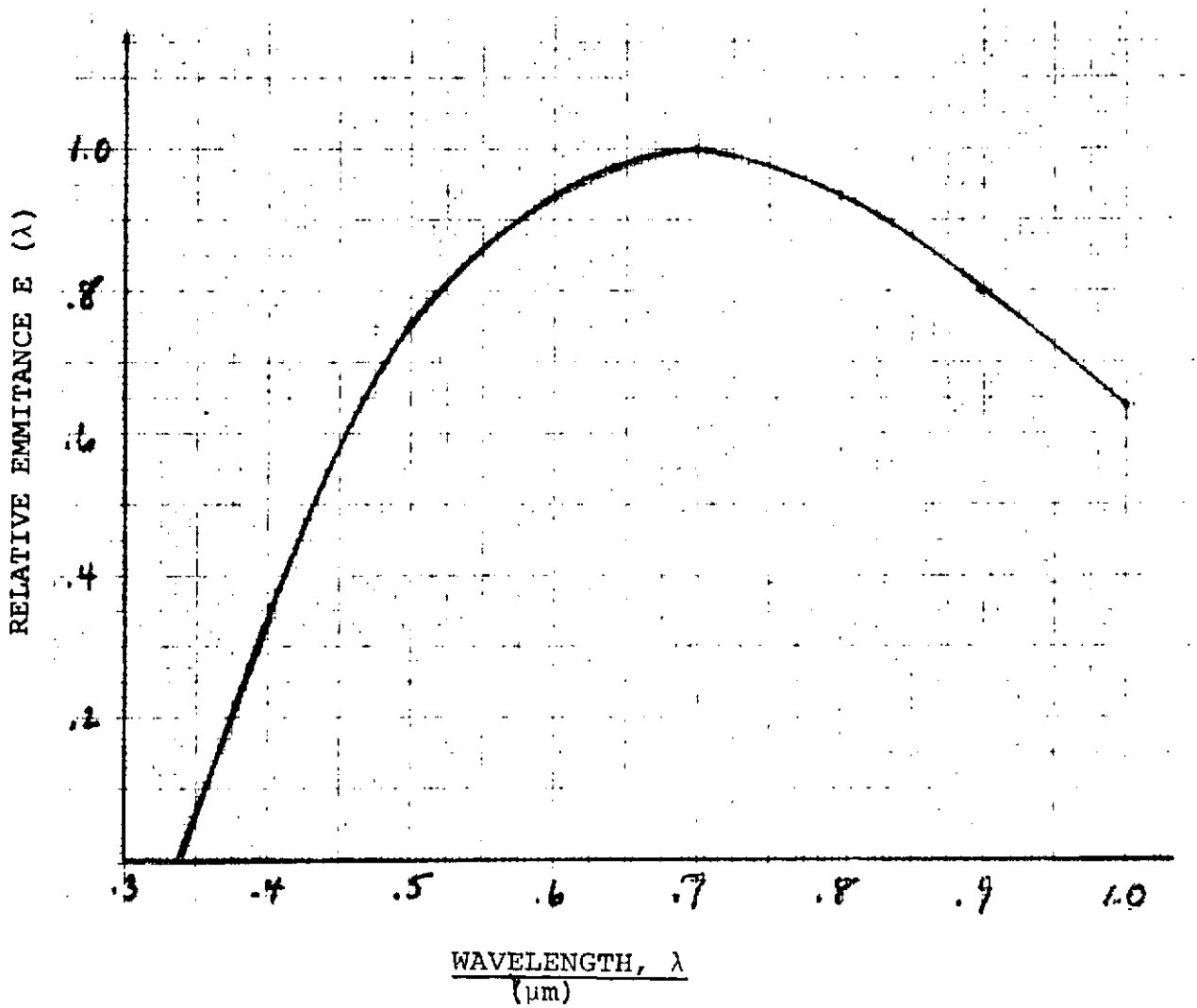

Figure IV-3. Relative Emittance of the Moon vs. Wavelength

Therefore:

$$H_{m,\,max} \simeq \frac{I_m}{\sum_{i=0}^{6} K(.425+.05i)\; E\;(.425+.05i)\; T(.425+.05i)\; X\; .05} \qquad (9)$$

from which $H_m(\lambda)$ can be determined.

Values of $H_s(\lambda)$ are available in Reference 4. However, the atmosphere for which those values were determined is not specifically defined. Hence, for consistency we used the same procedure to determine $H_s(\lambda)$ that we did for $H_m(\lambda)$ above. In this case also, we obtained I_s at sea level from Reference 6. Its value is 1.24×10^5 lumens/meter^2.

From $H_s(\lambda)$ and $H_m(\lambda)$ we get $R(\lambda)$ as shown in Table IV-5.

For each scene and wavelength of interest for moonlight observations, we then compute new radiance values $L_m(\lambda)$ from $L_s(\lambda)$ for the sun by

$$L_m(\lambda) = L_s(\lambda)\; R(\lambda) \qquad (10)$$

For observations of moonlit scenes, the radiances seen from the spacecraft will be quite low. With a frame camera, these low light levels are overcome by increasing the exposure time to increase the energy on the camera target. However, as noted in Chapter III, there are limits to the exposure time. Hence, another way to increase the energy could also be considered - widening the spectral band of observation. If this is done, however, there may be a decrease in contrast between the target and the background. A trade-off was made between these two effects of increasing the band in order to determine the correct size of the band for each application. The tradeoff results are given in Paragraph V-3-B.

C. Low-Light Multispectral Applications

The radiance values for these scenes are obtained as outputs from the ERIM computer simulation for the zenith angles specified in IV-2-C. Larger zenith angles are obtained by extrapolation.

TABLE IV-5. $R(\lambda)$ - CONVERSION FACTOR BETWEEN RADIANCE FROM SUN AND RADIANCE FROM FULL MOON AT SAME ZENITH ANGLE

Spectral Band (μm)	$R(\lambda)$ (10^{-6})
.35 - .4	.723
.4 - .45	1.17
.45 - .5	1.50
.5 - .55	1.91
.55 - .6	2.26
.6 - .65	2.64
.65 - .7	3.01
.7 - .75	3.40
.75 - .8	3.55

4. Radiance Tabulations

A. High Resolution Scenes - Daylight

As noted in Section 3-A above, the total radiance from any element in a scene is made up of a target radiance, L_t, a forward-scattered ground radiance, L_g, and a back-scattered sky radiance, L_s. For the scenes of interest, Equations (1) and (3) of Section 3-A were used to compute L_t and L_g for intervals of 0.05 microns from 0.35 to 0.75 microns. L_s for various wavelengths was computed by ERIM using their atmospheric model (Reference 5) for the zenith angles noted in Table IV-1. Figure IV-4 gives the results of ERIM's computations.

Total radiances for the high resolution, daylight scenes were computed only for the band from 0.55μm to 0.70μm since adequate highlight illumination is available in this band for the scenes of interest even for large zenith angles. In addition, the contrast is better if we cut off the lower end of the band at 0.55μm. Table IV-6 gives the total radiances for the observables in the scenes. Note that these values differ somewhat from scene to scene depending upon the background element. This is due to the forward scattered radiance from the ground, L_g. For high cumulus clouds, we assumed that L_g was negligible because of the altitude of the clouds. Hence, in this case only one set of radiances is given.

B. Moonlight Observations

Total radiances for moonlight observations were computed for intervals of 0.05 microns from 0.35 to 0.70 microns by obtaining corresponding data for sunlight at the same zenith angle and then converting to full moon using Equation (4) and Table IV-5 of Section IV-3-B. Full moon to partial moon conversions were then obtained using ratios in Table IV-7.

Since the total radiances under moonlight conditions were quite low,

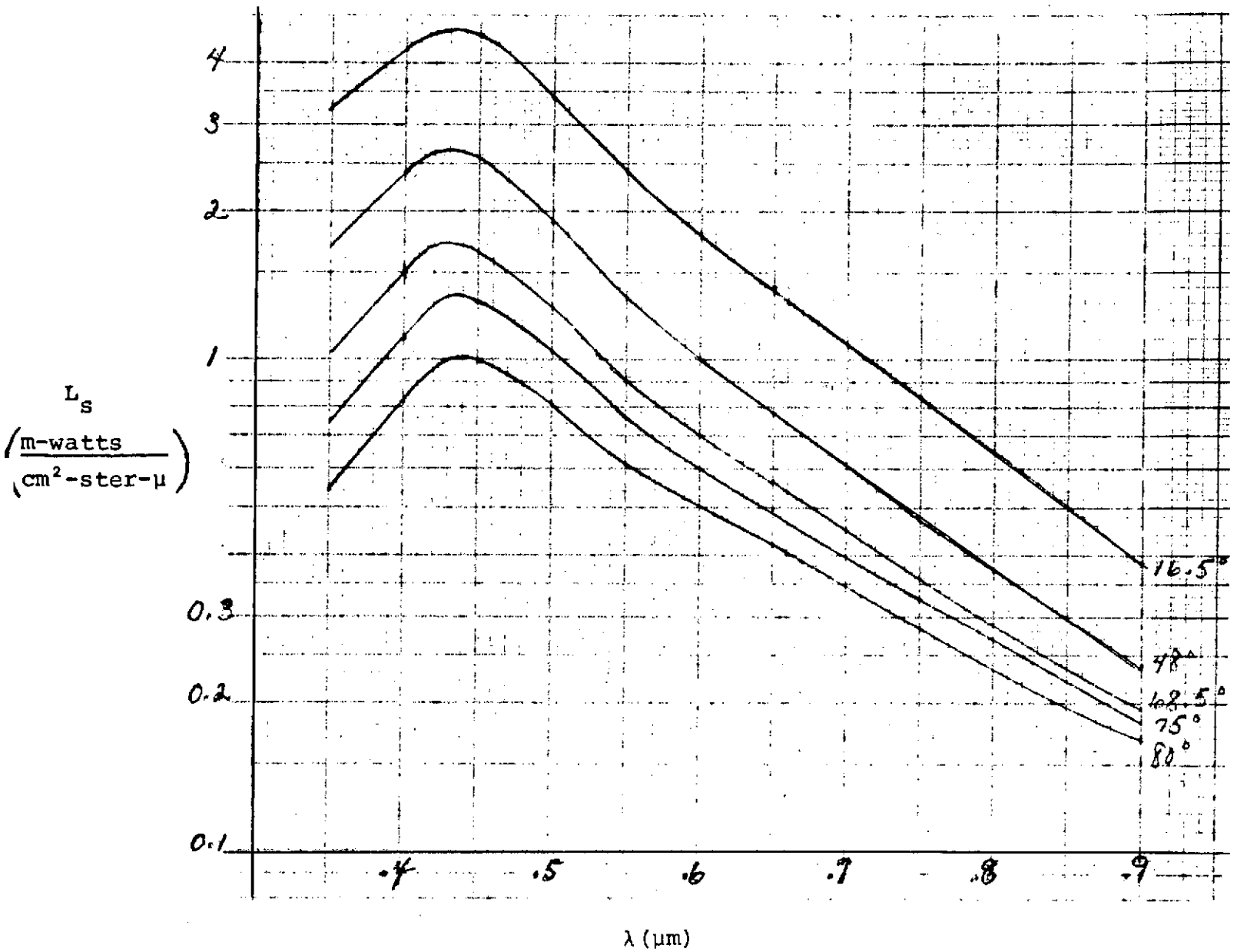

Figure IV-4. Back-Scattered Sky Radiance, L_s, for Various Zenith Angles

TABLE IV-6. TOTAL RADIANCES FOR HIGH RESOLUTION, DAYLIGHT SCENE OBSERVABLES FOR THE 0.55 - 0.70μm BAND

Observable	Background	Radiances (mwatts/cm^2-π ster) 16.5°	48°	68.5°	75.5°	80°
High Cumulus	All	16.64	11.15	5.54	3.43	2.07
Low Stratus	Water	9.63	5.98	2.56	1.39	.722
	Vegetation	9.90	6.09	2.60	1.41	.730
	Soil		6.23	2.66	1.44	.740
Water	High Cumulus	1.59	.921	.498	.355	.256
	Low Stratus	2.53	1.51	.740	.478	.313
	Vegetation	1.66	1.02	.538	.375	.264
Vegetation	High Cumulus	3.22	1.93	.888	.547	.328
	Low Stratus	3.99	2.42	1.09	.651	.378
	Water	3.05	1.83	.848	.537	.320
Soil	High Cumulus		3.34	1.44	.819	.429
	Low Stratus		3.68	1.59	.892	.469
	Snow		3.71	1.58		
Snow	Soil		6.50	2.66		

TABLE IV-7. RATIOS OF RADIANCES, PARTIAL MOON-TO-FULL MOON

Moon Fraction Visible	Radiance Ratios
Full Moon	1
2/3 Moon	.28
1/2 Moon	.12
1/3 Moon	.032

computations were made for spectral bands of several different widths. The wider the band, the greater the radiance, but also, the lower the contrast (especially if the band is made wider by extending into the blue). Table IV-8 gives the radiances for full moon only for five bandwidths and five zenith angles.

C. Low-Light Multispectral Applications

Total radiances for these applications were determined by ERIM as part of their SEOS earth resources applications study (References 2 and 3). The results of these computations are given in Table IV-9.

Only two zenith angles are shown for each application. For poorer (i.e., larger) zenith angles, a rough extrapolation can be obtained by using data available from intermediate steps of the high resolution and moonlight cases of Sections IV-4-A and B. The earth resources applications all deal with either water problems or thematic mapping. The latter is reasonably well approximated by vegetation. Both water and vegetation data were computed for zenith angles as bad as 80° for the previous two applications. As can be seen from Table IV-9, the lowest radiances are in bands .65 - .69μm and .7 - .73μm for the water applications and band .60 - .65μm for thematic mapping. Figure IV-5 gives the total radiances in 0.05μm bands centered at .675μm and .725μm for water and at .625μm for vegetation plotted against zenith angle. By fitting the shape of these curves to the two points given by ERIM for each application, one could roughly extrapolate total radiance data to larger zenith angles. We have neglected small differences in spacecraft zenith angles arising from different target locations within the U. S. The results of this extrapolation are given in Section V-3-B where exposure times for the given zenith angles are presented and then the times for the larger zenith angles are estimated.

TABLE IV-8. TOTAL RADIANCES, FULL MOONLIGHT SCENES (10^{-6} MWATTS/CM^2-π STER)

ZENITH ANGLE		16.5°					48°				
SPECTRAL BAND		.35-.7	.4-.7	.45-.7	.5-.7	.55-.7	.35-.7	.4-.7	.45-.7	.5-.7	.55-.7
OBSERVABLE	BACKGROUND										
High Cumulus	All	72.7	70.6	64.5	55.1	43.6	48.3	47.0	43.0	36.8	29.2
Water	High Cumulus	8.41	7.93	6.87	5.52	4.14	4.84	4.57	3.97	3.21	2.42
Vegetation	High Cumulus	13.7	13.2	12.1	10.5	8.50	8.07	7.82	7.19	6.28	5.12
Soil	High Cumulus						13.4	13.1	12.2	10.8	8.85
Low Cumulus	Water	41.3	40.3	37.1	31.8	25.3	25.2	24.6	22.8	19.7	15.7
Low Cumulus	Vegetation	41.9	40.9	37.6	32.3	25.7	25.2	25.0	23.1	20.0	16.0
Low Cumulus	Soil						26.1	25.6	23.7	20.5	16.4
Water	Low Cumulus	12.8	12.2	10.7	8.70	6.58	7.41	7.08	6.24	5.10	3.86
Vegetation	Low Cumulus	17.5	16.9	15.4	13.2	10.5	10.4	10.1	9.22	7.95	6.38
Soil	Low Cumulus						15.2	14.8	13.7	12.0	9.73
ZENITH ANGLE		68.5°					75.5°				
High Cumulus	All	23.7	23.0	21.2	18.2	14.5	14.3	14.0	13.0	11.2	9.00
Water	High Cumulus	2.63	2.44	2.15	1.73	1.30	1.90	1.79	1.54	1.24	.925
Vegetation	High Cumulus	3.91	3.77	3.39	2.92	2.35	2.50	2.39	2.14	1.82	1.44
Soil	High Cumulus	5.89	5.73	5.31	4.66	3.82	3.44	3.33	3.05	2.67	2.18
Low Cumulus	Water	10.5	10.3	9.61	8.36	6.75	5.67	5.56	5.18	4.53	3.67
Low Cumulus	Vegetation	10.6	10.5	9.74	8.49	6.85	5.73	5.62	5.24	4.59	3.73
Low Cumulus	Soil	10.9	10.7	9.94	8.67	7.00	5.85	5.73	5.35	4.69	3.81
Water	Low Cumulus	3.67	3.51	3.10	2.53	1.93	2.40	2.29	2.01	1.64	1.25
Vegetation	Low Cumulus	4.78	4.62	4.20	3.60	2.88	2.94	2.83	2.54	2.16	1.72
Soil	Low Cumulus	6.58	6.40	5.92	5.16	4.20	3.76	3.65	3.35	2.92	2.37
ZENITH ANGLE		80°									
High Cumulus	All	8.47	8.33	7.75	6.76	5.45					
Water	High Cumulus	1.38	1.31	1.12	.897	.666					
Vegetation	High Cumulus	1.61	1.53	1.35	1.12	.863					
Soil	High Cumulus	1.96	1.89	1.69	1.44	1.14					
Low Cumulus	Water	2.97	2.90	2.69	2.35	1.91					
Low Cumulus	Vegetation	3.00	2.92	2.72	2.38	1.93					
Low Cumulus	Soil	3.03	2.96	2.75	2.41	1.96					
Water	Low Cumulus	1.60	1.52	1.33	1.08	.817					
Vegatation	Low Cumulus	1.81	1.73	1.54	1.28	.995					
Soil	Low Cumulus	2.12	2.04	1.84	1.57	1.24					

TABLE IV-9. ERIM RADIANCE LEVELS IN μWATTS/CM^2-π STER FOR EARTH RESOURCES APPLICATIONS

Application \ Spectral Band (μm)	.42-.46	.47-.52	.53-.57	.56-.6	.6-.65	.65-.69	.7-.73	.78-.82	.89-.95
Estuaries @ 15.5° Sun Angle									
Total Radiance	804	1875	697	829	144	314	135		
Path Radiance	656	1444	446	565	119	182	101		
Needed Detect. Change	18.5	48	27.9	29	12.6	25.4	17.3		
@ 75.3°									
T. R.	173	339	138	166	28	63	25		
P. R.	144	261	88	82	22	38	19		
N. D. C.	3.5	8.8	5.7	6.0	3.1	4.7	3.1		
Fish Areas @ 6.75°									
T. R.	804	1670	669	776	129	314	122		
P. R.	606	1112	336	424	88	138	75		
N. D. C.	25	62	37	39	20.4	33.9	23.6		
@ 48°									
T. R.	217	455	468	622	91	182	85		
P. R.	163	301	236	339	63	97	53		
N. D. C.	6.6	17	25.7	31.4	14.1	18.2	15.7		
Oil Pollution @ 6.25°									
T. R.		1859	707	816		477			
P. R.		1112	336	424		138			
N. D. C.		125	74	78.5		68			
@ 68°									
T. R.		336	144	163		97.3			
P. R.		201	69.1	84.8		28.3			
N. D. C.		22.6	15.1	15.7		13.8			
Thematic Mapping @ 15°									
T. R.	1178	2304	1002	1448	433	1203	807	1652	2622
P. R.	807	1444	446	565	119	182	101	63	628
N. D. C.	37.1	57.5	55.6	58.7	15.7	25.4	35.2	19.8	49.9
@ 68°									
T. R.	267	524	251	433	107	301	201	440	656
P. R.	182	330	113	170	28.3	47	25	15.7	157
N. D. C.	8.5	12.9	13.8	17.6	4.1	6.3	8.8	5.3	12.6

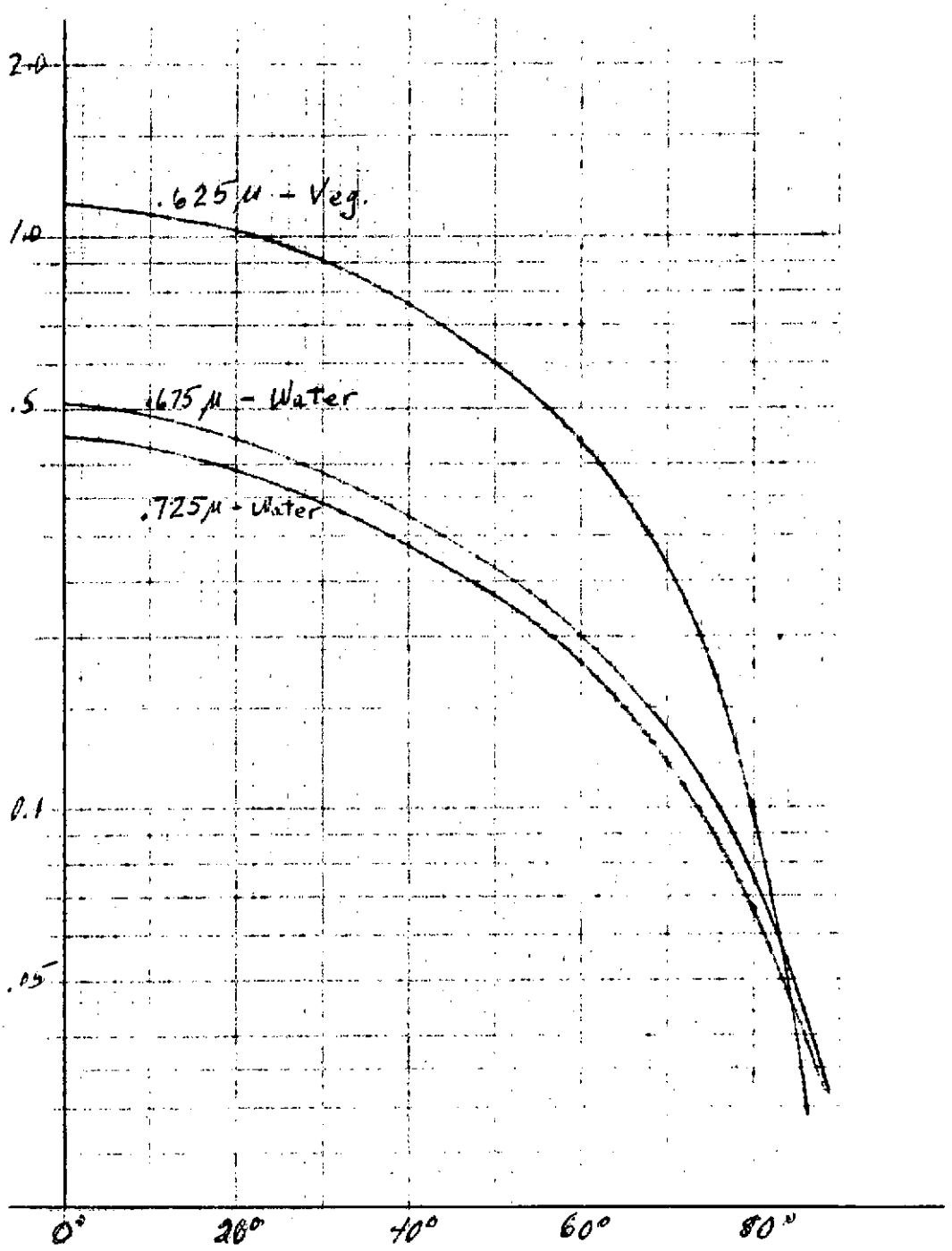

Figure IV-5. Variation of Total Radiance in 0.05μm Wide Bands

References

1. Selection of the Optimum Filter-Detector Combination for Cloud Observations from a High Altitude, Capt. S. Pilipowsky, 1968 Air Force Study Report (Internal Memorandum).

2. Earth Resources Applications of the Synchronous Earth Observatory Satellite (SEOS), D. S. Lowe, J. J. Cook, et al, Environmental Research Institute of Michigan, NASA CR-ERIM 103500-1-F, December 1973.

3. Handout for Discussion of Preliminary SEOS Results, ERIM, May 24, 1974, and Corrections to Radiance Calculations, Received from ERIM, June-August, 1974.

4. Handbook of Geophysics and Space Environments, S. L. Valley, Air Force Cambridge Research Laboratories, McGraw-Hill, 1965.

5. The Effects of Scattered Light on the Ability to Distinguish Target Radiance at a Synchronous Satellite Above the Earth, G. C. Goldman, ERIM, Contract 9510-A-0002.

6. Electro-Optics Handbook, RCA, Commercial Engineering, 1968.

7. Spectral Distribution of Night Illumination, J. Johnson, Engineering Research and Development Laboratory, Ft. Belvoir.

V. PERFORMANCE ANALYSIS

1. Introduction

This section is concerned with the analysis of performance and operating conditions for three candidate sensors. These candidates are desired for three generally different applications:

1. High resolution daylight pictures in one spectral band.

2. Primarily nighttime operation at medium resolution in a single spectral band.

3. Multi-spectral picture-taking at medium resolution over a substantial portion of daylight hours.

The sensors analyzed for these three applications were the 2-inch RBV with an ASOS surface for the first; a 40 mm SIT with a conventional S-20 for the second; and a 1-inch silicon vidicon for the multi-spectral application. Additionally, an SEC sensor was considered as a possible alternate for nighttime picture-taking.

The data presented in this section covers three areas of computation:

1. Coverage and resolution performance.

2. Exposure times as related to scene radiance computations in Section IV.

3. Camera operational rates and cycle times.

2. Coverage and Resolution Performance

A. High Resolution Daylight Camera

The 2-inch RBV has an available picture format of 25.4- by -25.4 mm. For a desired coverage of 150-by-150 km at nadir, the LEST (including correcting optics) focal length (F.L.) is:

$$\text{F.L.} = \text{Picture Width} \times \frac{\text{Orbit Altitude}}{\text{Ground Frame Width}}$$

$$= 2.54 \times \frac{35{,}770}{150} = 605.7 \text{ cm},$$

at synchronous altitude. For the assumed LEST of this focal length having a 1.5 meter aperture, the f number is given by

$$\text{f/no} = \frac{6.057}{1.5} \cong \text{f/4}$$

The field-of-view for the 150 km width of coverage is

$$\theta = \text{Tan}^{-1} \frac{150}{35{,}770} = 0.24°$$

Note that this angular view will result in ground coverage at nadir slightly larger than 150 km due to earth's curvature; at mid-continent the coverage is substantially greater. The finest resolvable ground element will depend on the scene contrast and consequent camera resolving power, but will be in the range of 37 to 49 meters per TV line. From synchronous altitude this corresponds to about 1 micro-radian for the IFOV of radiometer terminology.

The process followed for resolving power computation is that devised for multispectral RBV cameras for ERTS[1] and again reported in the RBV Camera Study for ERS.[2] Briefly, the mechanism consists of computing the average squre wave response for a camera system for a given contrast (the modulation available curve), and determining its intercept with a computed modulation required curve. The latter curve is a function of the SNR of the camera, the slope of the camera transfer characteristic (γ), the camera amplifier and raster characteristics, the scene mean radiance, and an empirically derived resolving power criterion.

The average square wave response is computed from the RBV and test lens response, (shown for a square wave input in Figure V-1) and the assumed LEST response (Figure II-1). The amplifier response is assumed flat over the range of interest. The RBV and test lens square wave response was first converted to sine wave form by the relationship shown in Reference 1 (Equation A-16)

$$r(f) = \frac{\pi}{4}\,\hat{r}(f) + \frac{r(3f)}{3} - \frac{r(5f)}{5} + \ldots$$

where $\hat{r}(f)$ is the square wave response

$r(f)$ is the sine wave response, and

f is the spatial frequency of interest

The MTF of the test lens (Figure A-10 of Refereence 1) was extracted, and the sine wave response of the RBV thereby obtained.

---

1. Two-Inch Return-Beam Vidicon Camera System, Quarterly Report No. 3, Contract NAS 5-11621, January 19, 1970, Appendix A.
2. Return-Beam Vidicon Camera System for the ERS Operational Mission, Configuration and Performance Study Report, Contract NAS 5-21094, July 31, 1973, Pages V:30 - V:45.

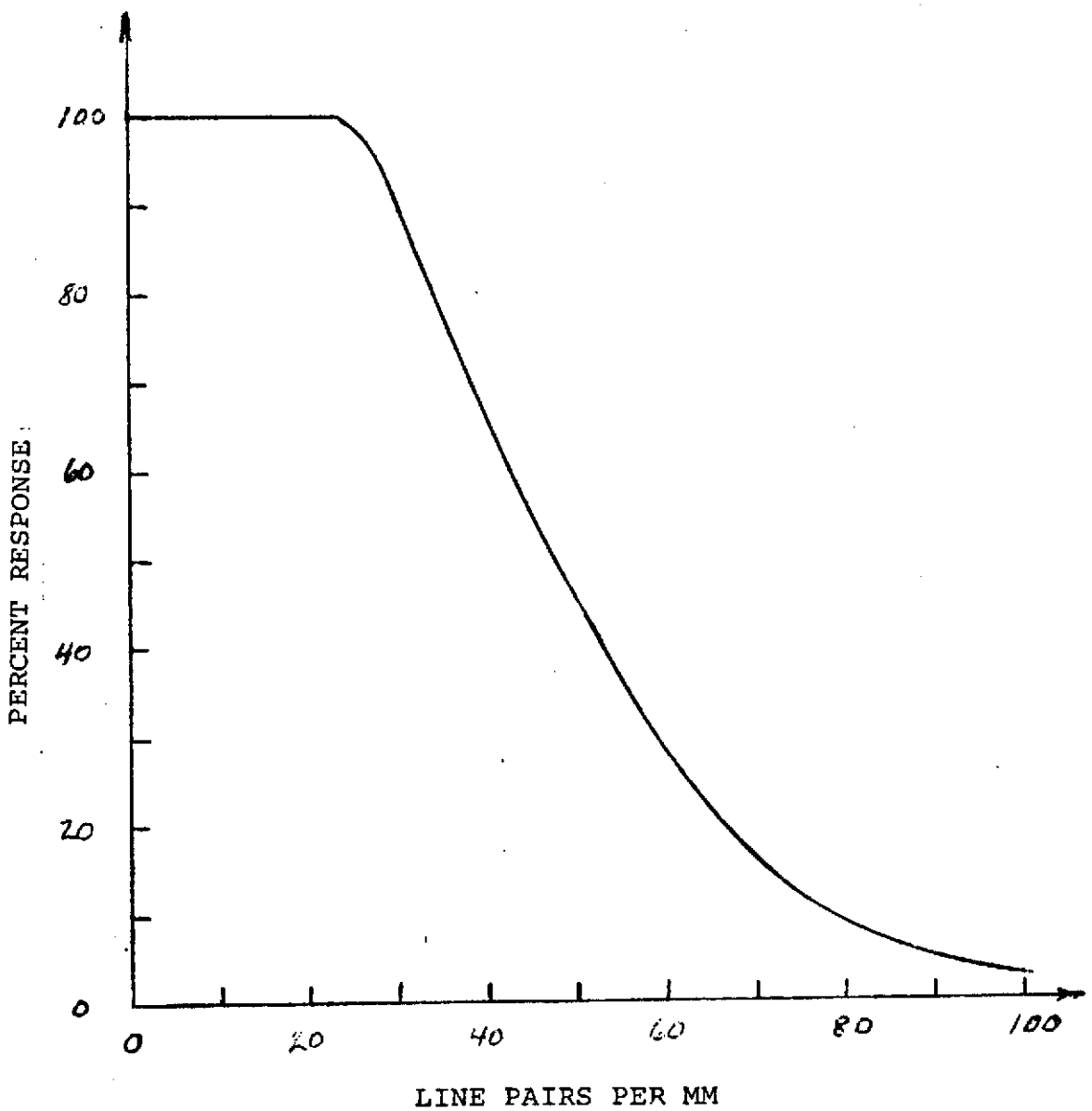

Figure V-1. Combined RBV and Test Lens Square Wave Response

The resultant sine wave response is shown in Figure V-2. The point-by-point product of this curve with the assumed LEST response shown in Figure II-1 yields the overall system sine wave response.

Next, this response was converted to a form representing response to a square wave target in order to utilize the empirically derived K factor. This factor was derived from numerous experiments with the Air Force tri-bar test target.[3] The conversion from sine wave form to average value of square wave response is accomplished via the method of Reference 1, by:

$$\bar{r}(f) = \frac{8}{\pi^2}\left[r(f) + \frac{r(3f)}{9} + \frac{r(5f)}{25}\right]$$

where: $\bar{r}(f)$ = Average value of square wave response

$r(f)$ = Sine wave response

The resultant modulation available curve is shown in Figure V-3 as the $C = \infty$ curve. This corresponds to maximum scene modulation (M) of unity. For lower values of contrast (C), the modulation is computed from,

$$M = \frac{C-1}{C+1}$$

and each point of the M=1 curve is reduced by the new modulation available factor. Also shown in Figure V-3 are the curves for modulation of .6, .5, .33, and .23 corresponding to contrast ratios of 4, 3, 2, and 1.6 respectively.

---

3. Schade, O. H., "An Evaluation of Photographic Image Quality and Resolving Power in Electron Imaging", Proceedings of the IRE, Vol. 48, P. 858, May 1960.

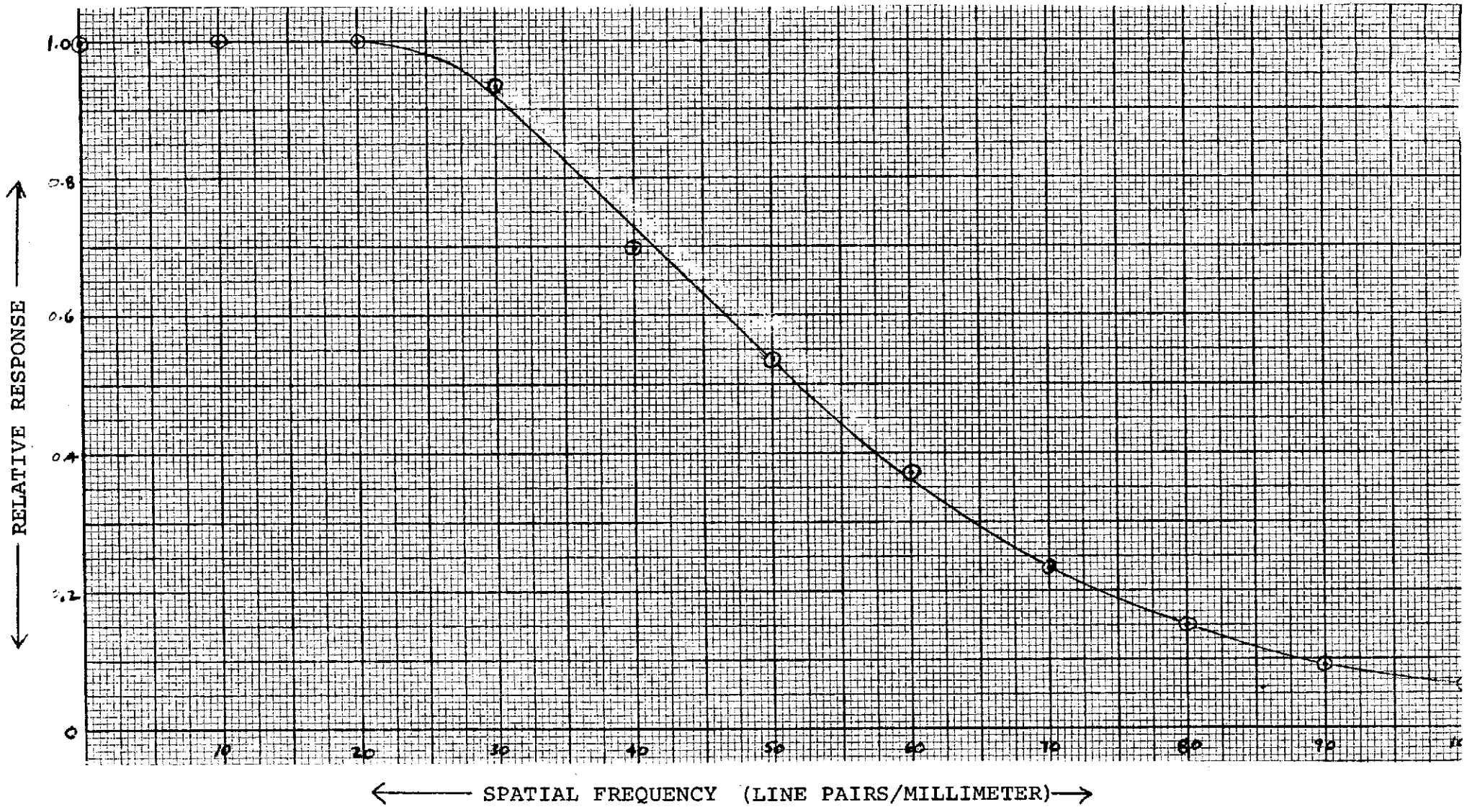

Figure V-2. RBV Sine Wave Response

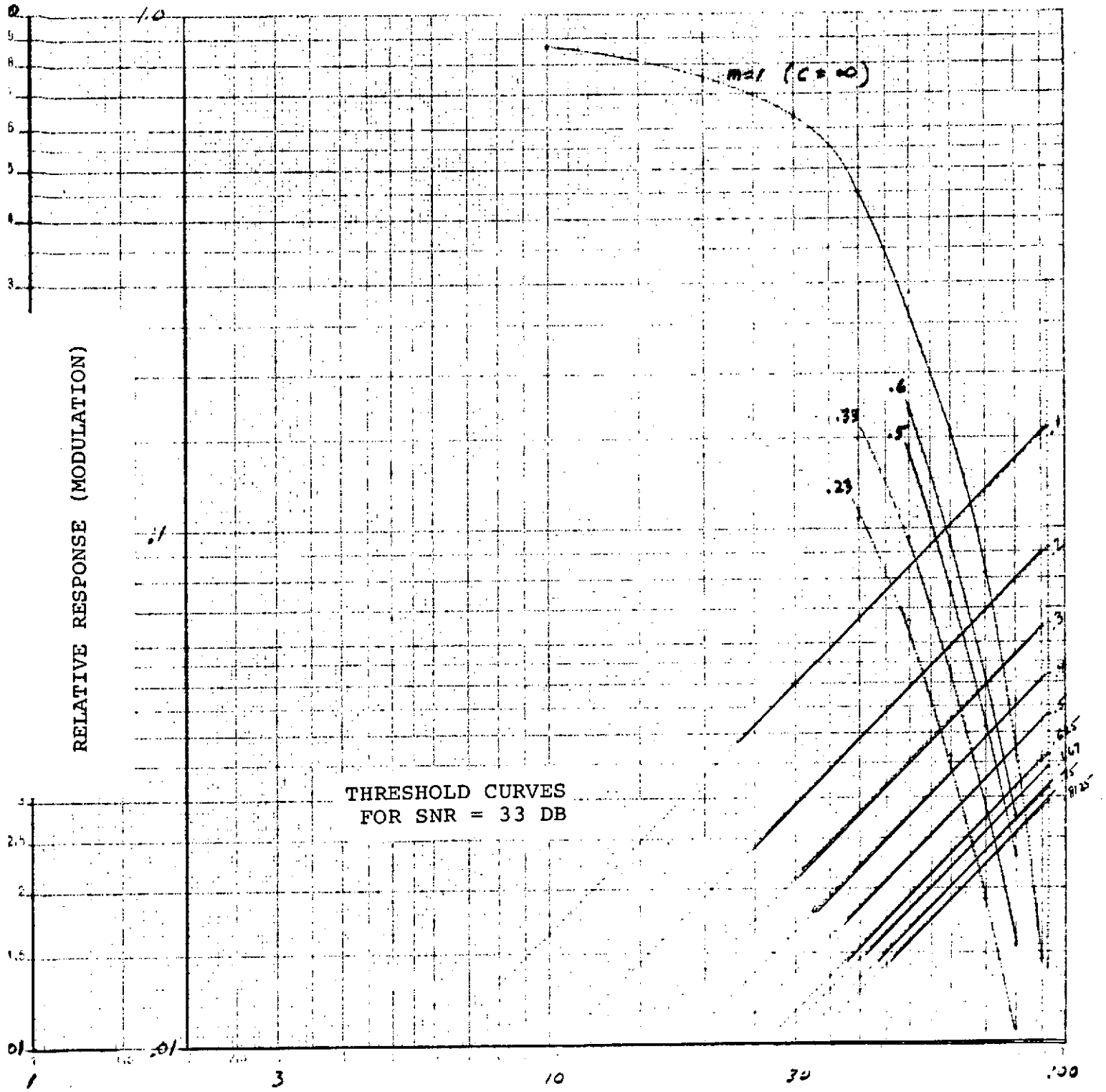

Figure V-3. High Resolution Camera Average Square Wave Response and Required Modulation

The modulation required curves shown on Figure V-3 are the 45 degrees straight line curves for an SNR of 33 dB (44.6:1), which were computed from Equation (A-34) of Reference 1:

$$M_o\,\bar{r}(f_r) = \frac{K}{\sqrt{5}}\left[\frac{1}{2\gamma\ SNR_{FS}}\left(\frac{E_{XFS}}{E_X}\right)^{\gamma}\ \sqrt{\frac{f_r\ F_A\ (f_r)}{f_n\ F_A\ (\infty)}}\right]$$

where: $M_o\,\bar{r}(f_r)$ = The product of the modulation and the average value of the square wave response.

f_r = The spatial frequency.

K = 4, the empirical constant, lying in the range 3.6 to 4.

E_{XFS} = Full scale exposure.

E_X = Mean Exposure

$F_A(f_r)$ = The amplifier response, assumed flat to f_r.

f_n = The Nyquist frequency of the raster (1/2 of the scan lines per mm).

$F_A(\infty)$ = Noise equivalent bandwidth of the amplifier.

The values associated with the modulation required curves, ranging from .8125 to .1, are the fraction of full scale exposure for each curve.

The value of γ used in this computation was obtained from measurements on actual RBV cameras. A typical RBV camera transfer characteristic is shown in Figure V-4. Note that the transfer

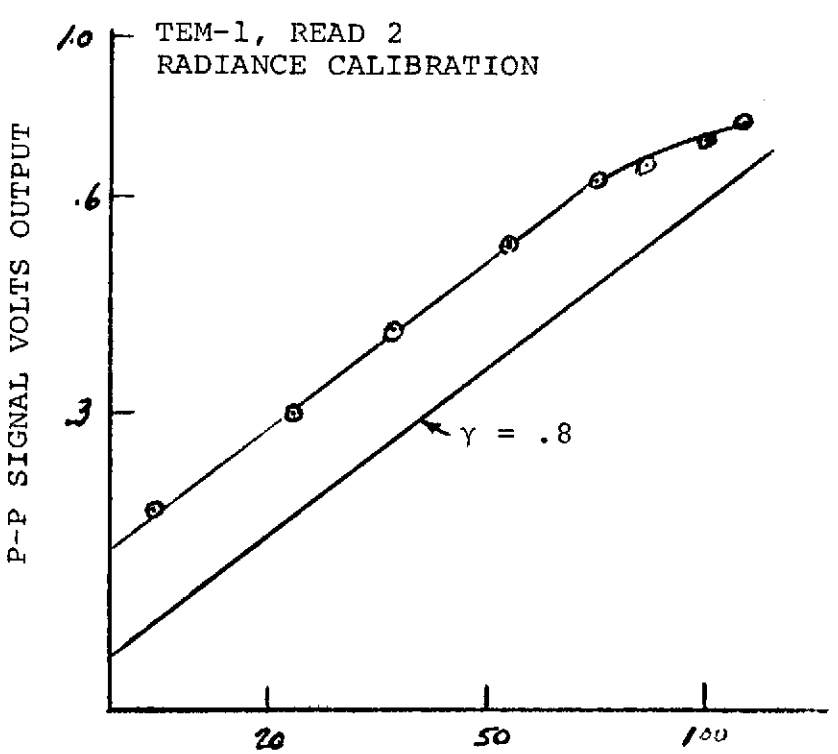

$$\frac{V_{OUT\ 2}}{V_{OUT\ 1}} = \left[\frac{\text{EXPOSURE 2}}{\text{EXPOSURE 1}}\right]^{\gamma}$$

$$\gamma = \text{LOG } 6$$
$$= .78$$

Figure V-4. RBV Light Transfer Characteristic From Camera Radiance Calibration Measurements

characteristic for this camera is relatively constant up to about 90 percent full scale radiance. For the computation performed here γ was assumed constant at 0.8. Somewhat higher resolving power results from lower gamma, especially for low contrast, high mean radiance conditions.

The number of scan lines required for full resolution is assumed, generally, to be somewhat in excess of the number of resolution elements. Numerically, the value should be in the range of 1.05 to 1.5 times the resolution elements (the Kell factor) depending on the sensor resolution capability and the desired system resolution. For this camera 4750 active scan lines are assumed corresponding to a Nyquist frequency of 93.5 lp/mm.

The amplifier response is assumed flat over the range of interest, 3.25 MHz for the computations. The noise bandwidth was equal to this value which is approximated by the use of a sharp cut-off filter. Both values are wider than required by the resulting system resolving power, but do not influence the numerical result.

The resolving power curves, generated from the family of intersecting points for a particular modulation available curve, are shown in Figure V-5. Note that the highest mean radiance point increases as the scene contrast decreases. This results from an assumed fixed peak highlight exposure setting of the camera. Clearly, for a high contrast ($C = \infty$) target, the mean radiance cannot exceed 50% of the peak. However, for conditions of contrast approaching zero, the mean radiance may approach the peak radiance without camera overload.

The abscissa of Figure V-5 is given for packing density on the sensor, as well as nadir ground resolution, since the former will vary much more slowly with earth look angle. The variation

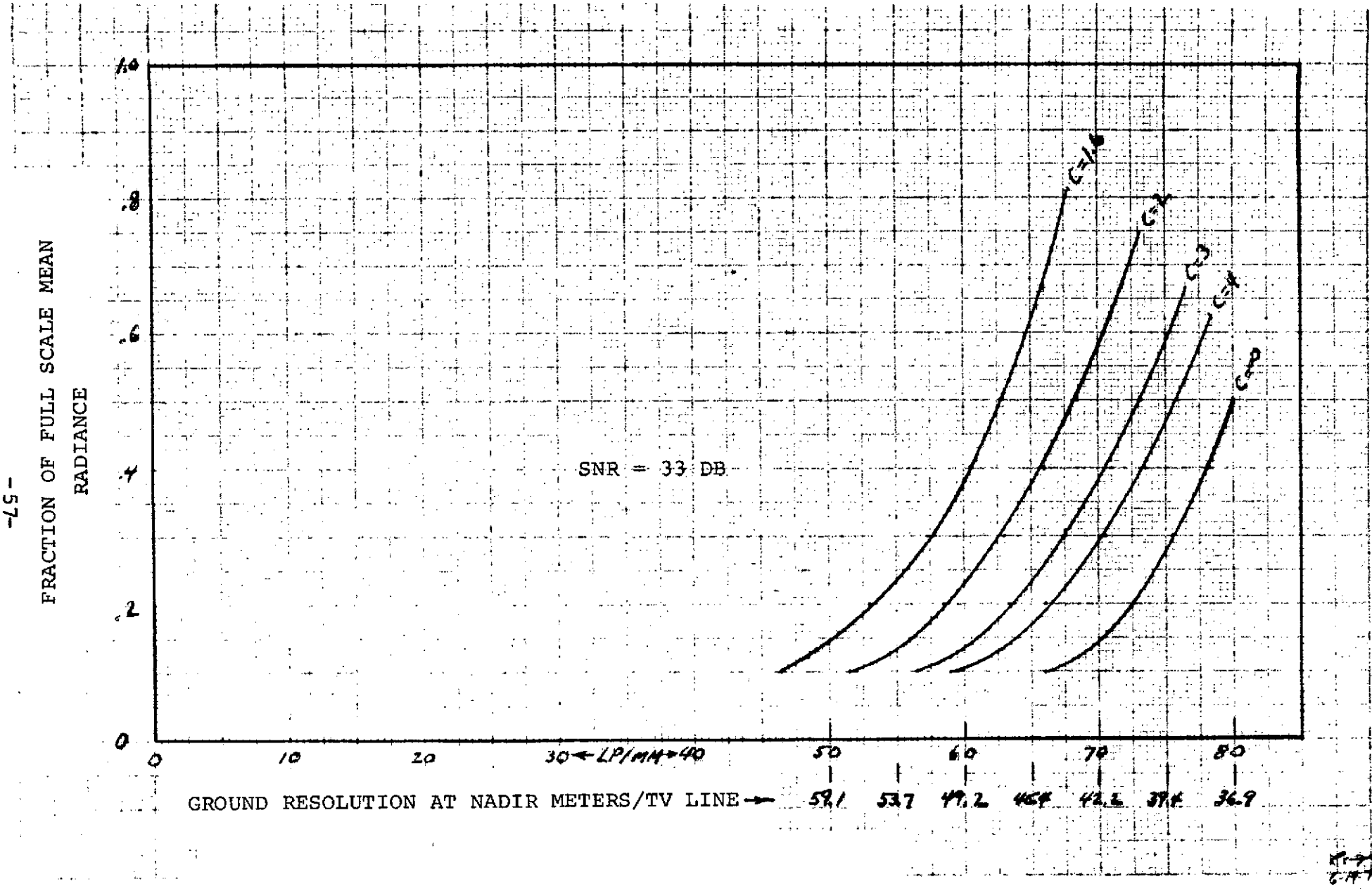

Figure V-5. Resolving Power Curves for High Resolution RBV Camera

of sensor packing density is due to the shift in scale of the LEST response relative to the sensor MTF. The ground resolution scale also shifts for this reason, as well as due to the varying distance to the earth surface (magnification) and, in the longitudinal direction, due to earth curvature.

The effect of earth look angle is illustrated in Table V-1 where ground resolution is given at 40° latitude (along the nadir line of longitude) for two packing density values. Following the usual practice, a mean value is computed for the two surface resolution values obtaining at locations other than at the nadir.

TABLE V-1. RESOLUTION AT NADIR AND AT 40° LATITUDE ALONG LINE OF LONGITUDE FOR HIGH RESOLUTION RBV CAMERA

NADIR POINTING		SURFACE METERS AT 40°		
SENSOR LP/MM	SURFACE METERS	LONG.	LAT.	MEAN (RSS)
70	42.2	64.0	44.2	53.2
80	38.3	58.1	40.1	48.3

In general, it is assumed that the scene content of interest, and sun angles, are known quantities and that the camera exposure is programmed to provide a peak highlight that is close to full scale. If multiple areas within the 150 x 150 km format are of interest, such as clouds against water and vegetation against soil, two pictures can be taken of the same area. This will yield the highest resolution data for each area of interest. However, the loss in resolution for the lower radiance area, on the shorter exposure frame, is unlikely to exceed 10 percent.

The resolving power curves may be thought of as boundary conditions. For detail finer than a curve applying to a particular contrast ratio, information will be lost. For coarser detail, the probability of resolving the information is quite high. Similarly, areas of scenes having slightly higher contrast are easily resolvable, while detail in lower contrast areas is rapidly lost.

Computations are given later in this section for exposure times that will provide the assumed 33 dB SNR with the sample target radiances referred to in Section IV. However, the camera capability may be estimated by extrapolating data previously computed.[4]

From previous computations a minimum of 33 dB SNR is obtained with a desert sand highlight radiance (about 20 percent reflectivity), at normal sun and viewing incidence, with a T/2.9 optical system and 5.0 milliseconds (msec) exposure time. For the f/4 LEST system, if a 50 percent transmission is assumed the T number is:

$$T/No = \sqrt{\frac{4^2}{.5}} = 5.66.$$

Then the required exposure time is increased to:

$$\text{Exposure Time} = \left(\frac{5.66}{2.9}\right)^2 \times 5 = 19 \text{ m.sec},$$

4. Reference 2, Page V4 to V13.

for 33 dB SNR. For sun and viewing angles providing 0.1 of this peak radiance, the exposure time should be .19 sec, and for .01 of the radiance the time should be 1.9 sec. The latter value represents about the maximum value of exposure time postulated for this camera and should be quite close to sunset conditions. It should also be noted that for cloud viewing, the exposure times should be reduced by a factor of about 4.

B. Nighttime Camera

a. SIT Sensor

A 40 mm silicon-intensifier target (SIT) vidicon is postulated for nighttime application. This sensor, an RCA C21145, has an available image diagonal of 40 mm providing for a square image of up to 28.3 mm. From available data sheet resolution information it is estimated that a resolving power of 800 TV lines per picture height (24 mm for the 3 x 4 aspect ratio of commercial TV) is practical. The square raster of 800 TVL/24 mm will then provide a total of 943 lines in each direction.

Scaling the LEST optics for 300 meters per TV line, the ground area at nadir will be 283 x 283 km, and the focal length will be:

$$\text{F.L.} = 28.3 \times \frac{35,770}{283} = 3.58 \text{ meters.}$$

The resulting f number for the 1.5m aperture telescope will then be f/2.39.

For this type of sensor, where an amplification process is incorporated within the device, the SNR will be established primarily by the noise source prior to the signal pre-amplifier. It is assumed in the following, that the primary source of noise within the device is due to random fluctuations in the electron stream emitted from the photocathode.

A cloud highlight at nadir, for a noon sun, of 10,000 foot-lamberts (fL) results in a faceplace flux density of:

$$\text{foot-candles} = \frac{10{,}000 \times .5}{4\ (2.39)^2} = 219,$$

for the assumed LEST transmission of 0.5. Then the total flux over the 28.3 mm square is 1.88 lumens. Assuming an effective exposure time of 10^{-7} seconds (obtained with a shutter having a more practical exposure of a few milliseconds and a neutral density filter), the faceplate exposure will be 1.88×10^{-7} lumen-seconds.

A tungsten illumination source at 2854°K color temperature provides a photo-cathode electron stream of 160 micro-amperes per lumen (μA/ℓ). Sunlight illumination is more effective on S-20 by a factor of 1.24 (see Table III-2) so that the electron stream due to this exposure will be: $1.88 \times 10^{-7} \times 1.24 \times 160 \times 10^{-6} = 37.3 \times 10^{-12}$ ampere-seconds (coulombs).

The estimated picture array of 943 x 943 elements results in a total of 88.9×10^4 elements. Then the number of electrons per picture element for the computed electron stream is computed from:

$$\text{Electron/Pixel} = \frac{\text{Charge Flow}}{\text{Charge/Electron}} \times \frac{1}{\text{Pixels}}$$

$$= \frac{37.3 \times 10^{-12}}{1.6 \times 10^{-19}} \times \frac{1}{88.9 \times 10^4} = 262$$

The electron stream SNR is:

$$SNR = \sqrt{\text{Electrons/Pixel}} = 16.2, \text{ or } 24.2 \text{ dB}$$

For full charge in the silicon target, the intensifier gain required is:

$$\text{Gain} = \frac{\text{Maximum Charge}}{\text{Charge Flow}}$$

Sensor data sheet information on the C21145 indicates a maximum target charge (for 8 volts target operation) of 25×10^{-9} coulombs. The required intensifier gain for this charge is 660, well below the maximum available gain of 2500 for the device.

The read rates and bandwidth are discussed in a later paragraph of this section. At this point, a frame rate of .12 seconds/frame and a bandwidth of 5.7 MHz is postulated. The peak output signal is then,

$$i_{out} = \frac{\text{Target Charge}}{\text{Read Time}} = \frac{25 \times 10^{9}}{.12} = 210 \text{ nanoamperes}$$

and the electron stream produced noise in the output, for the computed SNR of 16.2, is 13 nanoamperes. By contrast the amplifier noise in 5.55 MHz is approximated by:

$$i_{noise} = \sqrt{.012 \ (BW)^3} = 1.5 \text{ nanoamperes}$$

Improved SNR may be obtained by increasing the exposure to provide an increase in the number of electrons per element. A SNR of 20 times (26 dB) is obtained with the same faceplate illumination, by lengthening the exposure time to 1.5×10^{-7} seconds, and an SNR of 40 times (32 dB) at 6×10^{-7} seconds. For both of these cases, the amplifier noise is small by comparison to the electron stream noise. It should also be noted that increasing the electron stream requires that an accompanying reduction in intensifier gain be made to avoid overload in the target.

This camera is intended for operation at night. Exposure times may be approximated by scaling light levels from the bright sun levels assumed (more accurate times are treated in a later section.) Full moonlight is generally assumed to be 10^{-6} times sunlight, requiring an exposure time of .6 seconds. For a half moon (or perhaps somewhat less) the light level is 10^{-7} times sunlight. In order to avoid exposure times in excess of about 2 seconds, the SNR is assumed to fall within the range of 26 to 32 dB at light levels between 10^{-7} and 4×10^{-7} of full sunlight.

Resolving power computations have been made for both SNR values to permit bracketing the anticipated camera resolution. More exact exposure time computations including the effect of haze filtering are discussed in the following sections. Starting with the square wave response for the C21145 shown in Figure V-6, the response was converted to sine wave form and cascaded with the LEST response. The LEST scale was established at 1 TV line corresponding to 300 meters at nadir (.00167 line pairs per meter at the surface). The cascaded sine wave response was then converted to mean value of square wave response to establish the modulation available curve at high contrast ($C = \infty$) as previously described.

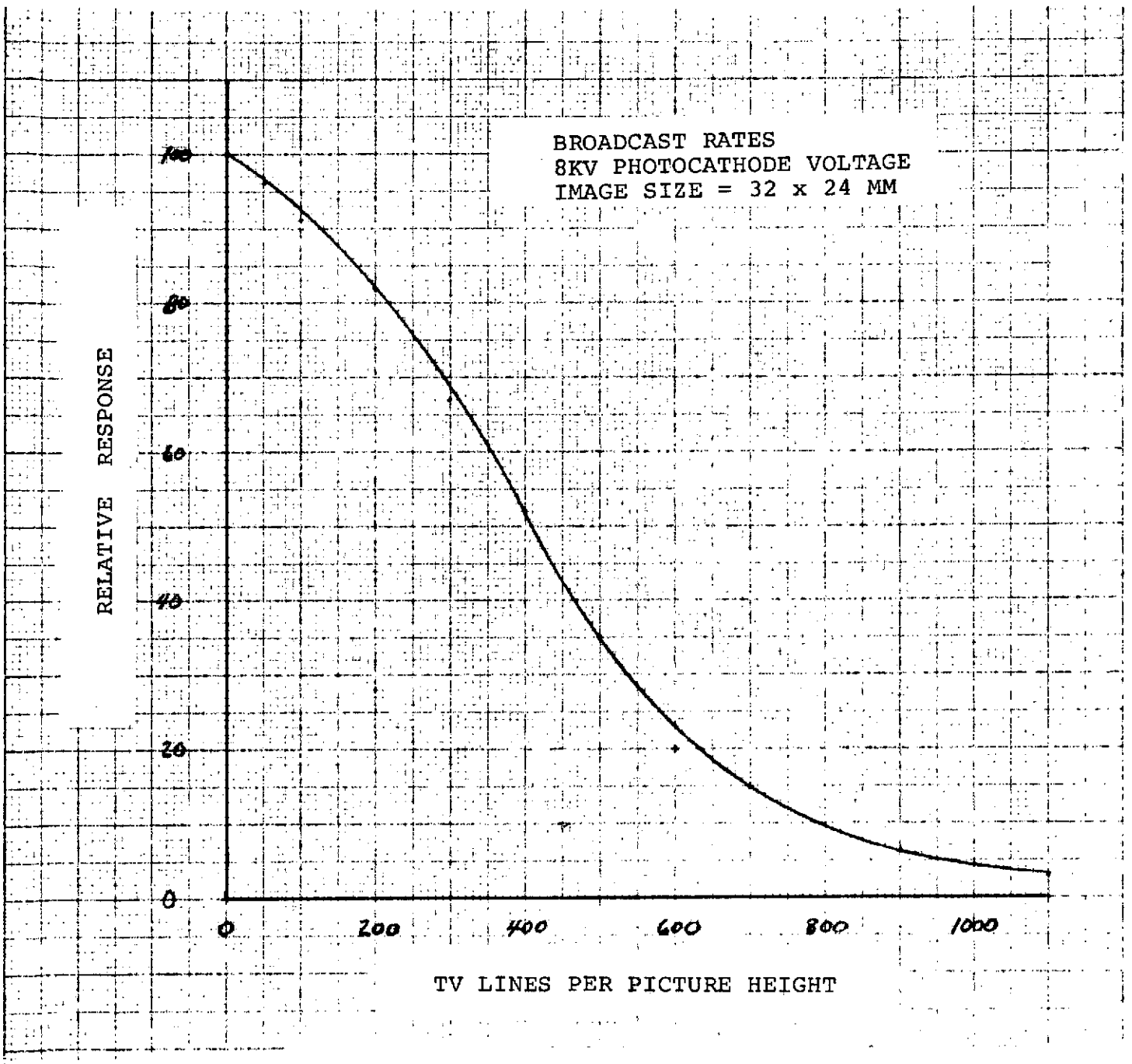

Figure V-6. Typical Square Wave Response of C21145 SIT Vidicon

The modulation required data was computed for a raster having 1200 scan lines and 943 horizontal elements per line (17 line pairs per mm), and a bandwidth (for signal and effective noise) of 5.7 MHz. The sensor light transfer characteristic, shown in Figure V-7, is virtually a straight line at 45 degree slope so that unity gamma is employed for the computations.

The family of modulation required and modulation available curves for 26 dB SNR are shown in Figure V-8. A similar set of curves are plotted in Figure V-9 for an SNR of 32 dB. The intercepts of these curves for very high contrast and a contrast ratio of 4, m=1 and m=.6 respectively, were then used to plot the resolving power curves shown in Figure V-10.

Shown on the abscissa of Figure V-10, is a nadir ground resolution scale as well as packing density on the sensor. Note that at a contrast ratio of 4 and, for example, 60 percent of maximum mean radiance, the resolving power is about 285 meters per TV line for the 32 dB SNR condition. For the 26 dB signal, the resolving power decreases by about 20 percent to 340 meters per TV line.

The potential for using increasingly longer exposure times will in part determine the SNR achievable at low levels of moonlight. Apart from the question of long times between picture frames, long exposure times may result in the degradation of information stored in the target. This is primarily attributable to dark current (reverse leakage) in the silicon diode target.

The SIT measurements quoted in data sheets are generally made at a faceplate temperature of 30° Centigrade. At this temperature a typical dark current of 30 nanoamperes obtains. During a 1.0 second exposure interval, a charge leakage of 15×10^{-9} coulombs could occur with a resulting loss of more than 50 percent of the stored charge.

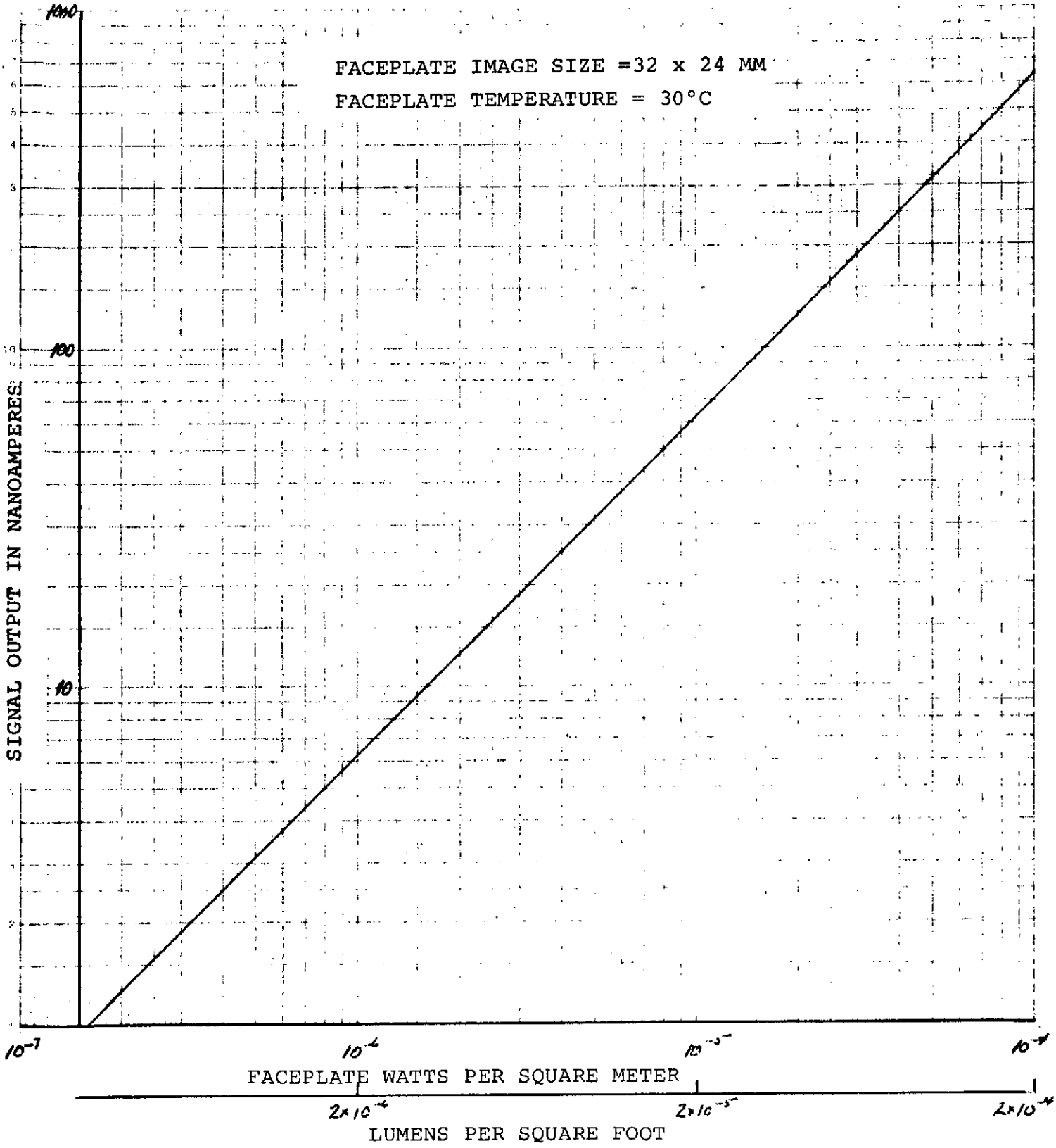

Figure V-7. Open Shutter Light Transfer Characteristic of C21145 SIT at Broadcast Rates

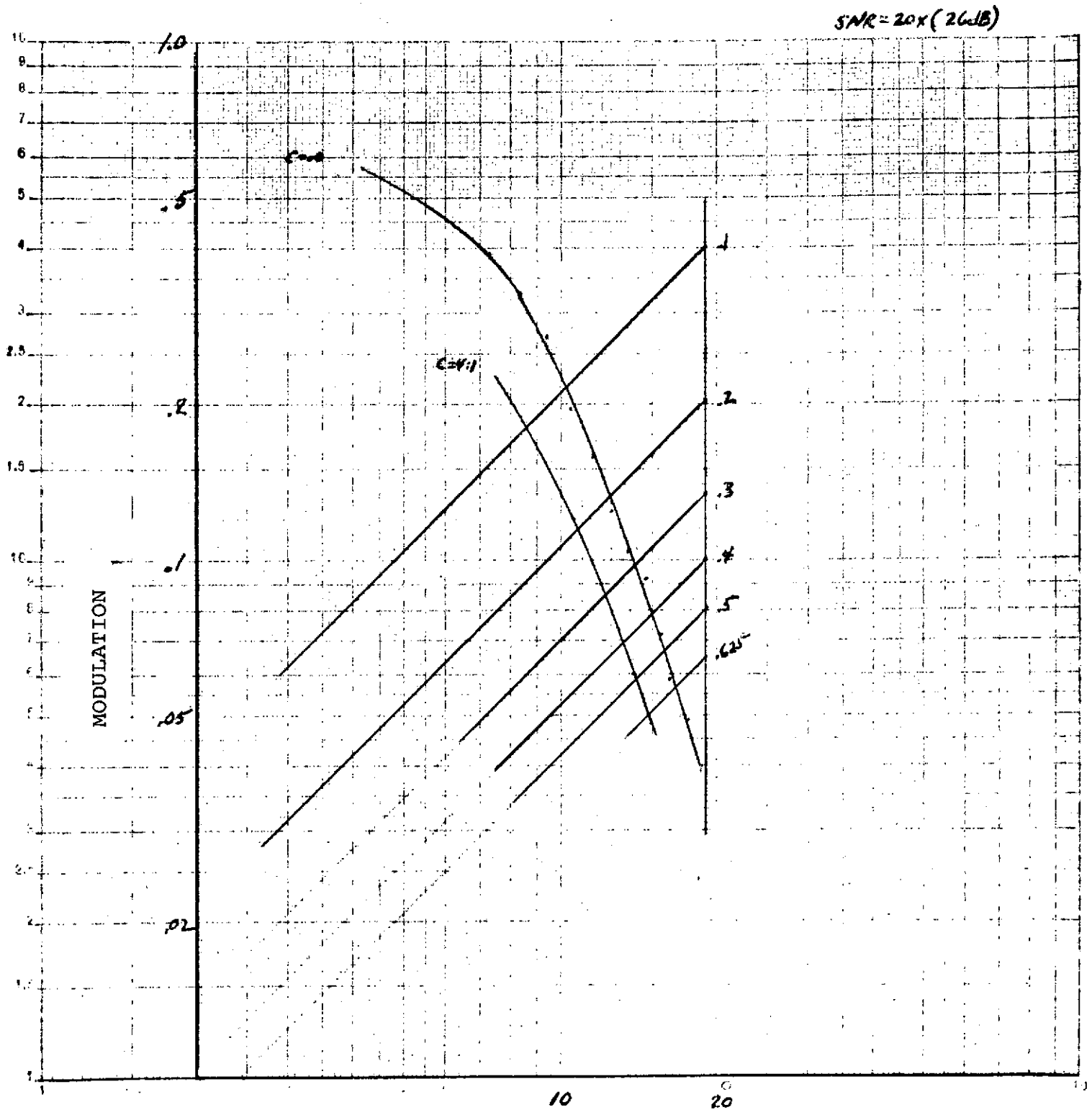

Figure V-8. Average Square Wave Response and Required Modulation for C21145 SIT at SNR = 26 dB

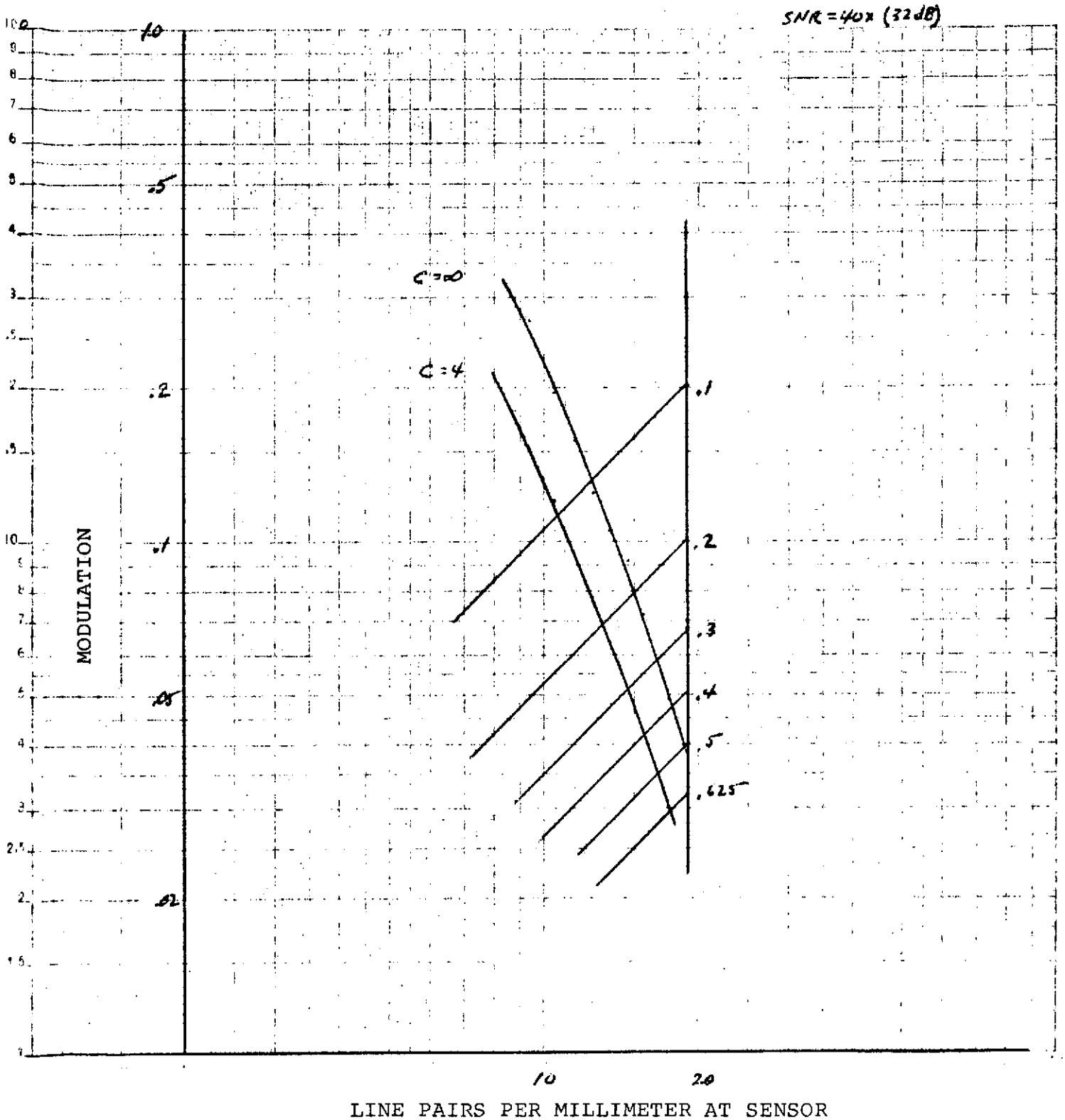

Figure V-9. Average Square Wave Response and Required Modulation for C21145 SIT at SNR = 32 dB

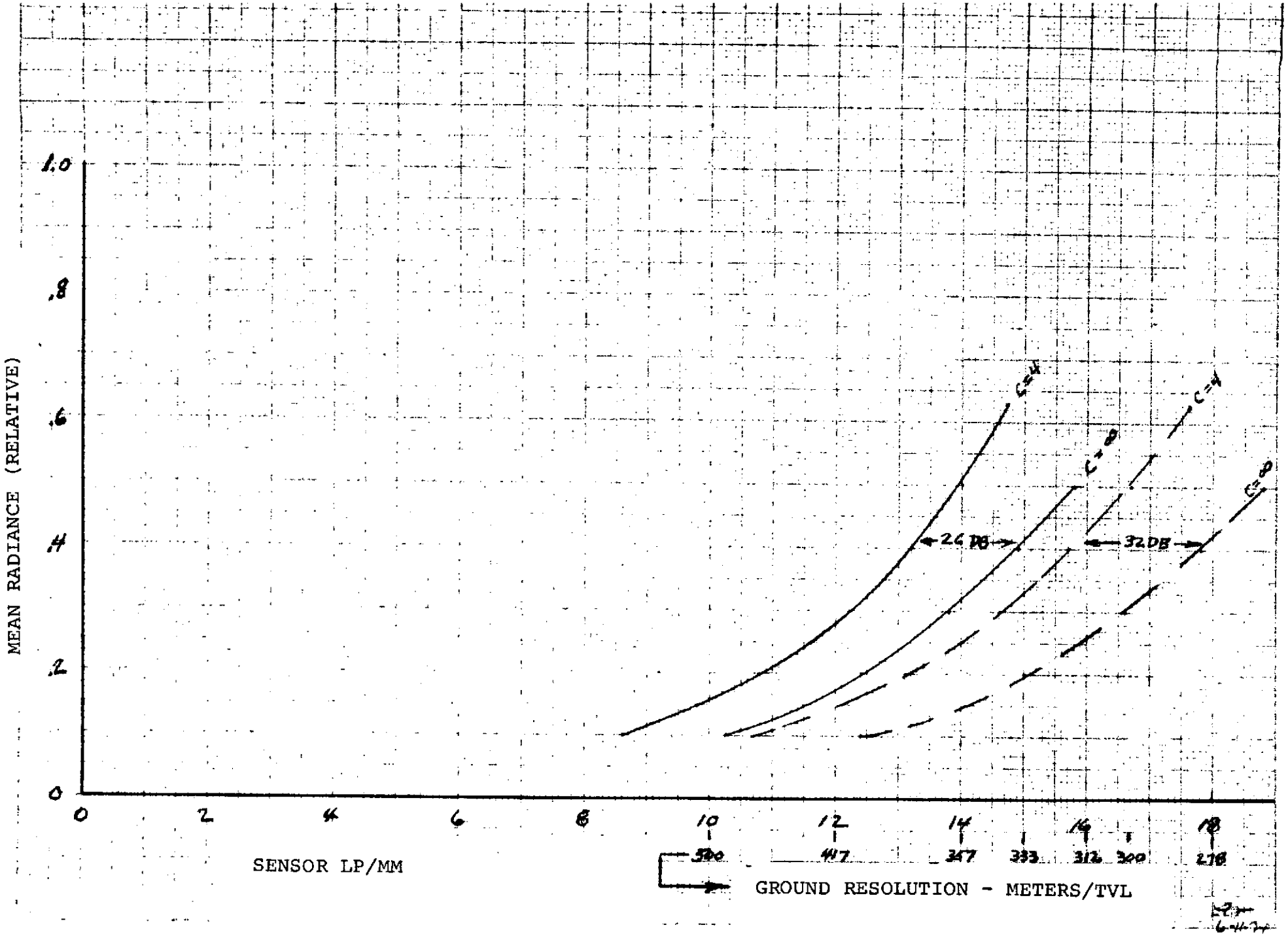

Figure V-10. Predicted Resolving Power for SIT Camera

Operation at cooler temperatures results in a decrease of dark current. Theoretically, reverse leakage current in silicon diodes should decrease by 2-to-1 for a 4.5°C decrease in temperature. This theoretical value is generally not achieved, a 7.5°C decrease being the typical value for a 50 percent reduction. If a leakage of up to 10 percent of useful information is assumed to be tolerable, the faceplate should be maintained at less than 5° Centigrade for a total expose and read times of 2 seconds. Even longer expose times are feasible if cooler temperatures are maintained, experiments having indicated quite satisfactory performance at -40° Centigrade.

b. SEC Sensor

Consideration has been given to the use of a secondary electron conduction (SEC) sensor as a possible alternate to the SIT for night picture-taking application. The single most important feature leading to the consideration of the device, is the virtual absence of dark current in the storage target. This permits extremely long exposure times without the necessity for careful target temperature control.

The tube considered as the basis for discussion in the following paragraphs is the Westinghouse WL-30893. This tube has a useable faceplate diagonal of 25.4 mm (1 inch), permitting the use of a square raster of 18 x 18 mm. The square wave response curve, shown in Figure V-11, indicates a potential resolving power of 600 TV lines for the 15 mm picture height of the 3 x 4 format.

A square raster should then permit a picture of 720 x 720 TV lines. Scaling the LEST optics to maintain 300 meters per TV line (as for the SIT), the ground coverage at nadir will be a 216 kilometer square. The required focal length is 2.98 meters and the resulting numerical aperture is f/2 ($\frac{2.98}{1.5}$ for the assumed 1.5 meter LEST).

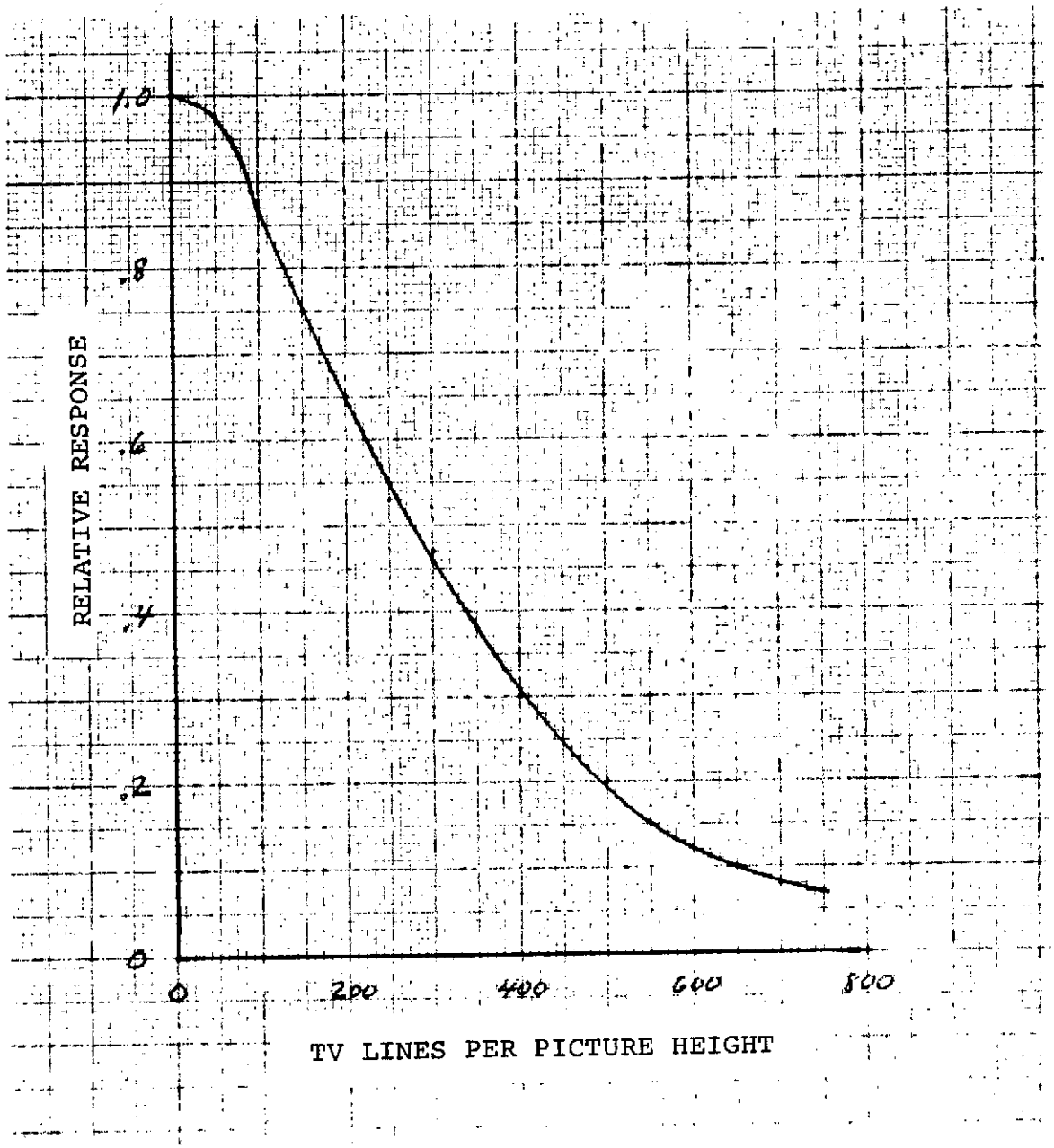

Figure V-11. Typical Square Wave Response of WL-30893 SEC Camera Tube

The reasoning followed to establish the exposure required for a desired SNR is similar to that used for the SIT. Unfortunately, the data sheet information does not provide sensitivity for the S-20 photocathode, but rather for the combination of photocathode and target. The assumption is made that the photoemitting material efficiency is sufficiently similar to that of the SIT to permit using the RCA data sheet number for photocathode efficiency.

The noon sun on clouds, providing 10,000 fL scene highlight, results in 313 fc available at the faceplate with the f/2 optical system and the assumed LEST transmission of 0.5. The total flux for the SEC format is then 1.09 lumens. The exposure required to provide full target charge, will be determined by the device gain and the target capacity. The light transfer characteristic for this device, shown in Figure V-12, is nonlinear particularly in the region of maximum charge, the device gain decreasing from 85 in the linear region to about 36 at maximum charge.

The maximum charge is computed at 3.33×10^{-9} coulombs so that the required charge flow is $3.33 \times 10^{-9}/36$ or 93×10^{-12} coulombs. Sunlight (6000°K) results in a luminous sensitivity of 198 microamperes/lumen so that the required exposure time for full charge is:

$$T_{exposure} = \frac{\text{Required Charge}}{(\text{Faceplate Lumens})\ (\text{Current/Lumen})}$$

$$= \frac{93 \times 10^{-12}}{(1.09)\ (198 \times 10^{-6})} = 4.3 \times 10^{-7} \text{ seconds}$$

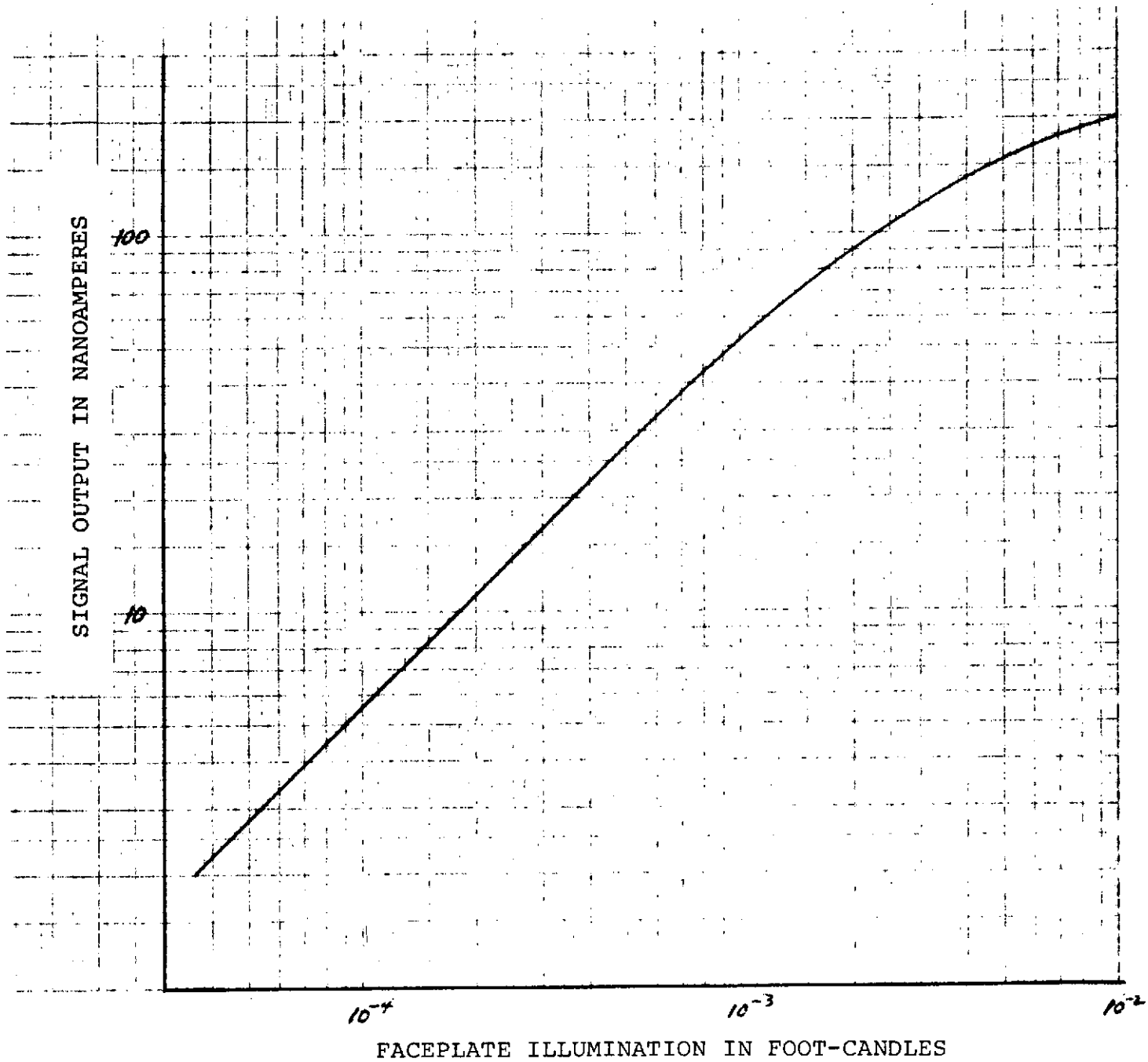

Figure V-12. Open Shutter Light Transfer Characteristic of WL-30893 SEC at Broadcast Rates With 2870°K Tungsten Illumination

With the charge flow produced by this exposure and the 720 by 720 picture element array, the electrons per picture element are computed at 1124. The electron stream SNR is given by $\sqrt{1124}$ or 33.5 (30.5 dB).

The relatively low storage capacity and gain of the electron multiplication process in the SEC requires that the readout rates be substantially lower than that employed for the SIT. This narrows the required bandwidth and reduces the pre-amplifier noise to levels which should be down by a factor of 3 or more as compared to the electron stream noise appearing in the output signal. A read frame time of 1.0 second appears to offer reasonable performance that is compatible with the 3-to-1 criteria, for SNR up to 40 times.

The SNR of 33.5:1 can be increased to 40:1 by increasing the exposure times by $(40/33.5)^2$. The required exposure time for the maximum sun condition is then 6.2×10^{-7} seconds.

For full moonlight, a factor of 10^{-6} of the assumed sunlight level, the required exposure time is .62 seconds. A maximum exposure time of 6.0 seconds is postulated permitting a light level of about 10^{-7} times that of full sun (about 1/2 moon operation). Note that there is no operational restriction other than the lengthy total frame time that prevents increasing the exposure time to permit picture-taking at even lower light levels.

The computations of LEST and sensor MTF were performed, as previously described, for high contrast ($C = \infty$) and contrast ratio of 4. The modulation available curves are shown in Figure V-13 together with the modulation required curves for a SNR of 40. Gamma was assumed to have a constant value of unity for these calculations which is slightly pessimistic due to the somewhat lower gamma at high radiance levels.

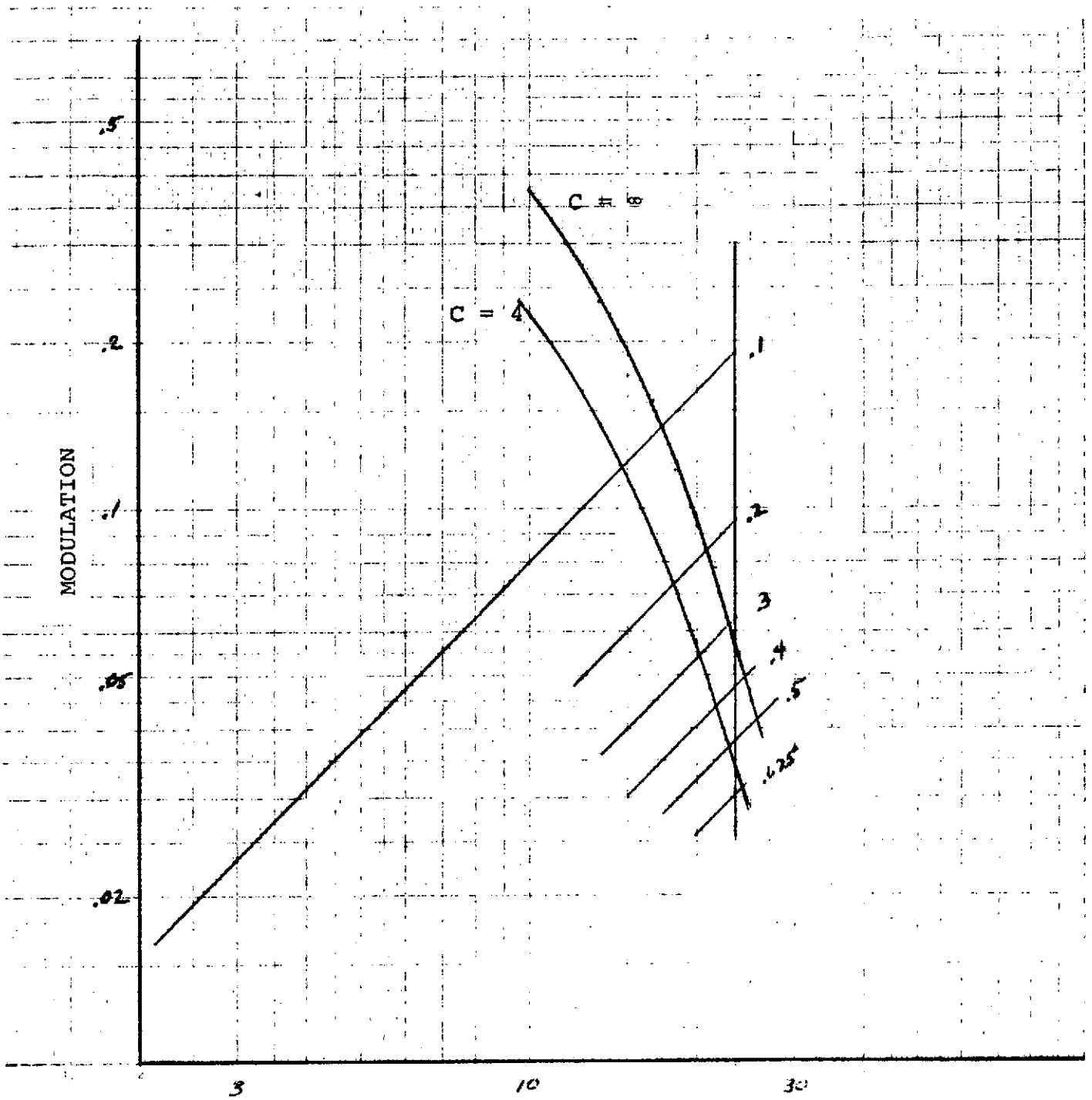

Figure V-13. Average Square Wave Response and Required Modulation for WL-30893 SEC at SNR = 33 dB

The resolving power curves are shown in Figure V-14 for the same two contrast levels. Note that the performance is slightly better in terms of ground resolution than the same curves for the SIT. The difference is primarily due to the initial estimates of packing density, apparently somewhat more pessimistic in the case of the SEC. Equalization of this performance is a somewhat tedious iterative process and was not carried out. However, the end result should be a slight narrowing of the coverage difference between the two sensors.

c. Comparison of SIT and SEC

Aside from questions of physical size and circuitry requirements, there are several differences between the two cameras described. The SIT is capable of greater ground coverage than the SEC, 283 Km as compared to 216 Km for the formats considered. The SEC is capable of longer exposure times, and consequent lower light level pictures, without regard to the temperature constraint imposed on the SIT. The SIT can be used for very long exposure times but the temperature of the target must be controlled.

Perhaps of greatest importance, the SIT is the more rugged of the two as regards incident illumination. Exposures to orders of magnitude above normal operating levels do not result in damage to the photo-emitter or target of the SIT. In fact, for some early cameras operating in an open shutter mode, short time pointing at the sun was survived without permanent degradation. By contrast, the SEC is rather sensitive in this regard, verified both by direct experience and by data sheet precautionary notes.

C. Multispectral Camera

Operation of the multispectral frame camera is based on the use of a 1-inch silicon vidicon such as the RCA 4532-A. Other potential vendors, producing a substantially similar

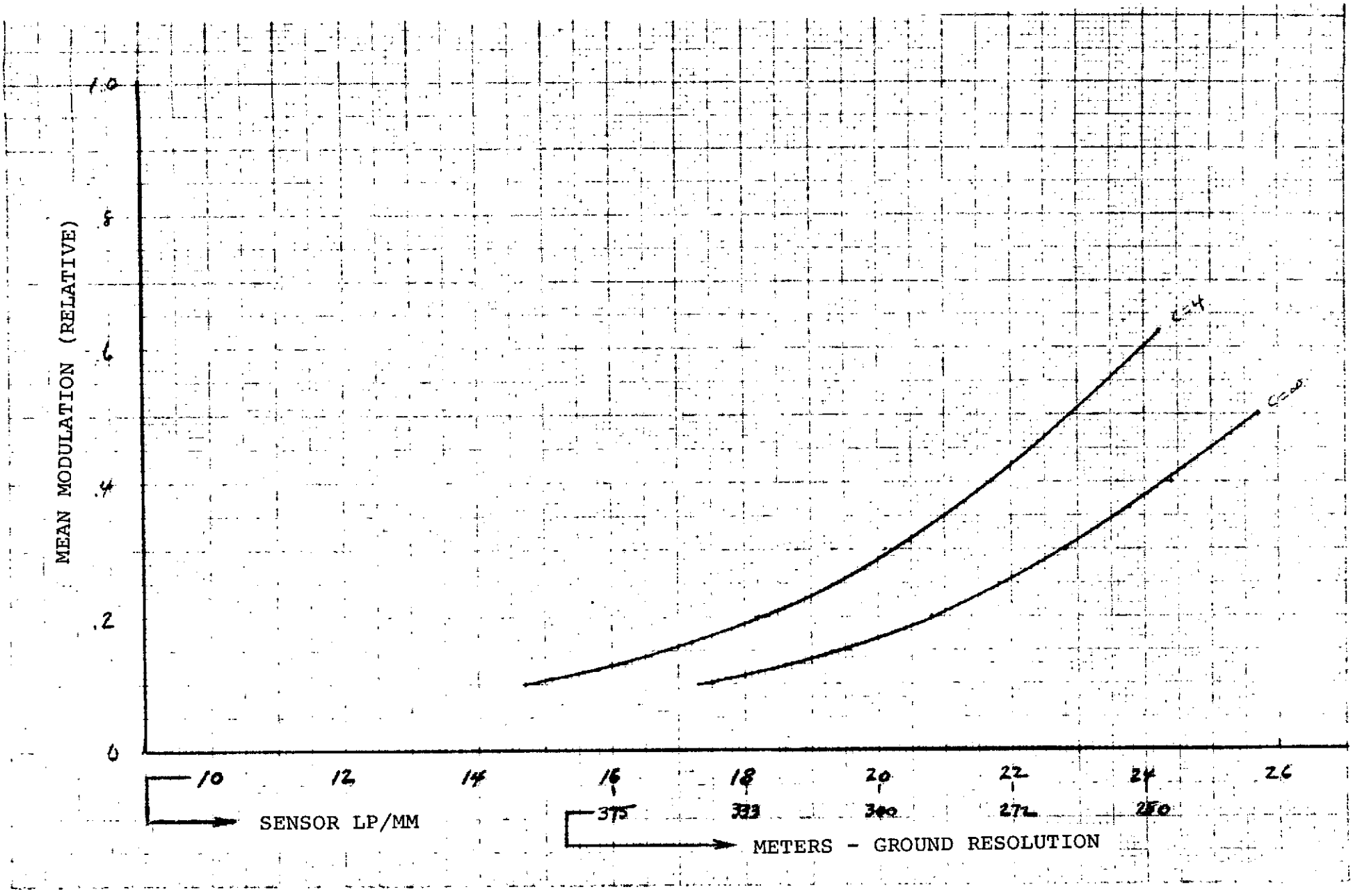

Figure V-14. Predicted Resolving Power for SEC Camera

product, are available for this device. The format available is up to 16 mm diagonally, permitting an 11.3 mm square format. A larger format version of the silicon vidicon would have the advantage of larger coverage for the same resolution, but is not available at this time.

The LEST optics are scaled to provide a frame coverage of 100 km square. From the sensor square wave response, shown in Figure V-15, it appears that 600 TV lines per picture height (31.3 line pairs per millimeter) is a practical limit for resolving power. In order to provide more margin a packing density of 30 lp/mm was assumed. This results in a total of 679 lines in both directions leading to a surface element of 147 meters per 1/60 mm at the sensor. The required focal length of the optical system is 4.05 meters with a numerical aperture of f/2.7.

This type of sensor does not incorporate any internal amplification process so that the primary noise source is attributable to the first stage of the amplifier chain. The output signal level and the bandwidth of the amplifier must be considered in establishing the required SNR.

Starting with a full spectrum cloud scene of 10,000 fL, the f/2.7 optical system provides 171 fc at the faceplate, assuming a transmission factor of 50 percent. At this illumination level, the exposure time will be adjusted so that with the scan rates chosen, an output signal of 78 nanoamperes will be obtained. This number results from the bandwidth requirement of 4.66 MHz and an SNR design objective of 37 dB (71 times).

The preamplifier noise is computed from $\sqrt{.017\ (\text{Bandwidth})^3}$ producing 1.1 nanoamperes. The required output signal at broadcast rates and 2854°K illumination is obtained with an exposure of $.25 \times 10^{-3}$ fc-second. (The unity gamma 4532A light

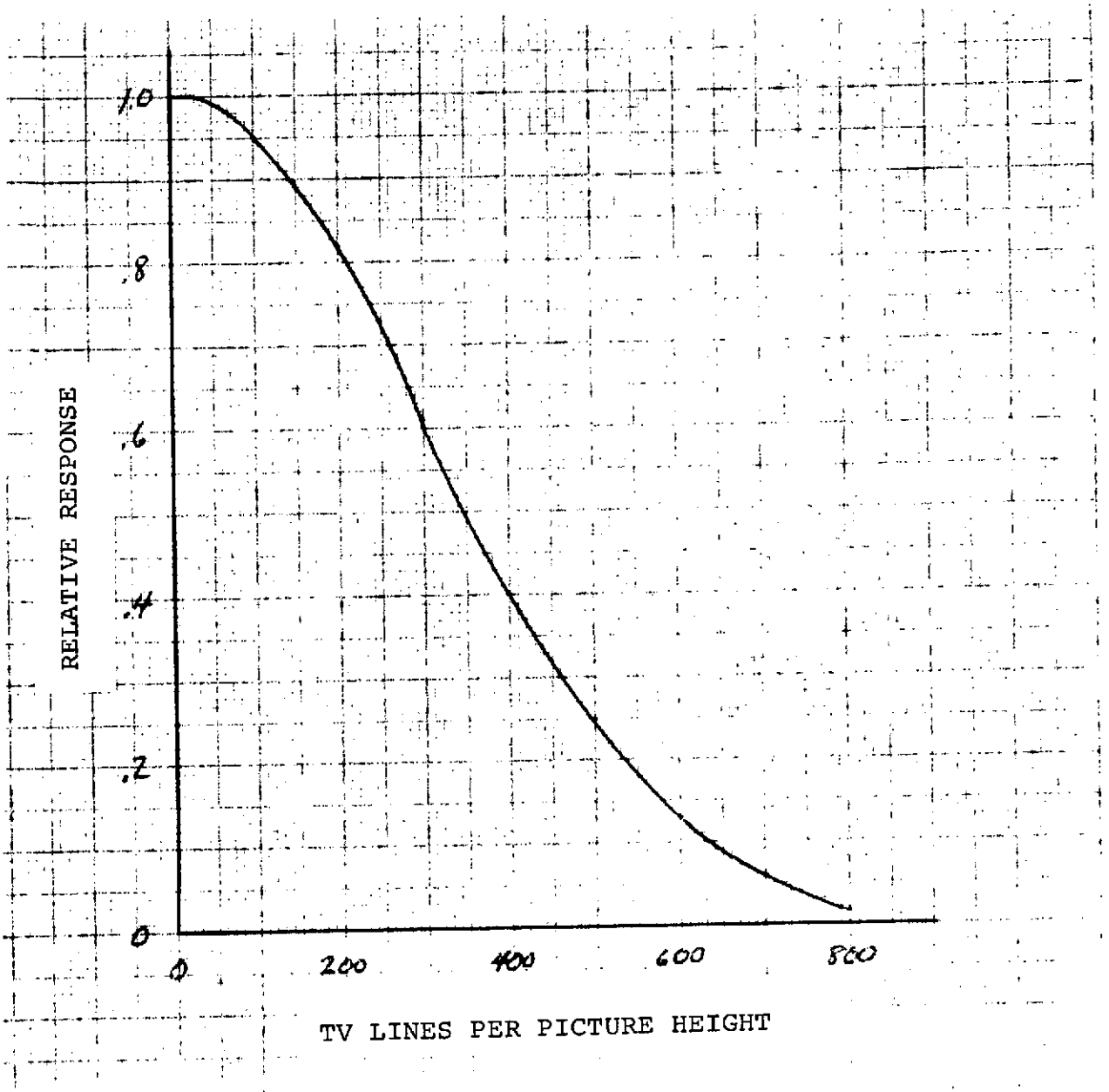

Figure V-15. Typical Square Wave Response of 4532A Silicon Vidicon

transfer characteristic at broadcast rates is shown in Figure V-16). For the 0.1 second frame time the exposure required is 1.5 x 10-3 at 2854°K and from Table III-2 ($1.5 \times 10^{-3}/.52$) = 2.9×10^{-3} fc-second at 6000°K.

The required exposure times with the 171 fc provided by direct sunlight is then 1.7×10^{-5} seconds. For a highlight such as sand having about 1/4 the radiance of clouds, the exposure time should be increased by four times to 6.8×10^{-5} seconds. For the multispectral application, where perhaps 10 percent of the total energy is available in a single band, the exposure time will increase by another factor of 10 to 6.8×10^{-4} seconds. (More accurate computations for actual targets are given in later paragraphs). This should still permit practical picture taking, for even lower reflectivity targets, over a substantial portion of the day with maximum exposure times of say 0.1 second. Temperature of operation may then be up to 30° Centigrade, or higher, without substantial effect due to dark current.

The computations for available modulation based on the silicon tube response, shown in Figure V-17, were performed as described for the other scenes. Since the camera is intended for operation over a wide range of contrast levels, and including low contrast scenes, the computations were carried over the range from $C = \infty$ to $C = 1.025$. The resulting family of resolving power curves are shown in Figure V-18. Recall that the estimated resolving power that established the LEST scale factor was based on an assumed 30 lp/mm while the actual numbers at contrast ratios above about 1.2 are somewhat higher. Some adjustment in the trade between coverage and detail may be in order, of course, taking into account the user requirements for definition as opposed to coverage.

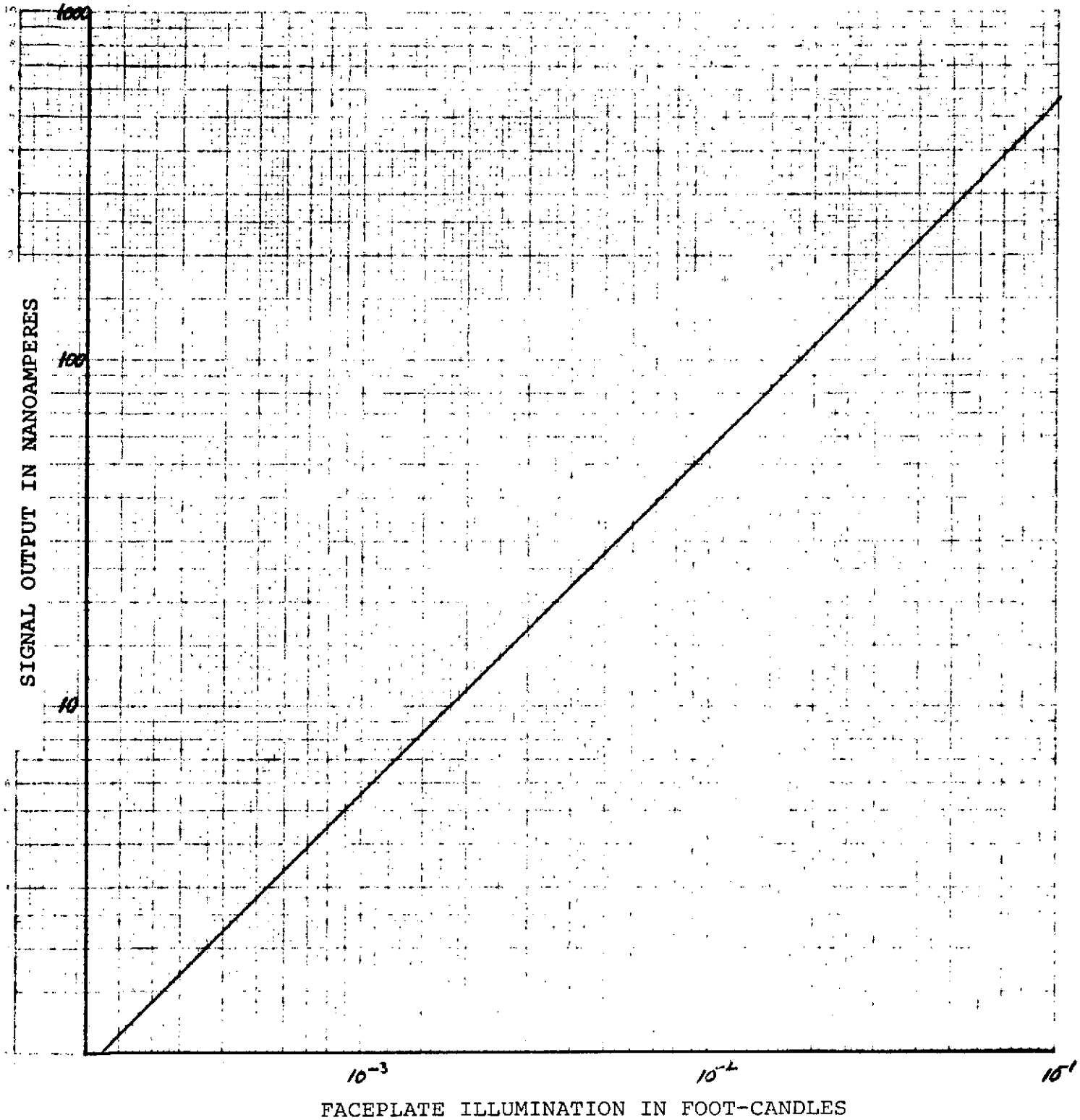

Figure V-16. Open Shutter Light Transfer Characteristic of 4532A Silicon Vidicon at Broadcast Rates with 2854°K Tungsten Illumination

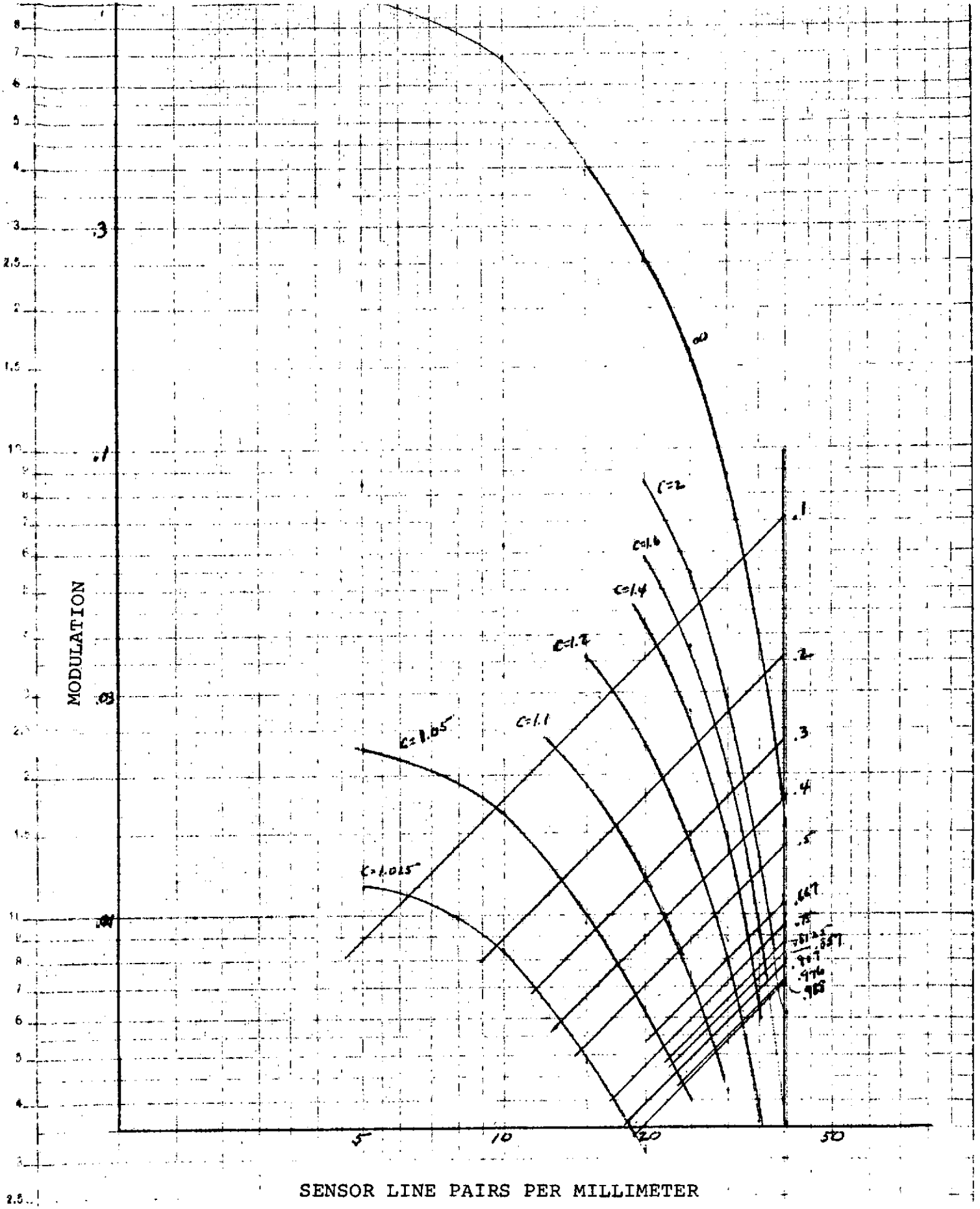

Figure V-17. Average Square Wave Response and Required Modulation For Silicon Vidicon Cameras at SNR = 37 dB

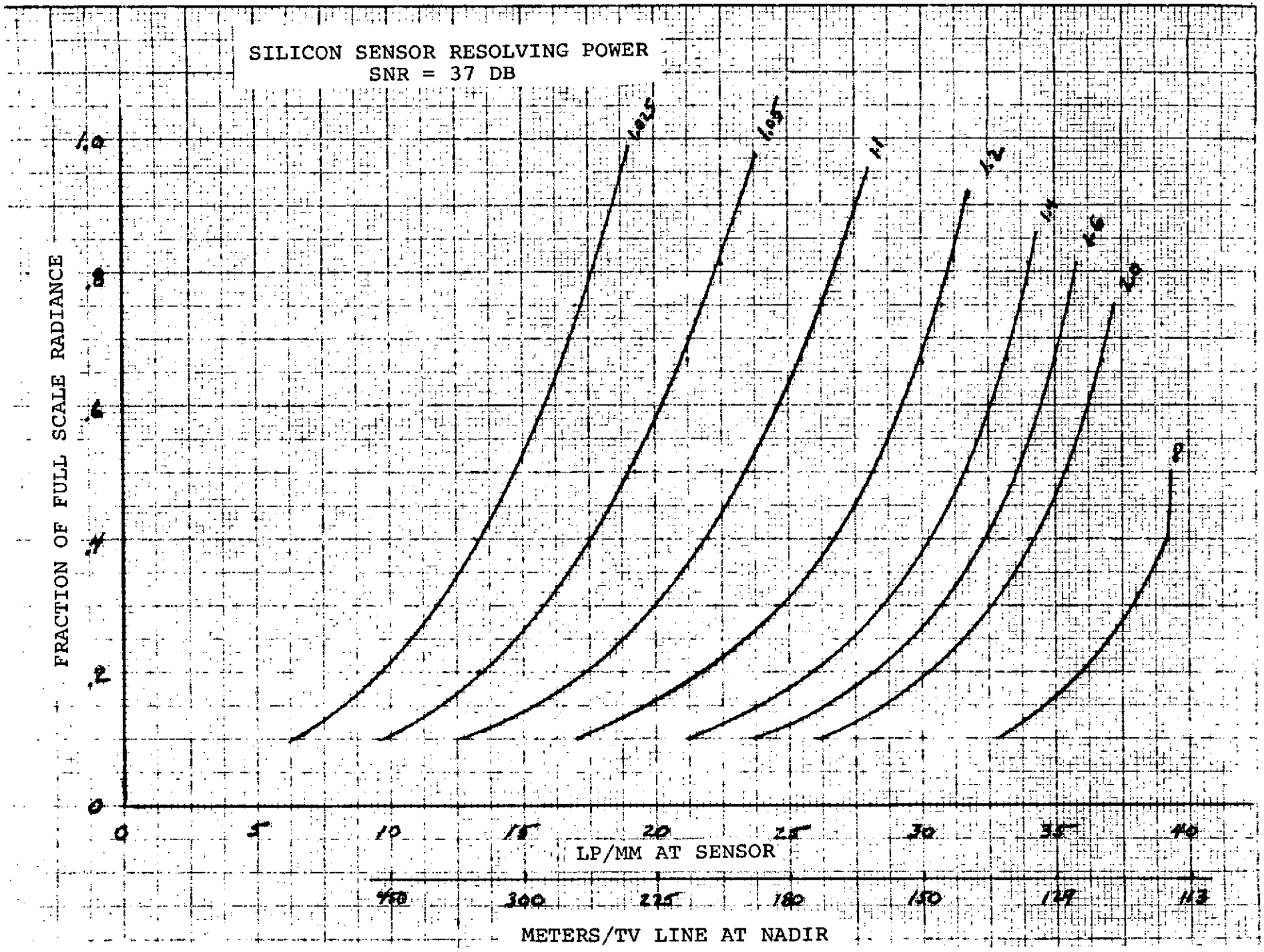

Figure V-18. Predicted Resolving Power for Multispectral Camera

3. Required Exposure Time

As noted above, a major advantage of an electron tube frame camera is the capability to have its exposure time adjusted to provide an acceptable level of energy on its faceplate. The acceptable level is determined from the desired signal-to-noise ratios for each camera as developed in Section V-2. The performance of each tube is defined in manufacturers' data sheets assuming a standard set of operating conditions. Therefore, it was necessary for us to convert the data for each scene to equivalent data under the standard conditions before exposure times could be determined. The next subsection describes the general procedure for obtaining exposure time, and the following subsections give the results for each camera and the scenes of interest.

A. Procedure for Determining Exposure Times

a. High Resolution Applications - RBV Camera

In Section V-2A, we indicated that a signal-to-noise ratio of 33 dB could be obtained for an RBV camera from desert sand and with normal sun and viewing incidence angles using 19 milliseconds exposure for a T/5.66 LEST system. This exposure corresponds to .6 microwatt-secs/cm^2. Exposure times can be obtained for this camera by computing faceplate highlight by:

$$F.P.H.L = \frac{\text{Scene Highlight}}{4(T/No)^2} \quad (\text{in } \mu\text{watts/cm})$$

and then

$$\text{Exposure Time} = \frac{.6\ \mu\text{watt-sec/cm}^2}{F.P.H.L.}$$

Scene highlights are available from Table IV-6 in Section IV-4-A.

b. SIT, SEC, and Silicon Vidicon Cameras

The general procedure for determining exposure time for the other camera application types is shown in Figures V-19 and V-20. Calibration data is available from tube manufacturers assuming as the light source a gas-filled tungsten filament lamp operating at a color temperature of 2854°K. This lamp has been adopted as the standard incandescent source by the International Commission on Illumination (CIE), which has accurately measured its relative spectral illuminance.[5] The operating temperature for a tungsten lamp at 2854°K color temperature is 2780°K.[6] It has been shown that the relative spectral emittance of such a lamp is reasonably approximated by the emittance of a blackbody at 2854°K.[7] Thus, the blackbody curve at 2854°K can be used to get relative spectral power distributions for the standard tungsten lamp. Since tube data sheets provide illuminance rather than irradiance data, we have also used the 2854°K blackbody curve to determine the conversion from lumens to watts (approximately 20 lumens per watt for the whole spectrum).[8]

The first step in determining exposure time requirements for the SIT, SEC, and silicon vidicon cameras and each application and band is to determine a multiplicative factor to convert observed radiance from a small spectral band to an equivalent radiance from the total spectrum for the standard source. Figure V-19 shows that the procedure requires the curves for tube response and the power density from the standard source. As can be seen, the multiplicative factor, (M_b) for any band b, is

---

5. "Applied Optics", Vol. 1, Leo Levi, Wiley, 1968, Table 11, P. 520.
6. Op. cit., Table 26, P. 554.
7. Op. cit., Eq. (5.2), P. 196.
8. Op. cit., Table 27, P. 555.

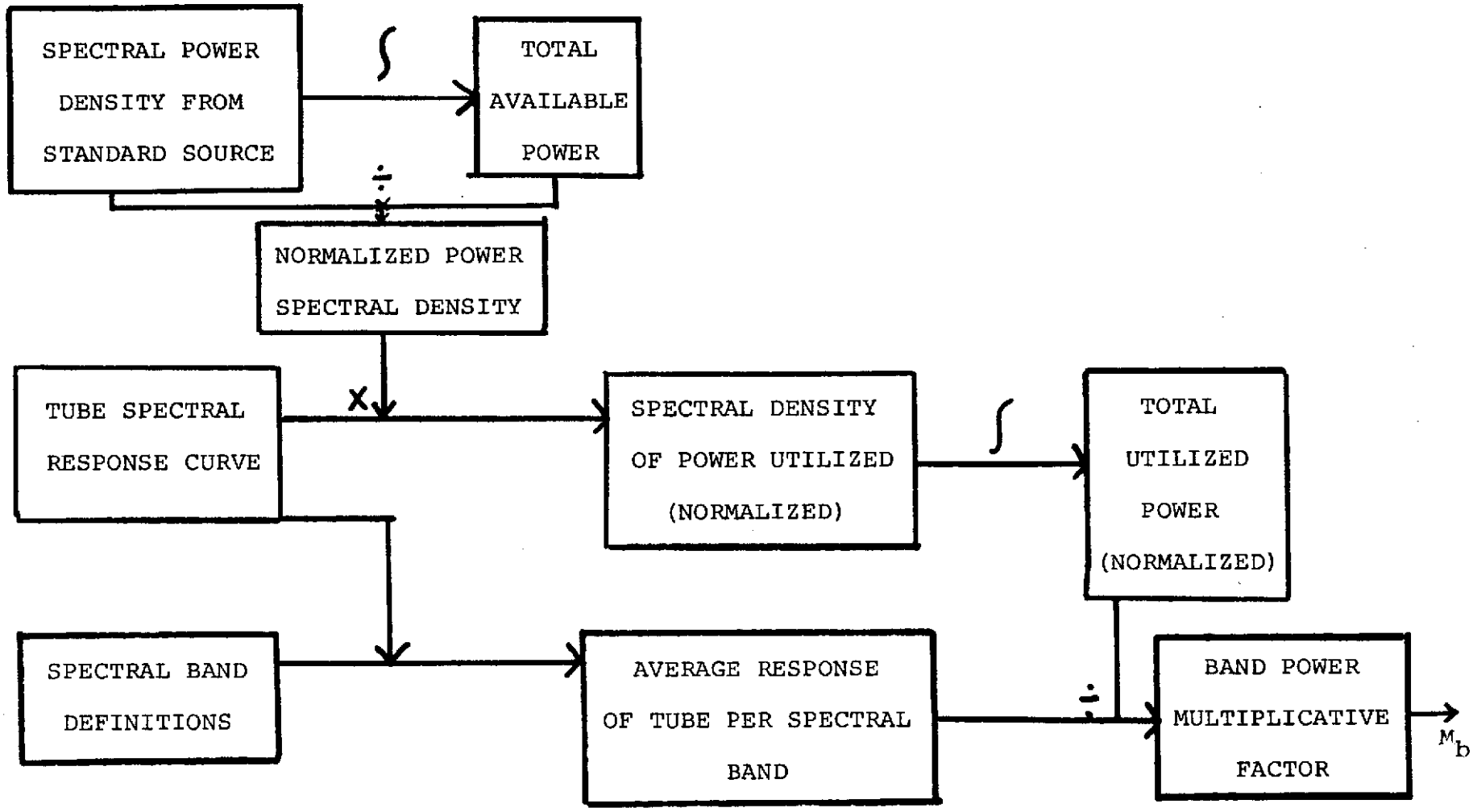

Figure V-19. Procedure for Determining Factor to Convert Scene Power Per Spectral Band to Equivalent Standard Source Total Power

C-2

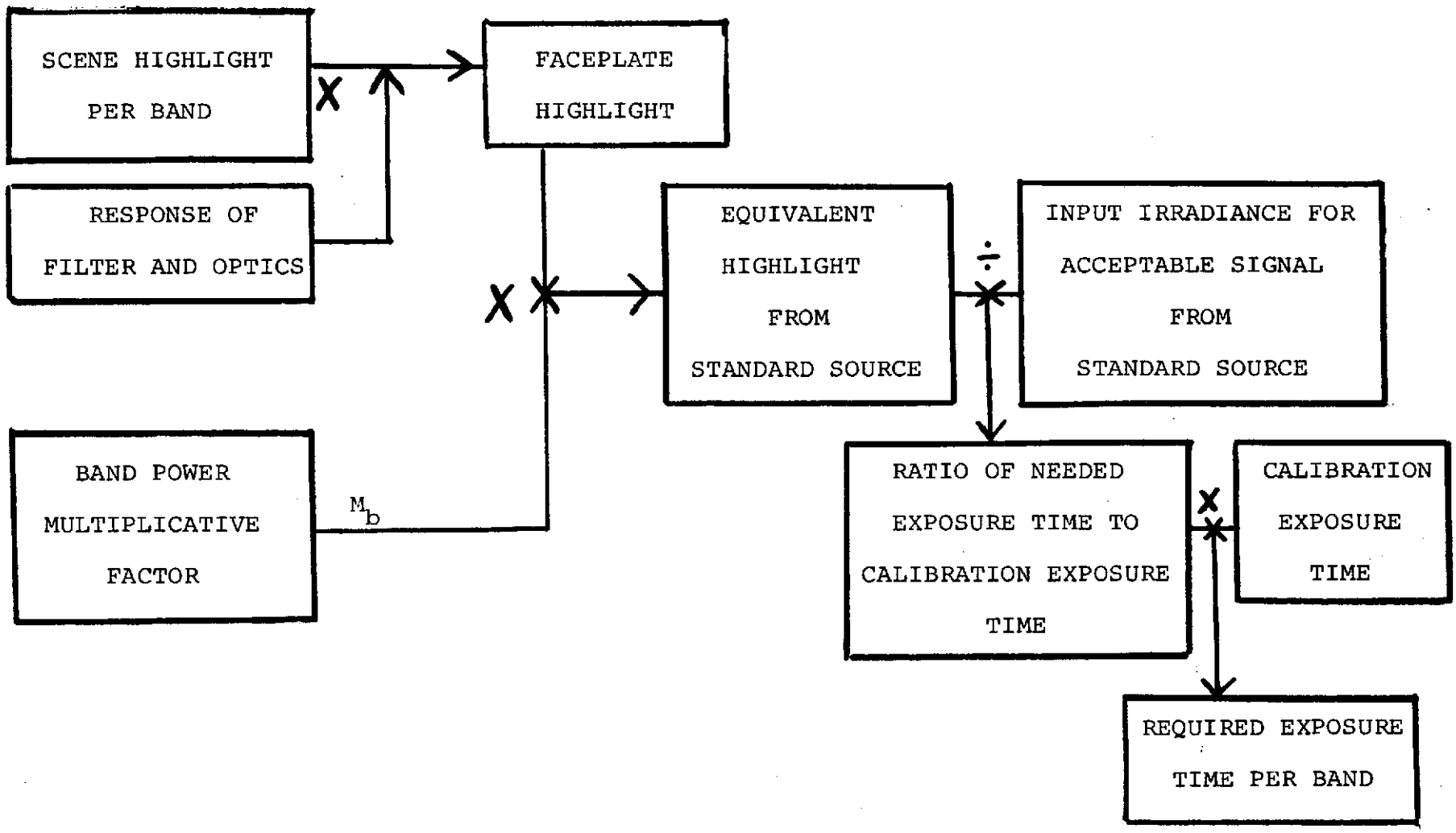

Figure V-20. Procedure for Determining Exposure Time for Each Scene per Spectral Band

$$M_b = \frac{R_b}{\int_0^\infty E(\lambda)\ R(\lambda)\ d\lambda}$$

where R_b is the average tube response for spectral band "b"

$R(\lambda)$ is the tube response at wavelength λ.

$E(\lambda)$ is the fractional spectral emittance density from the source at wavelength λ defined as:

$$E(\lambda) = \frac{e(\lambda)}{\int_0^\infty e(\lambda)\ d\lambda}$$

where $e(\lambda)$ is the spectral emittance density of the source at wavelength λ. In practice the integrals were determined by noting that $R(\lambda)$ is essentially zero except in the visible and near IR (see Figure III-4) and approximating them by summing over narrow bands.

The exposure time is computed in a second step as indicated in Figure V-20. The scene highlight is the radiant emittance given in $\mu w/cm^2$ determined by multiplying by π the basic scene radiance data provided in $\mu w/cm^2$-ster. The faceplate highlight (FPHL) is obtained by:

$$\text{F.P.H.L.} = \frac{\text{scene highlight x lens transmission x filter trans.}}{4(F/No)^2}$$

The filter transmission is taken as 1.0 for the wide bands used for the SIT and SEC cameras, but for the narrow bands for the multispectral observations with the silicon vidicon, a conservative value of 0.5 is used.

The equivalent highlight is then obtained by multiplying by the multiplicative factor. For each camera an acceptable output signal has been determined based on observed scene contrast and desired resolution as outlined in Section V-2. For cameras with SIT or SEC tubes, exposure requirements for an acceptable signal from a standard source can be determined from the bright sun calculations of Section V-2. For the SIT, the exposure time of 6×10^{-7} seconds provides a faceplate exposure of $6 \times 10^{-7} \times 1.88 = 11.28 \times 10^{-7}$ lumen-seconds which gives the desired SNR of 40. A standard tungsten source at a color temperature of 2854°K is less efficient than the sun by a factor of 1.24 for the SIT tube response. Hence, the exposure must be increased to 14×10^{-7} lumen-seconds to provide the desired SNR. Converting from photometric to radiometric units using a factor of 20 lumens/watt, the corresponding exposure is:

$$\frac{14 \times 10^{-7}}{20} = 0.7 \times 10^{-7} \text{ watt-seconds.}$$

The irradiance on the faceplate is given by:

$$\frac{\text{Exposure}}{\text{Time}} \times \frac{1}{\text{Area}} = \frac{.7 \times 10^{-7}}{6 \times 10^{-7}} \times \frac{1}{(2.83)^2} = 0.0146 \text{ watts/cm}^2$$

Thus for the SIT tube for the "standard source" input irradiance for Figure V-20, we use 0.0146 watts/cm^2, and for the calibration exposure time, 6×10^{-7} secs.

For the SEC camera, the exposure for 6.2×10^{-7} seconds is computed to be 6.76×10^{-7} lumen-seconds from the sun or 8.38×10^{-7} lumen-seconds from the tungsten source. In radiometric terms this gives 0.418×10^{-7} watt-secs exposure and a "standard source" irradiance (for Figure V-20) of 0.021 watt/cm^2 to go along with the exposure time of 6.2×10^{-7} seconds.

For the silicon vidicon, the scene data requirements, Section IV-4-C, indicate the need for a high signal to noise ratio; 71:1 was chosen. Using the manufacturer's data sheets based on a standard exposure time of 1/60 second, the required exposure is 77×10^{-9} watt-seconds/cm^2 for the desired SNR, and the standard source faceplate irradiance is 4.62×10^{-6} watts/cm^2.

B. Tabulated Exposure Times for Each Camera

Tables V-2, V-3, and V-4 give the exposure times and contrasts for the scene conditions determined in Section IV-4 for each camera type. Using these contrasts with the resolving power curves of Section V-2 above, one can determine the resolution achieved at the faceplate highlight and,at any other point in the frame with a radiance of a fraction of that highlight. For Tables V-2 and V-3, note that only one set of results is given for the low stratus cloud scenes even though the total radiances varied somewhat depending on the background. The variation was small (< 4%); so, we conservatively used the lowest total radiance for all backgrounds.

Table V-2 shows that the high resolution observations can be easily achieved even at 80° zenith angles within the allowable one second exposure time for the RBV. Even for the vegetation vs. water observations where the best spectral band was not chosen (better contrast being achieved for longer wavelength), less than 1/4 second exposure is required at 80° zenith angles. Thus, the radiance could be decreased by a factor of four, which would give a zenith angle very near sunset, and the exposure time could still be less than one second.

In Table V-3, for the moonlight scenes, note that there is only one set of exposure times and contrast given (not two) for both the SIT and for the SEC. This is sufficient since both tubes use the same S-20 surface and, therefore, have the

TABLE V-2. EXPOSURE TIME REQUIREMENTS FOR RBV CAMERAS* FOR HIGH RESOLUTION SCENES

Scene	Parameter \ Solar Zenith Angle	16.5°	48°	68.5°	75.5°	80°
High Cumulus	Exposure Time (msec)	4.6	6.82	14	22.2	37.5
vs. Water	Contrast	10.4	12.1	11.1	9.6	8.09
Vegetation	Contrast	5.2	5.75	6.23	6.21	6.27
Soil	Contrast		3.36	3.82	4.15	4.8
Low Stratus	Exposure Time (msec)	8.0	12.8	30	54.5	107
vs. Water	Contrast	3.85	3.94	3.46	2.96	2.31
Vegetation	Contrast	2.48	2.52	2.39	2.17	1.93
Soil	Contrast		1.69	1.67	1.62	1.57
Vegetation	Exposure Time (msec)	26.1	42.9	90.9	143	240
vs. Water	Contrast	1.84	1.79	1.58	1.43	1.21
Snow	Exposure Time (msec)		11.8	28.6		
vs. Soil	Contrast		1.76	1.68		

* 0.55 - 0.70 μm Spectral Band

TABLE V-3. EXPOSURE TIME REQUIREMENTS FOR SIT AND SEC CAMERAS FOR MOONLIGHT SCENES

MOON PHASE		FULL MOON							
SCENE		HIGH CUMULUS VS				LOW STRATUS VS			
			WATER	VEG	SOIL		WATER	VEG	SOIL
PARAMETER		EXP TIME (SEC)	CONTRAST			EXP TIME (SEC)	CONTRAST		
ZENITH ANGLE	SPECTRAL BAND								
16.5°	.4 - .7μ	.35	8.9	5.34		.60	3.31	2.41	
	.45 - .7	.42	9.35	5.32		.73	3.46	2.44	
	.5 - .7	.57	10	5.24		.98	3.66	2.45	
	.55 - .7	.87	10.6	5.1		1.5	3.84	2.45	
48°	.4 - .7μ	.52	10.3	6.03	3.58	.99	3.47	2.48	1.73
	.45 - .7	.625	10.8	5.97	3.51	1.2	3.65	2.51	1.73
	.5 - .7	.85	11.5	5.86	3.42	1.6	3.86	2.52	1.71
	.55 - .7	1.3	12.1	5.71	3.3	2.4	4.08	2.52	1.68
68.5°	.4 - .7μ	1.1	9.25	6.1	4.01	2.4	2.94	2.27	1.67
	.45 - .7	1.3	9.83	6.25	3.99	2.8	3.1	2.36	1.68
	.5 - .7	1.7	10.5	6.25	3.91	3.8	3.3	2.36	1.68
	.55 - .7	2.6	11.2	6.19	3.8	5.6	3.5	2.38	1.67
75.5°	.4 - .7μ	1.7	7.78	5.85	4.2	4.4	2.43	1.99	1.57
	.45 - .7	2.1	8.44	6.07	4.26	5.2	2.59	2.06	1.6
	.5 - .7	2.8	9.09	6.17	4.21	6.9	2.76	2.13	1.61
	.55 - .7	4.1	9.73	6.23	4.14	10	2.94	2.17	1.61
80°	.4 - .7μ	3.0	6.4	5.43	4.42	8.5	1.9	1.69	1.45
	.45 - .75	3.5	6.92	5.74	4.57	10	2.03	1.77	1.49
	.5 - .7	4.5	7.53	6.05	4.7	13	2.18	1.85	1.54
	.55 - .7	6.9	8.18	6.31	4.79	20	2.34	1.94	1.58

same spectral response. Note also that we have only given full moon data for all the spectral bands examined. One can see that the widest spectral band, .4 - .7 μm, offers a substantial reduction in exposure time over the other bands, e.g., almost 2.5:1 over the narrowest band, .55 to .7 μm. This is achieved at a very small sacrifice in contrast - about 20% reduction between the two extreme bands. Hence, it is logical to recommend the selection of the .4-.7 μm band. Figure V-21 shows the exposure times required for partial moons vs. lunar zenith angle. As can be seen, both the cooled SIT tube (2 secs. max) and the SEC (9 seconds max) offer possibilities for observation under partial moon conditions. Cooling the SIT further, could improve its capabilities, but 9 or 10 seconds is probably a reasonable limit on holding the spacecraft stable.

Table V-4 provides the results for the silicon vidicon camera for the multispectral earth resources observations. In addition to exposure time, two contrasts are tabulated for each set of conditions. By maximum contrast, we mean the ratio of the scene highlight to the path radiance. This is actually the upper bound on the contrast that could exist in the scene. For resolving power determination, however, we must use the minimum contrast, which is the ratio of the highlight to the highlight minus the smallest change we wish to detect from Table IV-9).

The exposure times listed are for only two solar zenith angles. Recalling that the purpose of this camera is to extend the multispectral observations to poorer sun conditions (i.e., larger zenith angles), we must extrapolate the zenith angles until the limiting exposure time for the silicon vidicon (0.1 seconds as noted in V-2-C) is reached for the worst spectral band. For estuaries and fishing area observations, the band with the worst exposure time is .7 - .73 μm, for oil pollution it is .65 - .69 μm, and for thematic mapping, it is .60 - .65 μm. We extrapolate by taking the ratio R, of

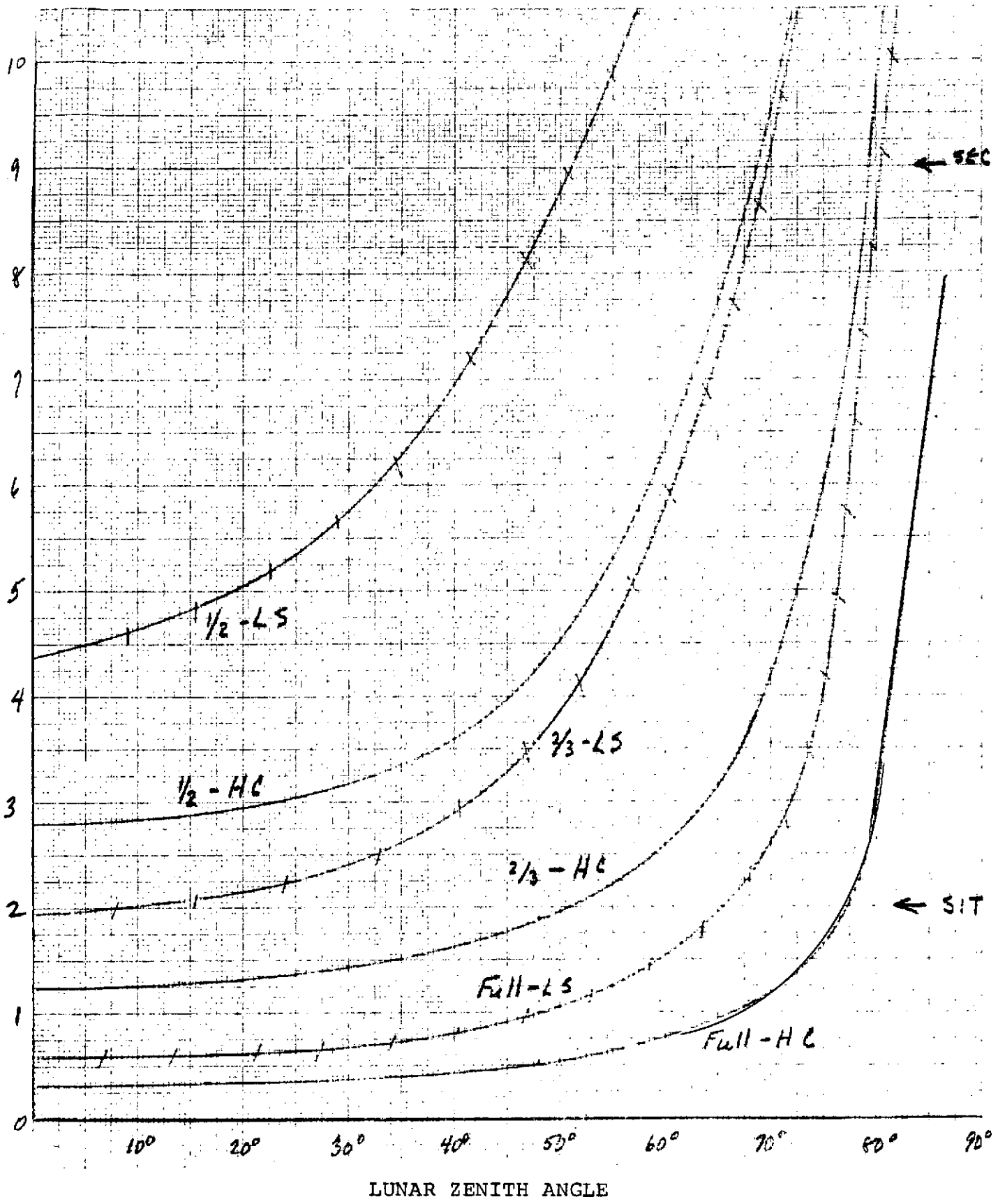

Figure V-21. Exposure Times for Partial Moonlight for High Cumulus and Low Stratus

TABLE V-4 EXPOSURE TIME REQUIREMENTS FOR SILICON VIDICON MULTISPECTRAL OBSERVATIONS

Spectral Band (μM)	.42-.46	.47-.56	.53-.57	.56-.60	.60-.65	.65-.69	.7-.73	.78-.82	.89-.95
Application									
Estuaries @ 15.5°									
Max Cont = Highlight / Parts Rad	1.22	1.3	1.56	1.47	1.21	1.73	1.34		
Min Cont = Highlight / HL - Smallest Change	1.02	1.03	1.04	1.03	1.10	1.09	1.15		
Exposure Time (msec)	3.34	1.08	2.20	10.4	12.4	5.6	12.6		
75.5° Max C	1.2	1.29	1.57	2.02	1.27	1.66	1.33		
75.5° Min C	1.02	1.03	1.04	1.04	1.12	1.08	1.19		
75.5° Exposure Time (msec)	14.5	6.0	12.6	10.4	64	28	66.8		
Fishing									
6.75° Max C	1.33	1.5	1.99	1.83	1.47	2.28	1.63		
6.75° Min C	1.03	1.04	1.06	1.05	1.19	1.12	1.24		
6.75° E. T. (msec)	3.34	1.2	2.6	2.2	14	5.6	14		
48° Max C	1.33	1.51	1.98	1.83	1.44	1.98	1.59		
48° Min C	1.03	1.04	1.06	1.05	1.18	1.10	1.22		
48° E T (msec)	11.8	4.4	6.0	2.8	19.6	9.2	20		
Oil Pol.									
6.25° Max C		1.67	2.1	1.92		3.46			
6.25° Min C		1.07	1.2	1.1		1.17			
6.25° E T (msec)		1.08	2.4	2.0		3.6			
68.6° Max C		1.67	2.08	1.92		3.44			
68.6° Min C		1.07	1.2	1.1		1.17			
68.6° E T (msec)		6.0	12.2	10.4		18			
Them. Map									
15.1° Max C	1.46	1.6	2.25	2.56	3.64	6.61	8.03	26.3	4.18
15.1° Min C	1.03	1.02	1.06	1.04	1.04	1.02	1.04	1.01	1.02
15.1° E T (msec)	2.2	.86	1.76	1.18	4.2	1.46	2.2	1.2	1.26
68.1° Max C	1.47	1.59	2.22	2.55	3.78	6.39	8.01	28	4.18
68.1° Min C	1.03	1.02	1.05	1.04	1.04	1.02	1.04	1.01	1.02
68.1° E T (msec)	9.4	3.8	7.0	4.0	17	5.8	8.6	46	5.0

0.1 seconds to the exposure time in these bands at the high zenith angles. Using Figure IV-5, which was generated for this purpose, we find the angle for which the radiance value of the corresponding band has the inverse ratio, $\frac{1}{R}$, to the value at the given zenith. For example, for fishing, at 48° zenith angle, $R = \frac{.1}{.020} = 5$. From Figure IV-5, the 0.725 μm graph gives 0.248 at 48° and 0.05 at about 83°. Hence, 83° can be taken as a rough approximation of the limiting zenith angle for fishing area observations. Similarly, we get the other values in Table V-5. We also show the corresponding diurnal time for each zenith angle at the same locations and at the summer solstice. At other times of the year, the diurnal time would be different.

TABLE V-5. MAXIMUM ZENITH ANGLES FOR MULTISPECTRAL APPLICATIONS

APPLICATION	MAXIMUM ZENITH ANGLE	LATEST TIME* OF OBSERVATION AT SUMMER SOLSTICE
Estuaries	81°	1830
Fishing Areas	83°	1823
Oil Pollution	89°	1852
Thematic Mapping	84°	1846
* Same target locations assumed.		

4. Camera Operational Sequence

A. High Resolution Camera

The operational sequence for the high resolution RBV camera consists of an erase/prepare interval, an expose interval, and a time devoted to reading out the information stored in the photoconductor. The total time devoted to a picture frame is 13 seconds as illustrated in Figure V-22.

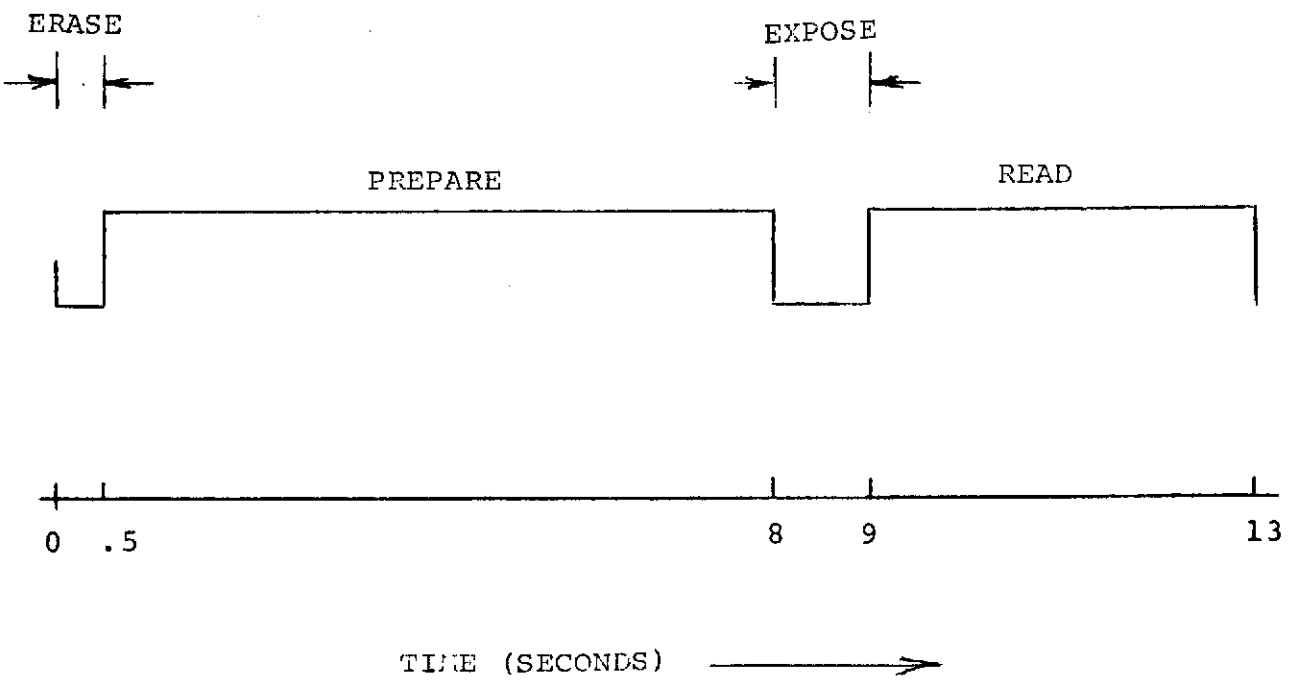

Figure V-22. High Resolution Camera Operational Sequence

The 0.5 second erase interval is devoted to flashing a set of target lamps to erase old information. A total of 7.5 seconds, consisting of 15-1/2 second frames is spent in charging the photoconductor in preparation for the next exposure. During this time, the cathode current of the RBV is operated at a relatively high level to ensure that a uniform potential is obtained on the photoconductor.

It appears, based on the computations of the previous section, that 1.0 second is adequate for the complete range of exposure times required. At the minimum, the exposure time will be 4.5 milliseconds. The lower extreme is based on extensive experience with the ERTS shutter mechanism, which provides excellent exposure uniformity for times in excess of this value.

Several factors lead to the choice of a 4 second read interval. Reading more rapidly requires an increase in RBV beam current (which tends to reduce resolution) in order to read out the same photoconductor charge in a shorter time interval. In addition, the bandwidth required to handle the signal information increases as the read interval is decreased. On the other hand, lengthening the read interval increases the total frame time and decreases the total number of frames that can be taken during the daylight hours.

The horizontal scan rate postulated here is the same as that employed for the ERTS cameras, 1250 lines per second. Of the 800 microseconds horizontal time, 90 percent is active with the remaining 10 percent, devoted to retrace and signal processing, being blanked. The required bandwidth for a maximum of 90 lp/mm (4600 picture elements) is computed by:

$$BW = \frac{\text{Pixels/Line}}{2} \times \frac{\text{Scan Rate}}{\% \text{ Active}}$$

$$BW = \frac{90 \times 2 \times 25.4}{2} \times \frac{1250}{.9} = 3.2 \text{ MHz}$$

The vertical read interval of 4 seconds permits an active read time of 3.8 seconds and an instrumentation and data interval (time code, calibration, etc.) of 0.2 seconds. A total of 4750 active scan lines will result. This value is adequate for the reproduction of more than 4500 elements in the vertical direction. (A somewhat smaller ratio of active lines to available resolution elements was used on the ERTS camera where spacecraft motion was a factor).

These operating rates are compatible with the sensor performance as related to SNR. Minimum specification value of 33 dB can be obtained to permit the resolving power performance computed in the previous section. In general, somewhat better performance can be expected for most of the units.

B. Nighttime Camera

a. SIT Sensor

The operational sequence for the SIT camera, shown in Figure V-23-a is similar to that described for the RBV camera. Since erasure of the silicon target is easier, two simplifications are noted: erase lamps are not required, and the number of scans required to erase and prepare is much smaller. Two scans at the normal read rates should lower residual signal to less than 3 percent.

The total time devoted to a single picture frame is 2.6 seconds. Three 0.1 second erase frames are postulated with a total prepare interval of 0.4 seconds followed by a two second expose interval. The read time is accomplished within a 0.2 second interval following exposure, with 0.12 seconds being active read information time and .08 seconds available for instrumentation data.

The horizontal scan rate is 10,000 per second. For an active frame time of .12 seconds, this rate results in 1,200 scan

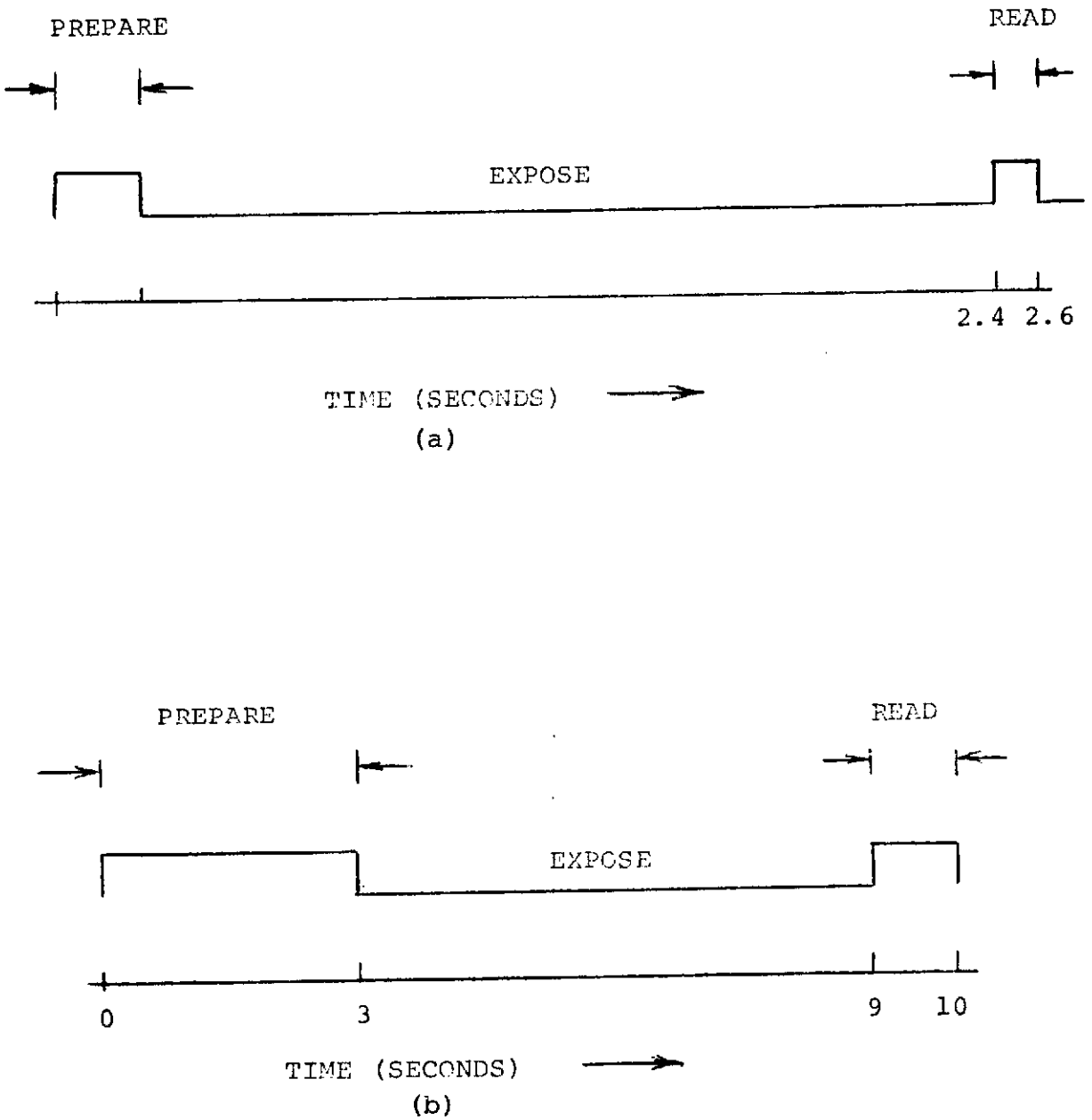

Figure V-23. Nighttime Camera Operational Cycle, a) SIT, and b) SEC Sensor

lines per frame. A total of 943 picture elements per line was initially assumed in the resolving power computations requiring a bandwidth of (943/2) x (10,000/.85) = 5.55 MHz with an active line time of 85 percent. This bandwidth is increased to 5.7 MHz to permit full resolution on high contrast scenes.

The vertical time of .12 seconds provides 1200 active scan lines per frame. This is sufficiently above the 943 element picture content to permit full resolution in the vertical direction.

The horizontal rate assumed here is sufficiently close to the data sheet rates (broadcast standard) to permit direct use of the information on MTF, dark current and erasure. Generally, the read rate may be increased until either the amplifier noise becomes significant compared to the electron stream noise, or the increased read current starts to degrade the MTF performance. Conversely, the rate may be slowed until the total frame time is too long or dark current causes an intolerable loss in signal information. Within these limits, there is a relatively broad area of satisfactory performance.

b. SEC Sensor

The operational sequence for the SEC camera, considered a possible alternate to the SIT, is shown in Figure V-23-b. The lower photocathode-to-target gain of the sensor requires that the read-out rate be slowed down to lower the amplifier noise relative to the electron stream noise. The read time as shown in the figure is 1.0 second in contrast to the .12 second interval for the SIT. Other than lengthening the frame time, no negative effects accrue to the operation of the SEC. The virtual absence of dark current in this target permits frame times substantially longer than are tolerable for the silicon target.

The scan rate for the SEC is established at 1000 lines per second. With 720 elements per scan line and 85 percent active time, the required bandwidth is $\frac{720}{2} \times \frac{1000}{.85} = 424$ kHz. A further reduction in scan rates is quite feasible with this sensor, although the rather lengthy resulting frame time would appear to be a potential disadvantage. A shortening of the read time does not appear to be feasible since a degradation in SNR will result.

c. Multispectral Camera

Daylight, multispectral, picture taking may be accomplished with a silicon sensor in a total frame time of 0.54 second. The operational cycle is shown in Figure V-24 for a read time of .14 second with the final 40 milliseconds devoted to an instrumentation interval.

During the active time of 0.1 second, the target is scanned at a 10,000 line per second rate. At the design packing density of 35 lp/mm and the 11.3 mm target dimension, the required bandwidth is 4.66 MHz. For this read rate, target temperatures may range to 30°C without substantial degradation due to dark current. Controlling the target temperature to lower values would permit scanning more slowly resulting in decreased amplifier noise and with an improvement in the 37 dB SNR postulated for the resolving power computations. Improved resolving power would, of course, result. (Note that the signal decreases linearly with scan rate while the noise decreases as the 3/2 power, approximately, in the range of operating rates).

A total of 1000 scan lines per frame are employed. This value is sufficient to obtain the full resolution capability (about 800 elements) of the silicon sensor.

Following the read interval, three erase/prepare cycles totaling .3 seconds will be employed. This should be adequate to remove old information and fully charge the reverse-biased silicon

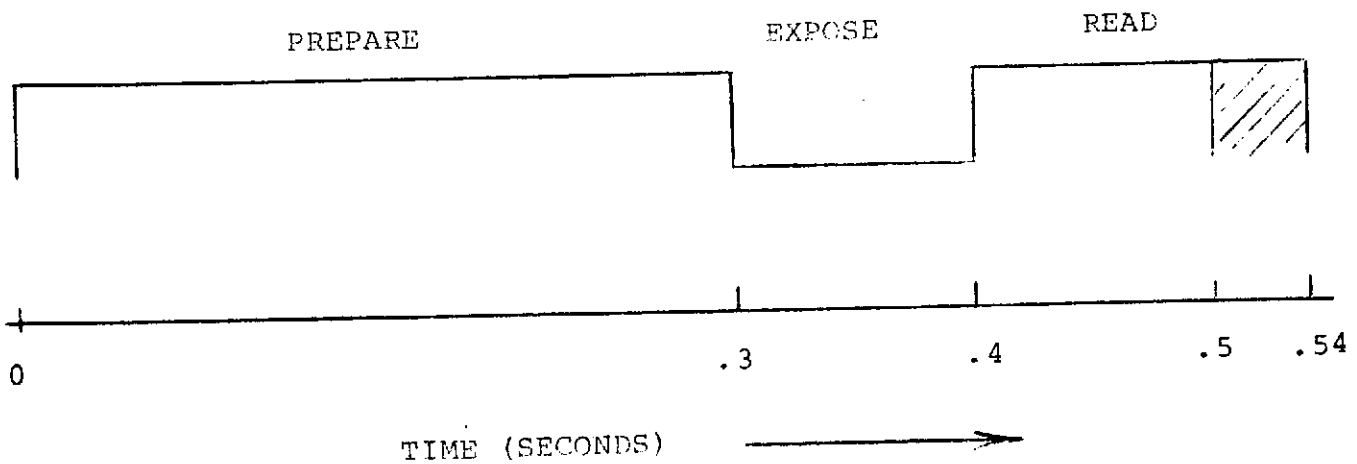

Figure V-24. Multispectral Camera Operational Sequence

diodes for the next exposure. Computations in the previous section indicate that a maximum exposure time of 0.1 second is adequate for the range of scene data over a substantial portion of daylight hours. A minimum exposure of 4.5 milliseconds will be employed, further reduction in faceplate irradiance, when required, being accomplished with neutral density filters.

VI. OPERATIONAL MODES

1. Introduction

Throughout this study we have assumed that all three of the frame cameras may be available on SEOS for use at different times for their respective applications. As noted in Section V-4, the total operational cycle times for all the cameras for a single scene observation are quite short. The maximums are 13 seconds for the RBV camera, 2.6 seconds for the SIT camera, 10 seconds for the SEC camera, and 4.9 seconds for the silicon vidicon camera. The latter value results from assuming sequential use of the camera for 0.54 seconds for each of the nine bands desired for thematic mapping applications. With such short times, it should be easily possible to fit the operation of any of the cameras for single scenes within the time used by other instruments (e.g., scanning IR radiometers or pushbroom scanners) sharing the LEST. It should even be possible, for larger area coverage, to fit in multiple frame camera cycles with the camera being pointed for each frame, either within a fixed, total LEST field or by pointing the whole LEST-plus-cameras configuration.

There are, therefore, three major items that should be considered for the operations of the three cameras with LEST. First, one must consider how to switch from one frame camera to another. Second, a concept is needed to permit changing of spectral filters to change the spectral band or adding of neutral density filters to cut the exposure to lower levels than can be achieved with the shutter alone. Third, a concept for pointing a frame camera within the LEST field would be desirable to avoid having to point the complete LEST for each small change in scene location. It is assumed for the purposes of this discussion that LEST is an f/6 telescope with a 400 x 400 km field of view at nadir from synchronous altitude.

2. Switching Between Frame Cameras

Several different alternatives exist for mounting the three cameras and switching between them. Two alternative possibilities are suggested.

The simplest and perhaps most easily visualized is a "lollipop" mirror with the input energy coming in along the axis of the lollipop (Figure VI-1a). The three cameras would be placed at say 120^{o} intervals around the lollipop mirror at different distances to accommodate the different focal lengths (Figure VI-1b). Rotation of the lollipop directs the input scene to the selected camera. Such a system would appear to be quite feasible and relatively compact.

Another alternative using two relay mirrors is shown in Figure VI-2. Camera 1 is used when mirror M_1 is in the horizontal, dotted line position; Camera 2, when M_1 and M_2 are both in the (solid line) diagonal positions, and Camera 3 when M_1 is on the diagonal and M_2 is in the vertical, dotted line position. Other alternatives are possible also.

3. Spectral and Neutral Density Filters

As indicated in Section V-3, the range of exposure times for the RBV camera is approximately 5 milliseconds to one second. For the silicon vidicon, it may be in the range of about 0.5 millisecond to 0.1 second. For moonlight scenes for the SIT it is about 0.3 - 2 seconds and for the SEC, 0.3 - 9 seconds. If we wanted to consider the possible use of these low light cameras for sunlight scenes, e.g., in the case of a failure of another instrument, then the exposure time could be reduced by about 10^{-6} since the sun provides about 10^{6} as much light as the full moon.

As noted previously, the existing shutter which has been used for the RBV camera on ERTS can accurately provide exposure times down to about 4.5 milliseconds. It would appear, therefore, that the shutter alone is adequate for the high resolution, daylight observations. For the SIT or the SEC, no

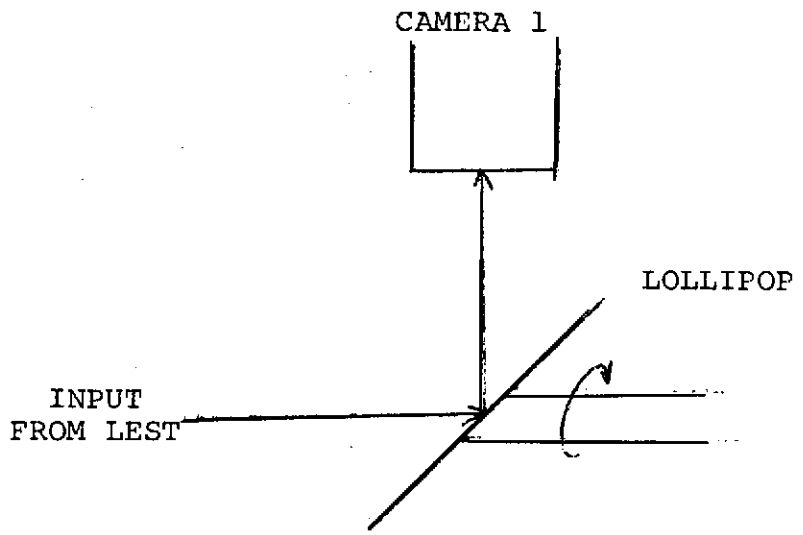

Figure VI-1a. Reflection of LEST Input Using Lollipop Mirror

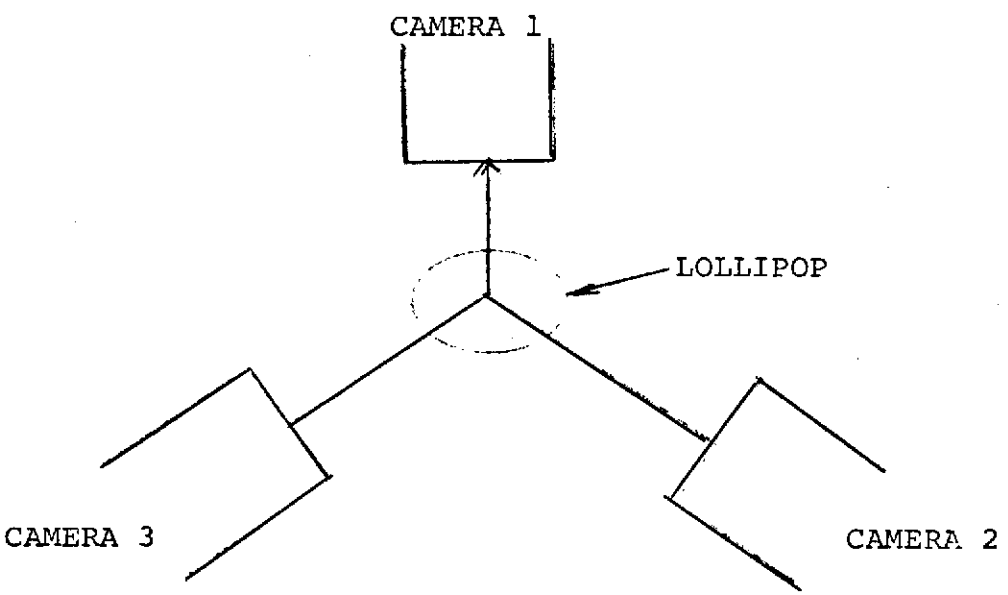

Figure VI-1b. Camera Arrangement Using Lollipop Mirror for Switching

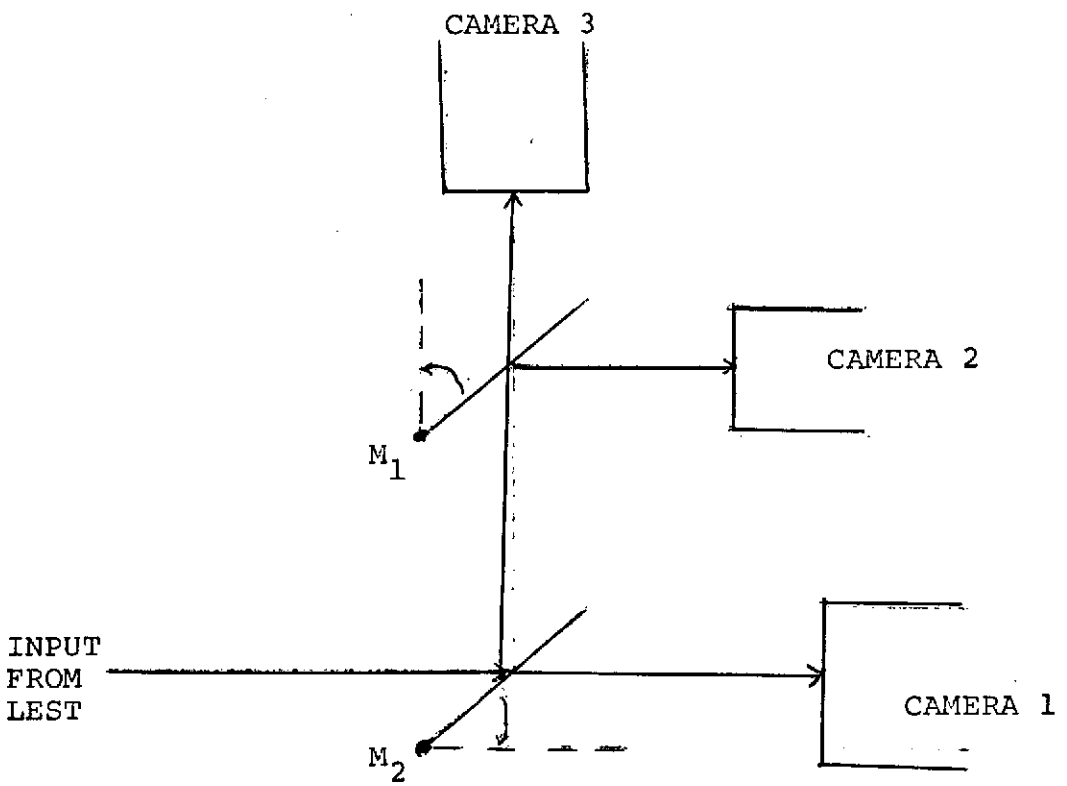

Figure VI-2. Camera Switching Alternative 2

neutral density (N.D.) filters would be necessary to supplement the shutter for moonlight operations, but filters would be necessary if sunlight operations are permitted with this camera. Two N.D.'s, one with an attenuation factor of 10^4 for mid-day sunlight and the other with a 10^2 attenuator for near sunset and sunrise, are suggested. They could be mounted on a segmented wheel along with a transparent segment with no attenuation for moonlight operations. (Alternatively the electron gain of the intensifier section could be reduced to lower the range required of the N.D. filters.)

For the silicon vidicon, a filter wheel is suggested since nine spectral filters will be needed for 9 bands. From Table V-4, neutral density filters with attenuation filters of 10 are sufficient for each band along with a no-attenuation position. For some bands it might be sufficient to have the 1/10 filter alone, but conservatively we can assume either an 18-position filter wheel with two positions for each band, or a 9 segment filter wheel in cascade with a second 2-position attenuator.

4. Optical Pointing

The proposed frame cameras will not cover the desired 400 x 400 km field of view with the desired resolution. With an object distance of 35,800 km and an entrance pupil diameter of 1.5 m, a camera with a 25.4 mm square raster operating at f/4 will cover a 152 x 152 km area, a camera with an 11.3 mm square raster operating at f/2.7 will cover a 102 x 102 km area, and a camera with a 28.3 mm square raster operating at f/2.4 will cover a 283 x 283 km area. If it is not feasible to point the entire camera optical system to obtain coverage of all regions within the 400 x 400 km area, it is possible to design an optical system with moving components to accomplish the same objective. Translation of the cameras provides an obvious solution to the problem, but if this also is considered impractical, there seem to be few

methods which are practical. In fact, the design described below is the only one so far identified which is consistent with the geometry of a large Cassegrain type primary objective system and which results in what might be considered to be reasonable requirements on the first order characteristics of the optical components.

The operational principles of the proposed approach are explained with reference to the first order layout shown in Figure VI-3. The first two components at the left, a positive lens followed by a negative lens, represent the action of the Cassegrain primary objective in bringing the incoming energy to focus at the primary focal plane. The dashed line traces the path of the chief ray for an off-axis image point, which, since the primary mirror of the Cassegrain objective is the entrance pupil of the system, passes through the center of the primary mirror. The next lens is primarily a field lens since choice of power of this lens is used to control the point along the optical axis at which, in the absence of the final lens, the chief rays of off-axis points would converge. The following lens is primarily a collimating lens, with its power so chosen that energy from a point in the primary image plane is collimated in the space between it and the final lens. (In practice, the powers of the field lens and the collimating lens are chosen in conjunction to produce the desired collimation and the desired intersection point of the chief rays.) The final lens is a focusing lens so placed that the intersection point of the chief rays (in the absence of this lens) lies in the focal plane of the lens. Translation of the final lens in a plane perpendicular to the optical axis produces the desired image motion at the camera faceplate.

Use of a translatable focusing lens in a collimated beam to produce image motion, as described above, is a fairly obvious technique. It is not as obvious that the relationship shown between the focusing lens and the chief ray intersection is

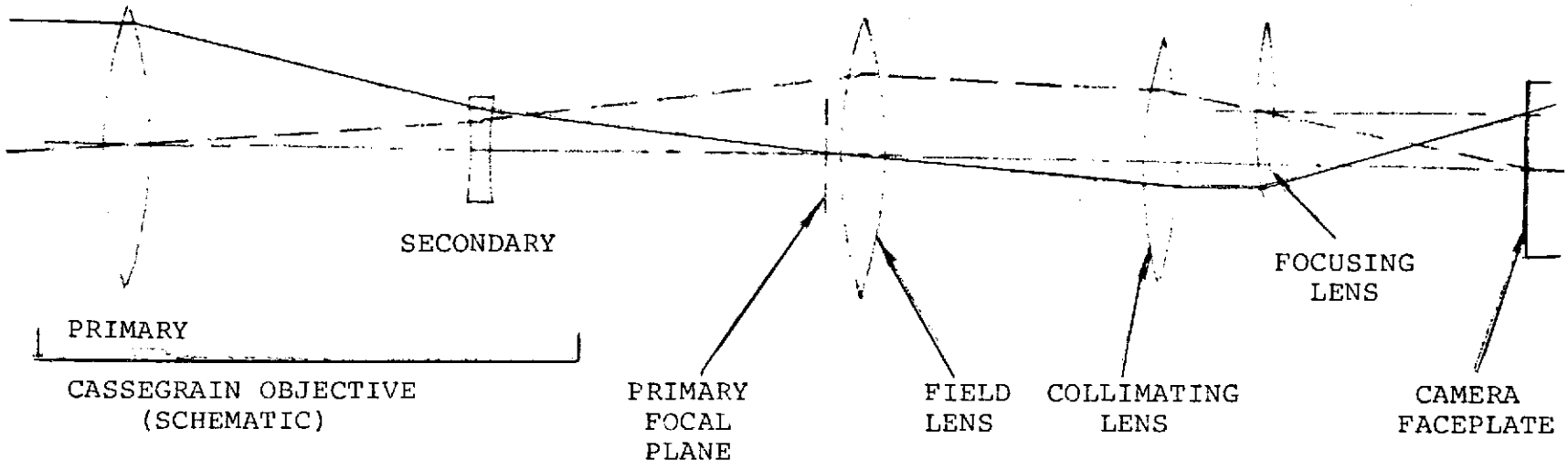

Figure VI-3. Schematic Optical Layout

necessary in order to avoid vignetting while at the same time keeping the diameter, and therefore the f-number, of the focusing lens within reasonable bounds. To assess feasibility, a sample design has been worked out, using first order ray tracing with thin lenses, to determine approximate values of lens focal lengths and diameters. Resulting values are given in Table VI-1 along with separations of successive elements. Assumptions used in this example were:

1. Primary mirror diameter is 1.5 meters,
2. Overall Cassegrain f-number is 7,
3. Mirror separation is 3 meters,
4. Distance from secondary mirror to primary focal plane is 3.5 meters,
5. Primary mirror is aperture stop,
6. Camera has 1/2 inch square raster,
7. f-number at camera faceplate is 2.7.

It should be borne in mind that the "thick" lenses which would have to be designed to replace the thin lenses used in the example would probably have diameters somewhat larger than those given for the thin lenses.

It might also be noted that the size of the relay system (collimating and focusing lenses) can be scaled down to some extent, with the principal result being an increase in the diameter-to-focal length ratio of the relay lenses.

If this optical pointing method is to be used with more than one camera, switching can be done with a movable mirror (e.g., a lollipop) between the final lens and the camera faceplate. If the cameras are operated at different f-numbers, this infers also different overall focal lengths, and a change in the optical system is required. This change

TABLE VI-1. SAMPLE DESIGN PARAMETERS

ELEMENT	FOCAL LENGTH (METERS)	DIAMETER (METERS)	SEPARATION (METERS)
Primary Mirror	4.5	1.5	3.0
Secondary Mirror	2.63	0.55	3.5
Focal Plane	N.A.	0.17	0.1
Field Lens	1.15	0.18	0.66
Collimating Lens	0.77	0.20	0.13
Focusing Lens	0.27	0.11	0.27
Camera Faceplate	N.A.	0.018	

can be effected by replacing the focusing lens with a lens of different focal length. For example, if an f/4 imaging cone is desired at the camera faceplate, the 0.27 meter focusing lens must be replaced by a 0.40 meter lens. If space permits, this lens should also be so placed that the intersection of the chief rays lies in its focal plane; and in this case the principles shown in Figure VI-3 are still applicable. If the lens cannot be so placed, the camera faceplate must be relocated to coincide with the focal plane of the lens, with the result that the chief ray to the center of the camera faceplate will not pass through the center of the focusing lens (when the focusing lens axis is displaced from the collimating lens axis). This causes an increase in the required diameter of the focusing lens. For the example of the 0.40 meter lens placed at the same location as the 0.27 meter lens, the diameter would have to be 0.144 meter as opposed to 0.136 meter for ideal placement of the lens.

VII. MECHANICAL AND ELECTRICAL CHARACTERISTICS

1. Introduction

This section contains interface information which will be useful for potential mission planning purposes. Estimates are given for volume, weight, and power consumption for each of the three types of cameras described in the earlier sections. The basis for the estimates are spacecraft hardware containing the same or similar sensors that were designed and fabricated under previous NASA contracts with AED. Specifically, the ERTS RBV multispectral cameras and the Apollo color camera are similar in many respects to the cameras described.

It is assumed for estimating purposes that optical elements are treated separately and are not part of the cameras. This includes mirror or prism elements that may be required to direct the target view to a particular frame camera. Other elements separated from the estimate are neutral density and spectral filter mechanisms and associated electronics drive circuitry. These may be presumed to weigh in the 2 to 4 pound category for each mechanism with associated intermittent power consumption that will be negligible when averaged over typical operating times.

2. Volume and Weight Estimates

The mechanical estimates of volume and weight assume that there are three components which make up a camera system. Each camera will consist of a camera head, a camera electronics component, and a controller and formatter component. The units may be physically separated and interconnected with harnessing of appropriate length as in the ERTS design. Alternatively, all three (or any two) may be integral as in the case of the Apollo camera. Interfacing spacecraft constraints as well as equipment requirements will be determining in this regard.

The camera head components, including the sensing device, are listed in Table VII-1. These include the mechanical components, required to operate the sensor, and target control circuitry and high voltage power supply which are generally integral with this assembly. In the case of the silicon sensor where an electron multiplication process is not required, no high voltage supply is required.

The camera electronics consists of the remainder of the circuitry, exclusive of timing generation, required to operate the camera and amplify and process the video information. These functions are listed in Table VII-2. In total these may occupy between 12 and 15 circuit boards, where each board is in the order of 6 x 6 inches in size. The camera controller functions are listed in Table VII-3. These include three primary circuit areas: generation of all timing and formatting signals, such as sweep synchronization, clamp and blanking timing and shutter timing; command decoding and mode generation; and video formatting. The latter functions encompass such items as sync insertion, the addition of time code, and generation and addition of calibration signals. Including self contained power supplies, about 10 circuit boards are estimated for these elements. In the event that two, or all three, cameras are flown, the controller circuitry may well be shared leading to perhaps a 10 percent volume increase as compared to a single camera. However, the volumes shown are for an assumed single camera complement.

Volume estimates for the three cameras are listed in Table VII-5. Also shown, for comparison, are present weights for the ERTS camera system. The tabulation is given for the three major elements discussed above. Note that the primary difference between the ERTS camera and the high resolution camera is due to the elimination of the lens and lens mount arrangement for the SEOS camera.

TABLE VII-1. CAMERA HEAD COMPONENTS

IMAGING ASSEMBLY

- Sensor
- Deflection Yoke
- Alignment Coils
- Thermal Control Elements
- Target Voltage Controller
- Spectral Filter and Mount

ELECTROMAGNETIC FOCUS ASSEMBLY

- Housing
- Focus Coils

HIGH VOLTAGE POWER SUPPLY

MOUNTING FEET

SENSOR CIRCUITS

- Video Pre-amplifier
- Deflection
- Beam Current Regulator

TABLE VII-2. CAMERA ELECTRONICS FUNCTIONS

Low Voltage Power Supplies and Regulators
Focus Current and Alignment Current Regulator
Thermoelectric Controller
Shutter Drive
Video Amplifier
Shading Correction
Electronic Clamp

TABLE VII-3. CONTROLLER CIRCUIT FUNCTIONS

Command Decoder
Mode Controller
Timing
Frequency Divider
Expose Control
Gating Logic
Level Gating
Video Gating and Clipper
Power Supply

TABLE VII-4. CAMERA COMPONENTS VOLUME ESTIMATES FOR WIDTH x HEIGHT x LENGTH IN CENTIMETERS (DIMENSIONS IN INCHES ARE IN PARENTHESIS)

COMPONENT	ERTS	HI-RES	NIGHTTIME (SIT)	MULTISPECTRAL
Camera Sensor	20.3 x 21.6 x 60 (8 x 8.5 x 23.6)	20.3 x 21.6 x 48.3 (8 x 8.5 x 19)	20.3 x 20.3 x 56 (8 x 8 x 22)	12.7 x 15.2 x 40.7 (5 x 6 x 16)
Camera Electronics	15.2 x 15.2 x 33 (6 x 6 x 13)	15.2 x 15.2 x 33 (6 x 6 x 13)	15.2 x 15.2 x 33 (6 x 6 x 13)	15.2 x 15.2 x 33 (6 x 6 x 13)
Controller*	15.2 x 15.2 x 33 (6 x 6 x 13)	15.2 x 15.2 x 26.7 (6 x 6 x 10.5)	15.2 x 15.2 x 26.7 (6 x 6 x 10.5)	15.2 x 15.2 x 20.3 (6 x 6 x 8)

*Controller volumes listed assumed single camera complements. Double or triple camera installations will be approximately ERTS controller dimension.

TABLE VII-5. CAMERA WEIGHT ESTIMATES IN KILOGRAMS
(WEIGHT IN POUNDS ARE IN PARENTHESIS)

COMPONENT	ERTS	HI-RES	NIGHTTIME (SIT)	MULTISPECTRAL
Camera Sensor	17.7 (38.9)	14.5 (32)	15.9 (35)	11.4 (25)
Camera Electronics	6.3 (13.8)	6.3 (13.8)	6.3 (13.8)	6.3 (13.8)
Controller	4.2 (9.3)	3.9 (8.5)	3.9 (8.5)	3.4 (7.5)
Totals	28.1 (62)	24.7 (54.3)	26.0 (57.3)	21.0 (46.3)

3. Power Estimates

Power estimates for the three cameras are given in Table VII-6. These numbers are first order approximations, individual consumption for each circuit function was not estimated. An additional factor that requires careful treatment is the difference in levels drawn by the cameras during various portions of the operating cycle, i.e., read, erase, and prepare. Shutter power and target lamp power required for the high resolution camera are not included since these will generally be on the unregulated bus. Approximately 1.5 watts may be estimated for this function.

TABLE VII-6. CAMERA POWER ESTIMATES

CAMERA	POWER IN WATTS
High Resolution	60
Nighttime (SIT)	40
Multispectral	25

VIII. RECOMMENDED FUTURE PROGRAM

It is felt that the material contained in this report represents a realistic first cut at defining the operational characteristics of frame cameras for SEOS. Each of the three described cameras offers potentially attractive performance features. It is suggested that a next level definition study be undertaken to characterize the cameras in further detail, and with a higher level of accuracy, to permit the generation of definitive performance specifications for a practical SEOS equipment complement.

As a starting point, the LEST characteristics should be known with reasonable accuracy to permit tailoring the requirements of the secondary optics with a higher degree of accuracy. (It is presumed that presently funded NASA contracts should result in LEST definition in a relatively short time scale.) A follow-on study would also consider the possibility of using shared optics among the cameras. Reference to Table II-1 indicates, for example, a fairly close focal length requirement for the SIT and multispectral camera. Performance penalties may be small if a single optical system is established for these units.

Differences between the LEST assumptions used and newly defined values for aperture, focal length, and MTF will impact most of the computations described in this report. Also, as a result, cycle times and rates may well be influenced.

A follow-on study would also permit generation of complete block diagrams. Timing cycles, detailing of timing intervals, and instrumentation data would be specified. Equipment interface requirements would be established and both electrical and mechanical installation constraints could be defined. Finally, program estimates would be generated for development time and costs for the cameras and associated test equipment.

IX. ACKNOWLEDGEMENTS

This report was written by H. Gurk and L. Freedman of the staff of RCA Astro-Electronics Division. Contributions to the material contained in Section III were made by J. D'Arcy, to Section V-3 by J. Barletta and Section VI by J. Armington. At the initiation and through approximately 50 percent of the effort, J. Sternberg was Program Manager; for the final portion of the effort, B. Soltoff assumed this responsibility.

APPENDIX A
GLOSSARY

ASOS	Antimony Trisulfide Oxysulfide
BW	Bandwidth
c	Contrast
C	Centigrade
dB	Decibels
fc	Foot Candle
fc-sec	Foot Candle-Seconds
fL	Foot Lambert
K	Kelvin
LEST	Large Earth Survey Telescope
lp/mm	Line Pairs per Millimeter
RBV	Return-Beam-Vidicon
M	Modulation
mm	Millimeter
msec	Milliseconds
MTF	Modulation Transfer Function
SIT	Silicon Intensifier Target (Vidicon)
SEC	Secondary Electron Conduction (Camera Tube)
SNR	Signal-to-Noise Ratio
Ster	Steradian
$\mu W/cm^2$	Micro-watts per square centimeter

APPENDIX B
COLUMN DEFINITIONS (TABLE III-1)

SIZE: Generic Bottle Size - Format for computations will be that most frequently employed on data sheets for this type.

RESOLUTION: Defined as the number of line pairs per millimeter producing 20% response to a square wave test pattern.

SENSITIVITY: Exposure required for 30 dB S/N. When data is obtained from broadcast standard operation the exposure time is assumed to be 1/60 second. Note that illumination conditions may directly affect the sensitivity.

1) Illumination with color temperature 2850°K (Tungsten source).

2) Illumination with 6000°K (Sunlight)

DYNAMIC RANGE: The ratio of the peak highlight exposure (corresponding to 30 dB S/N) to the smallest exposure increment which equals or exceeds the rms noise. Step increments increasing by $\sqrt{2}$ are assumed for grey step specification.

SPECTRAL CHARACTERISTICS: Four spectral characteristics are encompassed by the tubes listed in the table. These characteristics are defined by the nominal curves shown in Figure III-4.

GEOMETRY: Class "A" is better than 1% linearity over entire format. Class "B" is better than 1% in the central region (80% ellipse or circle) and better than 2% to the edge of the raster. Class "C" is better than 2% in the center and better than 5% to the edge.

STORAGE: A qualitative rating of the ability to usefully integrate exposure information and to read out the data relatively slowly.

Class C: Storage times in the range of 10^{-3} to 10^{-1} second.

Class B: Storage times in the range of 10^{-3} to 10^{1} seconds.

Class A: Storage times in the range of 10^{-3} to 10^{2} seconds or larger.

SHADING: Shading is defined as non-uniformity in the output signal. Two types will occur:

1) Dark Field Shading - Fluctuation in output level over the format in the absence of input radiance.

2) White Field Shading - Fluctuation in output level over the format with a constant radiant input (usually measured at peak highlight).

SHADING (Contd.): Central and edge areas defined for GEOMETRY will be used here.

Class A: Better than 5% (with correction) in center and better than 10% to edge.

Class B: Better than 10% center and 25% to edge.

Class C: Better than 20% center and 50% to edge.